A Comparison of DEM-based methods for fluvial terrace mapping and sediment volume calculation: Application to the Sheepscot River Watershed, Maine

Author: Austin Jeremy Hopkins

Boston College Electronic Thesis or Dissertation, 2014

Boston College

The Graduate School of Arts and Sciences

Department of Earth and Environmental Sciences

A COMPARISON OF DEM-BASED METHODS FOR FLUVIAL TERRACE MAPPING AND SEDIMENT VOLUME CALCULATION: APPLICATION TO THE SHEEPSCOT RIVER WATERSHED, MAINE.

a thesis

by

Austin J. Hopkins

submitted in partial fulfillment of the requirements

for the degree of Master of Science

2014

ABSTRACT

A COMPARISON OF DEM-BASED METHODS FOR FLUVIAL TERRACE MAPPING AND SEDIMENT VOLUME CALCULATION: APPLICATION TO THE SHEEPSCOT RIVER WATERSHED, MAINE.

Austin J. Hopkins

Advisor: Noah P. Snyder

Fluvial terraces form in both erosional and depositional landscapes and are important recorders of land-use, climate, and tectonic history. Terrace morphology consists of a flat surface bounded by valley walls and a steep-sloping scarp adjacent to the river channel. Combining these defining characteristics with high-resolution digital elevation models (DEMs) derived from airborne light detection and ranging (lidar) surveys, several methods have been developed to identify and map terraces. This research introduces a newly developed objective terrace mapping method and compares it with three existing DEM-based techniques to determine which is most applicable over entire watersheds. This work also tests multiple methods that use lidar DEMs to quantify the thickness and volume of fill terrace deposits identified upstream of dam sites. The preliminary application is to the Sheepscot River watershed, Maine, where strath and fill terraces are present and record Pleistocene deglaciation, Holocene eustatic forcing, and Anthropocene land-use change. Terraces were mapped at four former dam sites along the river using four separate methodologies and compared to manually delineated area. The methods tested were: (1) edge detection using MATLAB, (2) feature classification algorithms developed by Wood (1996), (3) spatial relationships between interpreted terraces and surrounding natural topography (Walter et al., 2007), and (4) the TerEx terrace mapping toolbox developed by Stout and Belmont (2013). Thickness and volume estimates of fill sediment were calculated at two of the study sites using three DEM-based models and compared to in situ data collected from soil pits, cut bank

exposures, and ground penetrating radar surveys. The results from these comparisons served as the basis for selecting methods to map terraces throughout the watershed and quantify fill sediment upstream of current and historic dam sites. Along the main stem and West Branch of the Sheepscot River, terraces were identified along the longitudinal profile of the river using an algorithm developed by Finnegan and Balco (2013), which computes the elevation frequency distribution at regularly spaced cross-sections normal to the channel, and then mapped using the feature classification (Wood, 1996) method. For terraces upstream of current or historic dam sites, thickness and volume estimates were calculated using the two best performing datum surfaces. If all analyzed terraces are composed of impounded sediment, these DEM-based results suggest that terraces along the main stem and West Branch of the Sheepscot River potentially contain up to 1.5 x 10^6 m^3 of fill. These findings suggest powerful new ways to quickly analyze landscape history over large regions using high-resolution, LiDAR DEMs while relying less heavily on the need for detailed and costly field data collection.

ACKNOWLEDGEMENTS

This research was supported by **National Science Foundation Grant #645343** and the **Boston College Department of Earth and Environmental Sciences** summer research fellowship. I would also like to thank the **University of Maine Darling Marine Center** for providing housing during the summer of 2013 and **Dino Bellugi** for helping me develop a terrace mapping method using MATLAB.

NOAH and GAIL: For not only financial and academic support, but also lobster dinners, sailing trips to the Martha's Vineyard, and overall a great graduate school experience.

AAKASH and CALEB: Fieldwork wouldn't have been the same without you two. Can't thank you enough for the valuable feedback and assistance.

RANDI WALTERS: For always supporting me in my endeavors, and providing the greatest motivation I could ask for to complete this research.

All BC Graduate Students: Thanks for making graduate school memorable!

TABLE OF CONTENTS

LIST OF FIGURES

LIST OF TABLES

1 INTRODUCTION

1.1 Research Motivation

Fluvial terraces are remnants of surfaces that were once connected to a river but have since been abandoned, leaving behind a landform with a relatively flat surface (tread) adjacent to the scarp of an incising river (Campbell, 1929; figure 1.1). Terrace abandonment occurs in response to the fluctuation of forces exerting control on a river's gradient (e.g. tectonic activity or climate induced base level change). Analyzing terraces assists in constraining the timing and magnitude of these forces over a particular region. Terraces are generally discrete features that are not continuous along a river, so they must first be accurately identified and mapped before the processes that created them can be understood. Historically, mapping terraces has required detailed field surveying that was costly and time consuming. More recently, the availability of high-resolution light detection and ranging (lidar) digital elevation models (DEMs) has promoted digital mapping of terrace landforms. DEM-based mapping can be accomplished using manual delineation or through fully or semi-automated procedures. This study applied four mapping methods to a watershed in mid-coastal Maine, a landscape heavily influenced by late Pleistocene continental glaciation overlain by changes in land-use practices (figure 1.2), to compare each method's effectiveness at mapping terraces in unfamiliar terrain.

DEM-based mapping of terraces encourages further extraction of data from these landforms, such as their height above the river channel or their thickness and volume. Of particular interest in the mid-coastal Maine landscape is terraces upstream of current and former dam sites (figure 1.2). Strouse (2013) studied the effect of changing land-use practices within the Sheepscot River watershed along mid-coastal Maine, and found that terraces upstream of two former dam sites formed due to deposition of sediment in the millponds. After the breaching or

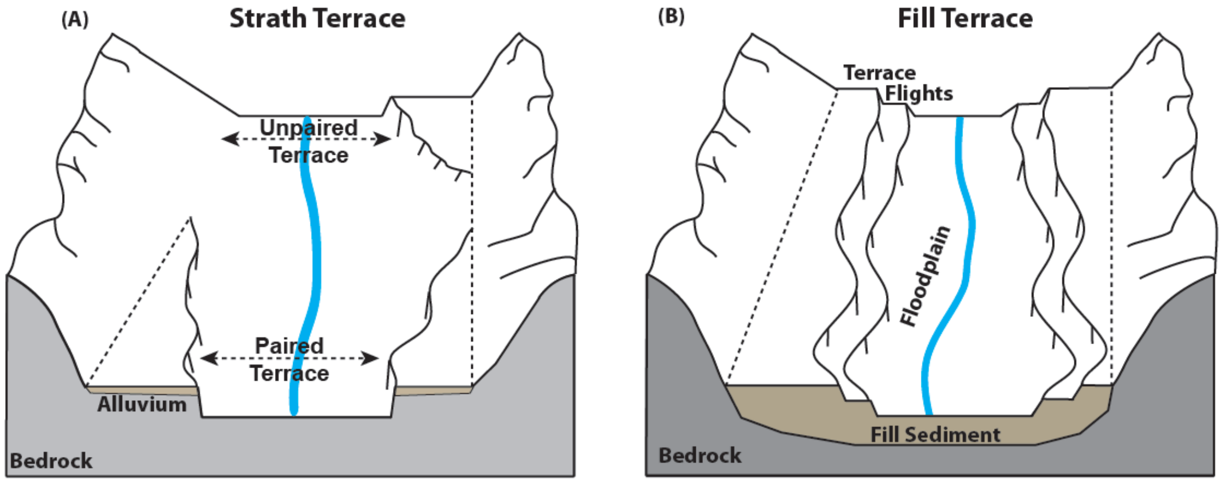

Figure 1.1: General schematic of (A) strath terraces and (B) fill terraces illustrating potential characteristics of terraces, such as being paired or unpaired or existing as multiple flights within a river valley. Figure modeled after figure 1 from Merritts et al. (1994).

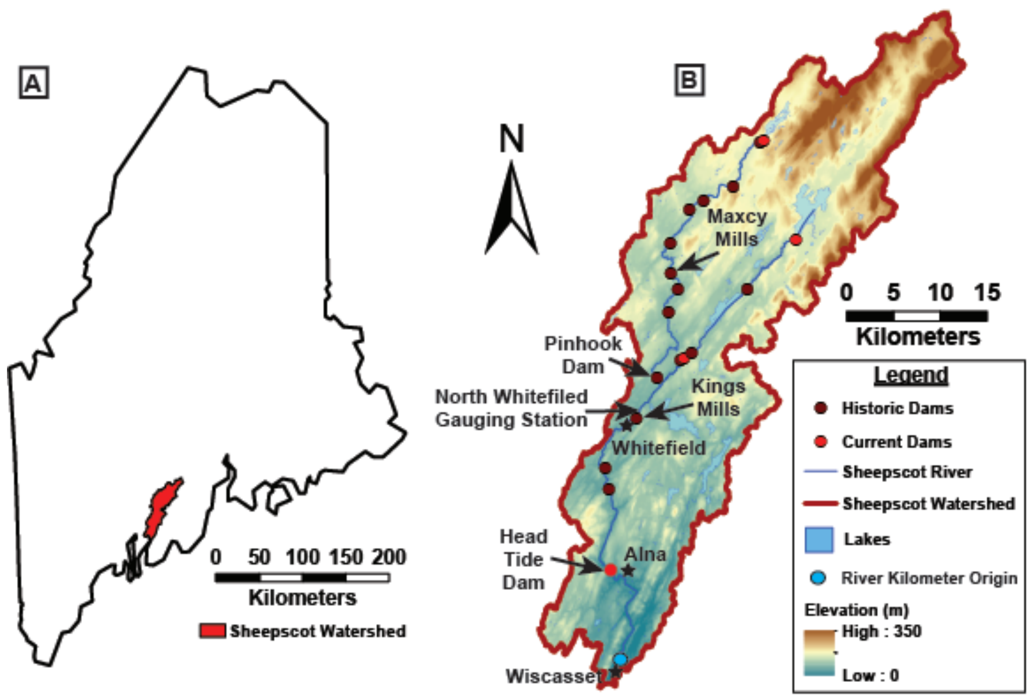

Figure 1.2: Location of the Sheepscot River watershed in mid-coast Maine (A) and DEM of Sheepscot River watershed showing current and historical dam sites (B).

removal of the dams, vertical incision into the impounded sediment occurred and produced the fill terraces. This type of terrace has been described in the mid-Atlantic Piedmont region of the U.S., and is commonly referred to as a reservoir or Anthropocene-sediment terrace (Walter and Merritts, 2008). Reservoir-sediment deposits are identifiable based on their characteristic stratigraphy of a massive fine-grained unit, often containing buried artifacts or organic matter, overlying paleo-valley deposits such as buried hydric soils, paleo-river channels, or floodplain strata (figure 1.3; Strouse, 2013). Within the Sheepscot River watershed, reservoir sediments typically overlie either glacial till or the glaciomarine clay known as the Presumpscot Formation (figure 1.3). These reservoir sediment terraces are potential point-sources for sediment and pollutants (Walter et al., 2007; Walter and Merritts, 2008), highlighting the need to obtain estimates of the volume of sediment being stored.

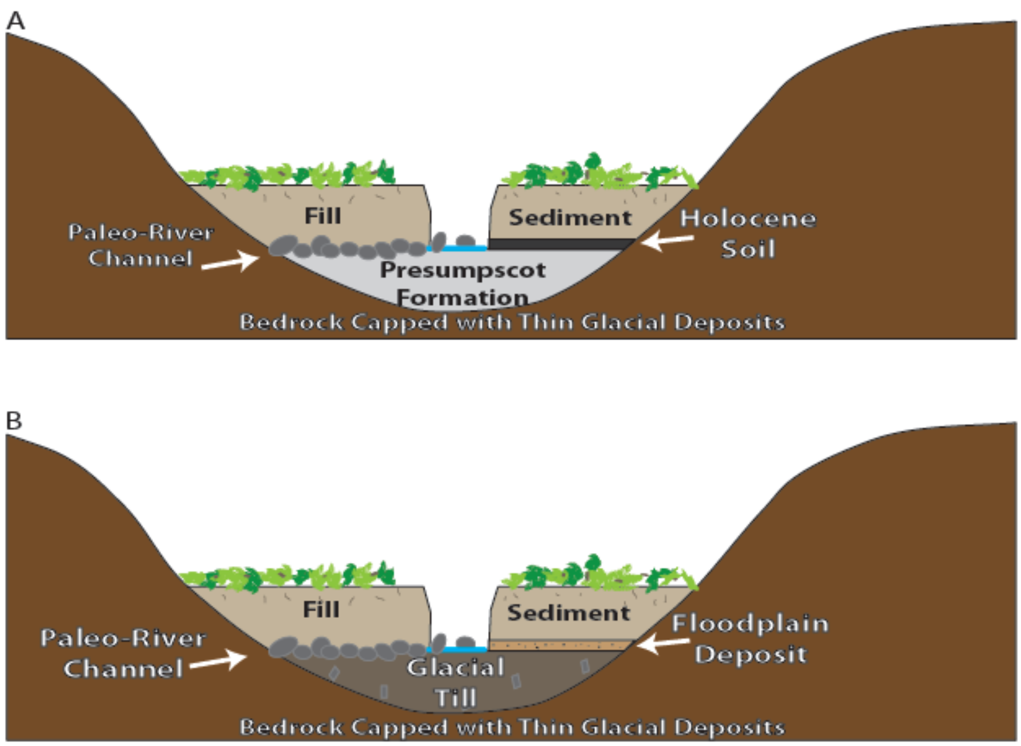

Figure 1.3: Idealized stratigraphy of reservoir sediment terraces within the Sheepscot River watershed, which typically overlay either (A) the glaciomarine Presumpscot Formation of (B) glacial till.

The Sheepscot River watershed historically included 44 dams (Halstead, 2002; table 1.1), with each site potentially storing Anthropocene sediment. To evaluate this, detailed field analysis would be required to first identify fine-grained deposits upstream of dams that correspond to reservoir sediment, and then map the thickness and aerial extent of these deposits to calculate the volume stored. Alternatively, I will discuss a first-order approximation of reservoir-sediment volume achieved using DEM-based approaches and assuming terrace landforms upstream of current and historic dam sites are comprised of reservoir-sediment.

1.2 Research Objectives and Thesis Structure

Existing algorithms and procedures used to objectively identify terraces in DEMs have primarily been supporting components of larger research studies and are often optimized for a specific field region or geologic setting. This work tests the regional applicability of methods by applying them to the Sheepscot River watershed, Maine, a landscape heavily influenced by late Pleistocene continental glaciation overlain by anthropogenic alteration (figure 1.2). This watershed contains both strath and fill terraces that record changes in climate, relative sea level, and land-use that have historically occurred in the region (figure 1.2).

The second chapter of this thesis focuses on a comparison of four DEM-based terrace mapping methods to determine which is best suited for large-scale implementation. The third chapter focuses on reservoir sediment terraces upstream of historic or breached dams. I initially compare three DEM-based datum surfaces used to calculate terrace thickness and volume in order to determine which is best suited for use within the Sheepscot River watershed. Results from mapping and thickness calculation comparisons were combined and the best methods were applied to all current and historic dam sites along the Sheepscot River and West Branch.

Dam Name	River	Purpose	Year Built	Height (m)
Sheepscot Falls	Main Stem	SP, SM, GM	~ 1760	4.3
Head Tide Dam*	Main Stem	SM,FM,GM	1762-1768	6.1
Joshua Little	Main Stem	SM	< 1800	?
King's Mills	Main Stem	SM, SH, GM	~ 1774	?
Turner Prebble	Main Stem	SM	~ 1775	?
Youngs	Main Stem	SH, SM, FM	~ 1807	?
Un-named	Main Stem	SH, GM	?	?
Cooper's Mills*	Main Stem	SM, SH, GM	1804	5.5
Un-named	Main Stem	SM	< 1869	3.7
Sheepscot Pond Dam*	Main Stem	SH, SM, GM, ST	1790	2.4
Pinhook	West Branch	SM	1804	?
Maxcys Mills	West Branch	SM,GM	1809	?
Haskell Pope	West Branch	FM, SM	< 1815	?
Chadwick Pratt	West Branch	GM	< 1829	?
Prescott	West Branch	GM, SH	~ 1829	?
Weeks Mills	West Branch	SM, GM	< 1807	?
Un-named	West Branch	T	< 1856	?
Pullen	West Branch	SM	< 1856	?
Hammond	West Branch	T, SM, SH	< 1856	?
Branch Mills*	West Branch	SM, GM	< 1800	4.3
Grays Tide Mill	Marsh/Deermeadow Brook	WS	~ 1850	4.0
Shattuck Tide Mill	Marsh/Deermeadow Brook	WS	1835	?
Allens Falls	Marsh/Deermeadow Brook	GM, SM	1660	?
Weeks Mills	Marsh/Deermeadow Brook	SM	~1800	2.4
Unnamed	Dyer River	SM, SH	< 1869	3.7
Match	Dyer River	M,	?	?
Fulling	Dyer River	GM, FM, SH, ST	< 1869	3.0
Boynton Trask	Dyer River	SM	1850	2.4
Chases Mill	Clary Lake	SM, SH	~ 1791	2.4
Streans	Clary Lake	SM, SH	1790s	3.0
David Bryant	Gully Brook	SH, ST	1850	1.8
Tolman Colburn	Dearborn Brook	SM, SH	1832	?
Solomon Bruce	Choate Brook	FM, ST	< 1832	?
Un-named	Meadow Brook	SM	< 1856	?
Turner	Colby Stream	SM	< 1819	?
Berry	Colby Stream	SM	< 1886	?
Dodges	Lovejoy Stream	SH	< 1869	?
French's	Lovejoy Stream	SM	< 1869	?
Colby	Lovejoy Stream	SM	1825	4.3
Greeley	Beech Pond	GM	1807	?
Head Mill	Trout Brook	SM	~1750	?
Trout Brook Dam	Trout Brook	SM	1940	4.9
Hodge	Ben Brook	SM	?	?
Mill Dam	Chisolm Pond	FM, SM	1820	6.1

Table 1.1: Current and historical dams in the Sheepscot Watershed (SVCA, 2009). Red entries indicate dams blocking Atlantic salmon passage. Entries with * denotes dams currently intact along river.

1.3 Overview of Fluvial Terraces

Terraces have been are commonly exploited for geologic and geomorphic studies, and are identifiable based on their characteristic morphology (figure 1.1). They exist in river valleys as either singular units or as a succession of remnant landforms preserved in flights (multiple, discrete units existing at varying elevations within a valley), and may be either 'paired' or 'unpaired' depending on whether cross-valley segments have correlating metrics such as elevation, soil development, or geochronological data (figure 1.1). Terrace genesis occurs during a time of fluctuating forcings, and represents the transient response of the landscape to either shifts in climate (Bull, 1991; Warner, 1992; Ritter et al., 2002; Fuller et al., 2009; Finnegan and Dietrich, 2011), tectonic activity (Riebe and Kirchner, 2001; Wegmann and Pazzaglia, 2002; Wegmann and Pazzaglia, 2009), changes in base-level (Pazzaglia et al., 1998; Gran et al., 2009; Belmont, 2011; Finnegan and Dietrich, 2011), anthropogenic activity (Walter and Merritts, 2008; DeLong et al., 2011), or through autogenic processes such as meander migration and cutoff (Finnegan and Dietrich, 2011). The vast majority of preserved terraces reflect historic conditions of modern rivers during the Quaternary, a time associated with high-amplitude and high-frequency glacial-interglacial cycles, and should be analyzed in this context (Pazzaglia, 2013).

Two end-member classifications exist for fluvial terraces based on the processes involved during development, thickness of alluvial deposits atop the tread (relatively flat surface of terrace), and basal contact topography (figure 1.1). The first end-member, known as a strath terrace (figure 1.1 A), is an erosional landform formed by the lateral migration of a river channel across a valley bottom that planes down underlying lithology prior to incision and abandonment. This produces a sub-horizontal base and leaves behind a thin mantle of alluvium on the terrace tread (figure 1.1 A). Strath terraces are often utilized in tectonically active regions to place timing on tectonic activity (Hancock et al., 1999), calculate rates of deformation (e.g. Rockwell et al., 1984; Lavé and Avouac, 2000), and quantify bedrock incision (e.g., Molnar et al., 1994; Lavé and Avouac, 2000; Pazzaglia and Brandon, 2001). However, recent work by Finnegan et al. (2014) has shown that incision rates derived using strath terraces cannot be assumed to reflect periods of equilibrium between river incision and external forcings over vast timescales (10^4 -10^7 years). Instead, strath terraces record stochastic episodes of erosion with rates that are strongly linked to measurement interval.

The alternative end-member is a fill terrace, which forms through aggradation in valleys and subsequent entrenchment (figure 1.1 B). Basal contacts for these deposits reflect the paleotopography of valley floors (figure 1.1 B). Aggradation occurs over time when the input of sediment exceeds transport capacity. This can be a product of changes in base-level, climate, land-use, or sediment concentrations in rivers (Ritter et al., 2002). The supply of sediment eventually ceases, halting deposition and inducing vertical incision by the river and entrenchment into the fill, thereby forming the fill terrace. Fill terraces are useful for deducing paleo-hydrologic and paleo-sedimentologic conditions (Blum, 1993; Pazzaglia and Brandon, 2001), as well as preserving a record of changes in land-use practices (Walter and Merritts, 2008).

1.4 Prior Work on Terrace Mapping

1.4.1 Manual Methods

All studies utilizing terraces involve some component of mapping. Mapping endeavors often required detailed field campaigns along with analysis of topographic maps and aerial photography, all of which can be costly and/or time consuming. Two studies that exemplify early mapping methodologies are Merritts et al. (1994) and Lavé and Avouac (2000). Over a period of several months, Merritts et al. (1994) surveyed terraces along a 40 km stretch of the Mattole River in California using a total geodetic station. In total, 1300 data points were collected and mapped not only terrace surfaces but also active channel width and bottom, gravel bars, and floodplains (Merritts et al. 1994). Although time consuming, the robustness of this dataset illustrates one of the benefits of field mapping and why it is still of such value today. Included in Merritts et al. (1994) is a discussion on the potential introduction of human bias when correlating terrace points and reconstructing paleo-river longitudinal profiles based on inadequate resolution in survey data (figure 1.4). Thus, studies seeking to use terraces to infer past conditions must obtain a sufficient amount of data to draw appropriate conclusions.

In a more recent study, Lavé and Avouac (2000) mapped terraces in the Siwaliks Hills, Himalayas of central Nepal using a combination of aerial imagery and field studies. Terraces were initially classified based on their spectral signature in a Landsat thematic mapper image (figure 1.5). Identified landforms were then further calibrated in the field through analysis of weathering color, strata facies, and thickness of alluvial veneer and overbank deposit. Terrace surface and basal contact elevations and were also measured in the field using digital altimeters (accuracy of 3-4 m after correction of barometric changes). These efforts produced two maps of terraces along Bagmati and Bakeya rivers (figure 1.6), which were used to quantify Quaternary uplift rates and base level changes occurring within the Siwaliks Hills.

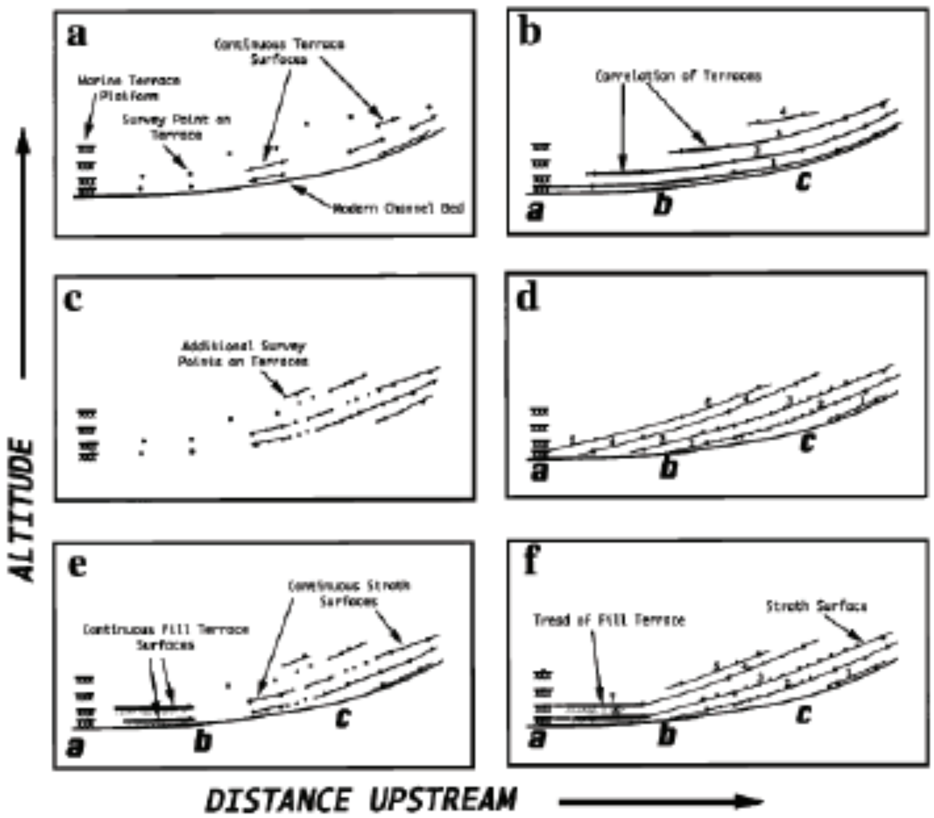

Figure 1.4: Potential erroneous terrace interpolations due to natural human bias and an insufficient amount of surveyed data points atop terrace surfaces. Figures a, c, and e show idealized terrace survey data with three alternative interpretations that could be reached (b, d, and f) based on the correlation of available data. Figure taken from Merritts et al., (1994).

1.4.2 Fully and Semi-Automated DEM-Based Methods

Beginning in the 1970s with the development of digital terrain models (DTM), researchers first began designing computer algorithms to digitally analyze terrain in watersheds (Collins, 1973). Subsequent development of coarse resolution (90, 30, 10 m grid spacing) DEMs provided only limited improvement in mapping endeavors because they lacked the vertical and horizontal resolution necessary to discriminate subtle variations between multiple terrace landforms (figure 1.7; Stout and Belmont, 2014). Adequate resolution for DEM-based mapping has recently been achieved through topographic datasets collected from airborne lidar surveys.

Lidar DEMs have high horizontal (1-3 m grid spacing) and vertical (5-20 cm elevation accuracy)

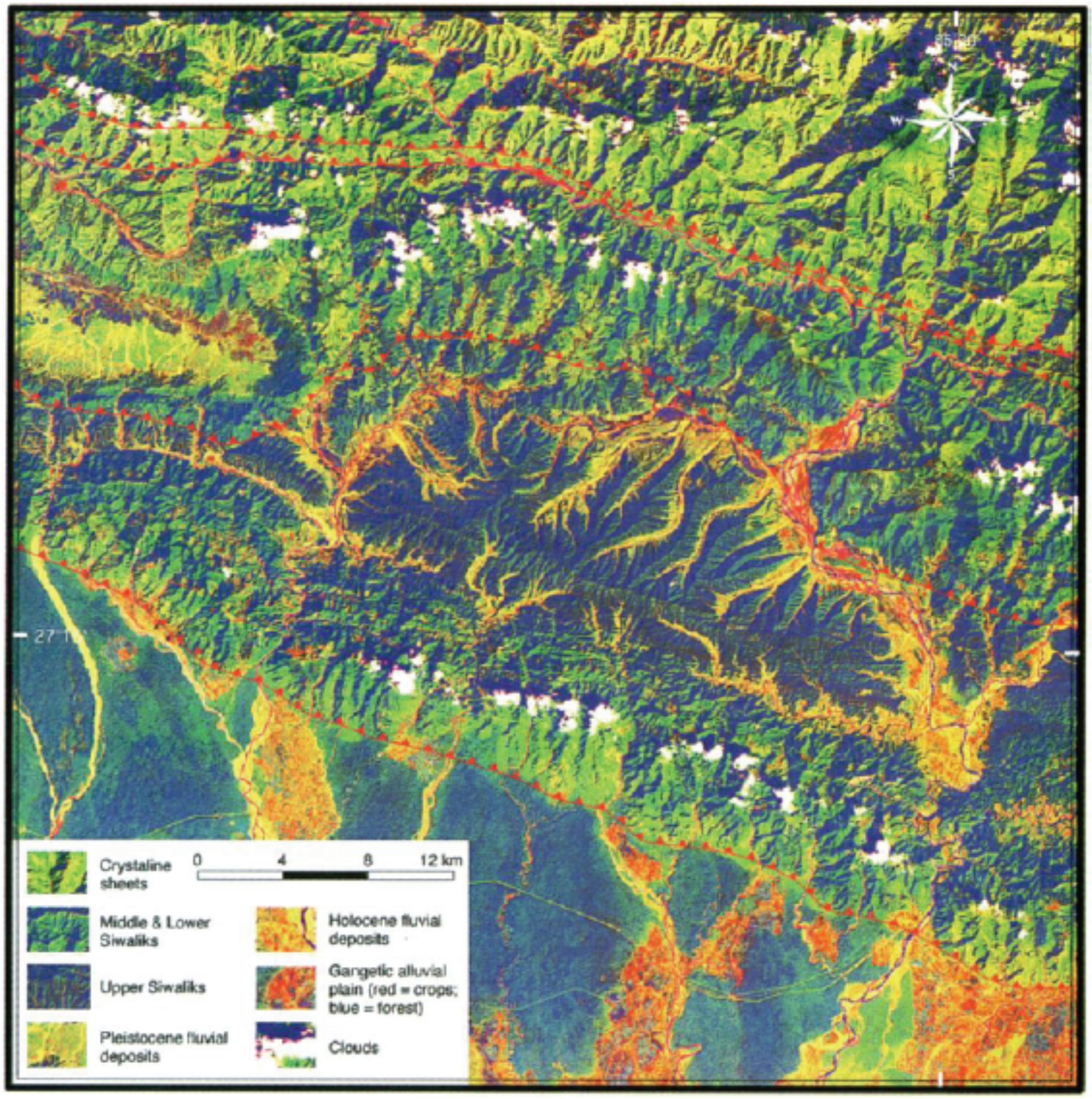

Figure 1.5: Landsat TM image (linear combination of channels 1, 2, 3, 4, 5, and 7) used by Lavé and Avouac (2000) to map fluvial terraces based on their unique spectral signature. Red colored regions within this image correspond to the terraces mapped in the study. Image taken from Lavé and Avouac (2000).

resolution. Additionally, lidar data can be filtered to produce bare-earth DEMs that remove vegetation in order to make surface textures and landforms more apparent to visual examination (figure 1.7). This aspect of lidar imagery is a notable improvement over aerial photography, particularly in forested landscapes, and may help alleviate the need to map terraces in the field (figure 1.7).

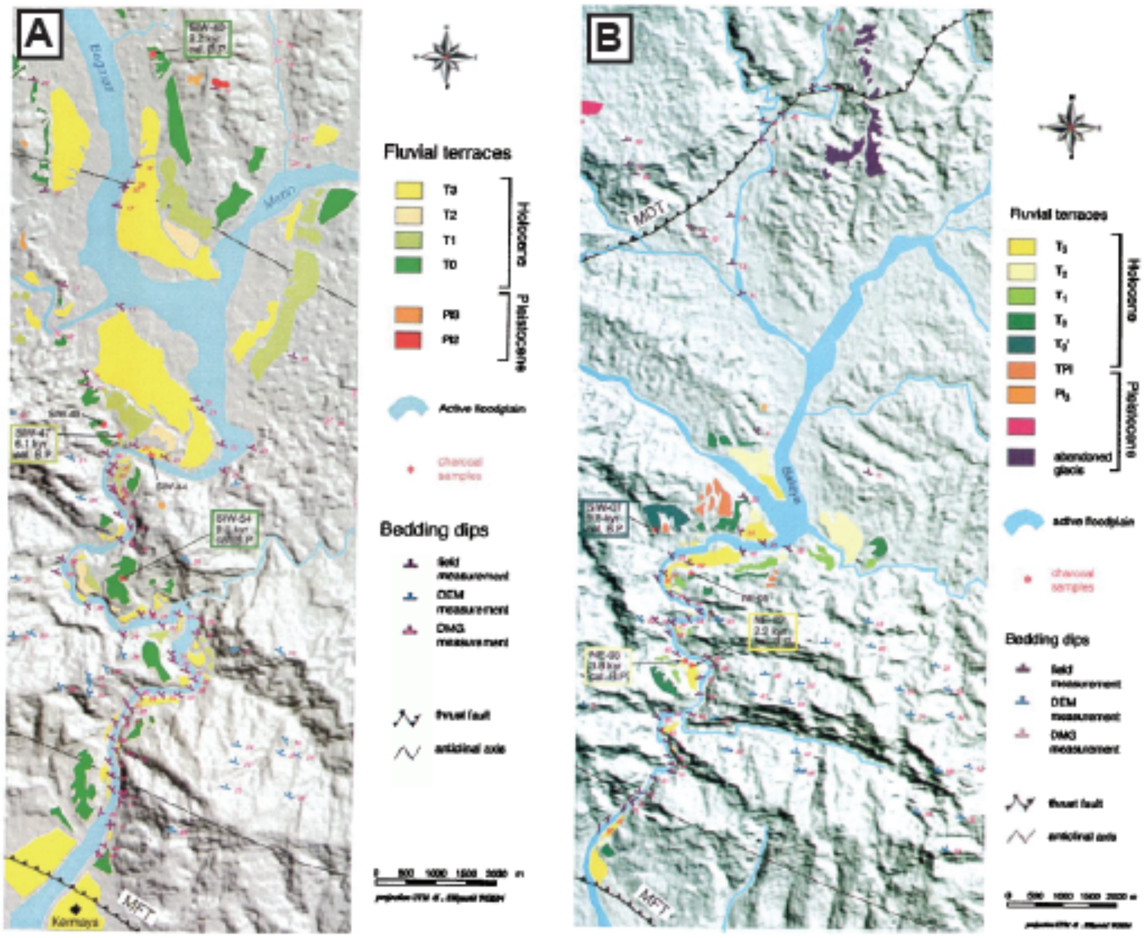

Figure 1.6: Maps of terraces along the (A) Bagmati River and (B) Bakeya River in Siwaliks Hills, Himalayas of central Nepal. Maps are overlain on a hillshade DEM of the region. Image from Lavé and Avouac (2000).

Capitalizing on the visibility of landforms such as terraces in bare-earth DEMs, several studies have developed automated techniques for classifying elevation datasets and extracting geomorphic and hydrologic features (MacMillan et al., 2003). Demoulin et al. (2007) worked with DEMs of the Vesdre Valley of eastern Belgium and developed an algorithm to extract fluvial terraces along longitudinal profiles based on topographic characteristics. Along river valley cross-sections, a flat terrace tread produces localized minima in slope values and a change of sign for profile curvature values, thus pinpointing the location of a terrace (figure 1.8). These artifacts serve as the basis for the Demoulin et al. (2007) mapping method, and were successful at mapping 74% of the terraces present in the Vesdre Valley. In direct response to Demoulin et al. (2007), subsequent studies have developed more effective means of mapping terraces along longitudinal profiles (i.e. Finnegan and Balco, 2013), the details of which are discussed in chapter 3.

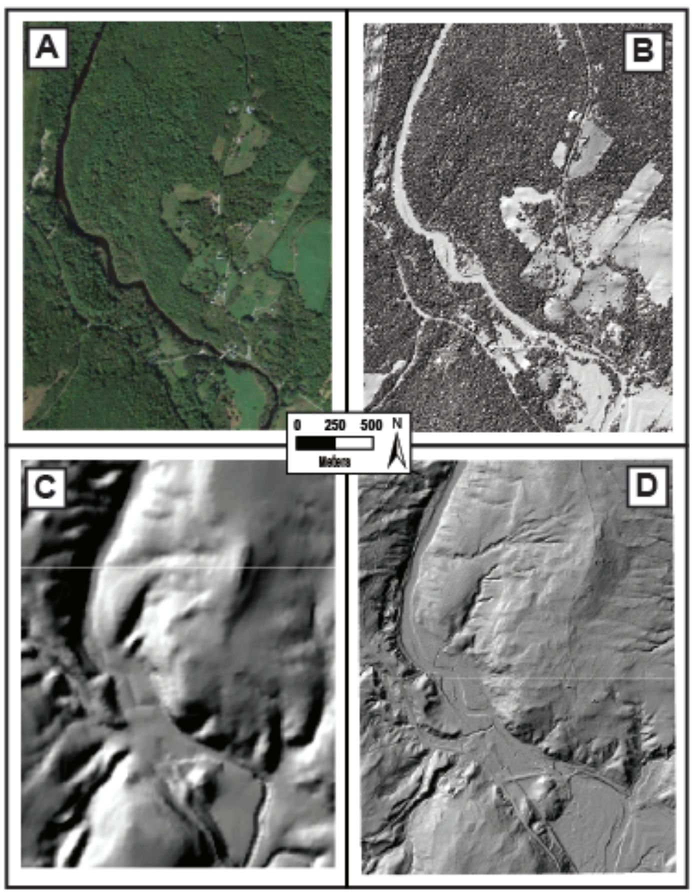

Figure 1.7: Benefits of using lidar DEMs illustrated by comparing (A) satellite images (~0.5 m/pixel spatial resolution from WorldView-2 satellite) obtained from Google Earth, (B) a first return hillshade raster computed using a lidar DEM, (C) a bare-earth hillshade raster computed using a 10 m resolution DEM and (D) a hillshade raster computed using a bare-earth lidar DEM.

The comparison of mapping methods will include automated and semi-automated DEM-based techniques. Chapter 2 discusses four more DEM-based mapping procedures, including edge detection in MATLAB, the Rahnis Method (Walter et al., 2007), feature classification algorithms (Wood, 1996), and the TerEx mapping toolbox (Stout and Belmont, 2014).

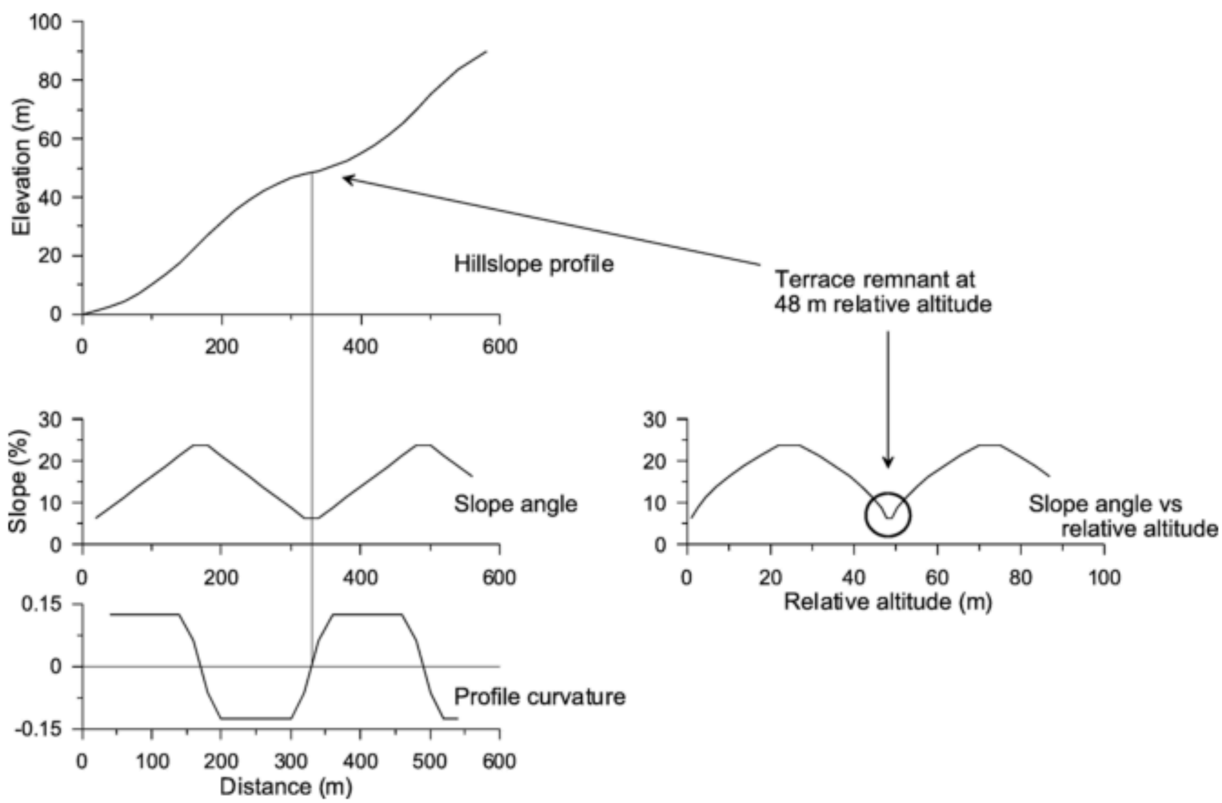

Figure 1.8: Multiple figures illustrating the potential for mapping terraces by defining them in terms of minimum slope values and where profile curvature values change sign. Image taken from Demoulin (2007).

1.5 Study Area

1.5.1 Geologic and Geomorphic Background of Mid-Coast Maine

The Sheepscot River watershed spans an area of 576 km^2 and flows 106 km through mid-coast Maine, into the Atlantic Ocean near the town of Wiscasset (figure 1.2). The river flows in a southwesterly direction and its path is heavily influenced by the underlying geology, consisting of metasedimentary rocks within the Norumbega shear zone (Osberg et al., 1985) that impart a strong NE-trending fabric onto the drainage pattern (Snyder et al., 2008). Glaciation has played a dominant role in shaping this landscape (Belknap et al. 1986; Belknap et al., 2002). At the last glacial maximum (LGM, ~25,000 ka), the Laurentide Ice Sheet flowed southeast across Maine, terminating on Georges Bank in the Gulf of Maine (Stone and Borns, 1986; figure 1.9 A). A warming climate resulted in deglaciation, with the ice sheet retreating to near the modern coastline at ~15 ka and later becoming nearly absent from the landscape at ~ 12.5 ka (Schnitker et al., 2001; figure 1.9 B-C). Glacial retreat is recorded by the common occurrence of glacial deposits throughout the landscape, including recessional moraines, kames, and eskers.

Sea level inundation occurred simultaneously with deglaciation, caused by isostatic depression of the lithosphere from the weight of the ice sheet and the extended amount of time necessary for rebound to take place (figure 1.9 B). During this time, a massive grey glaciomarine mud with interwoven sand-lenses known as the Presumpscot Formation (Bloom, 1963; Smith, 1985; Stone and Borns, 1986) was deposited in low-lying regions along the coast (figure 1.9 B). Today, the Presumpscot Formation can be found up to 130 m above modern sea level and is easily identifiable in stratigraphic sections, providing a clear datum from which to place time constraints on overlying units (Thompson and Borns, 1985; figure 1.9 C). Nearly the entire Sheepscot River watershed is seaward of the late Pleistocene shoreline (Smith, 1985), therefore fine-grained glaciomarine deposits dominate the river valley with sand and gravel outcrops present in zones of coarse glaciomarine and esker deposits in the western and northern parts of the watershed (Thompson and Borns, 1985).

The combination of glacial activity and bedrock control has produced the Sheepscot

River visible today. The Sheepscot River has a low gradient (mean slope ~0.0016 m/m) imposed-form channel that flows predominantly over glacial deposits. Bedload is most likely

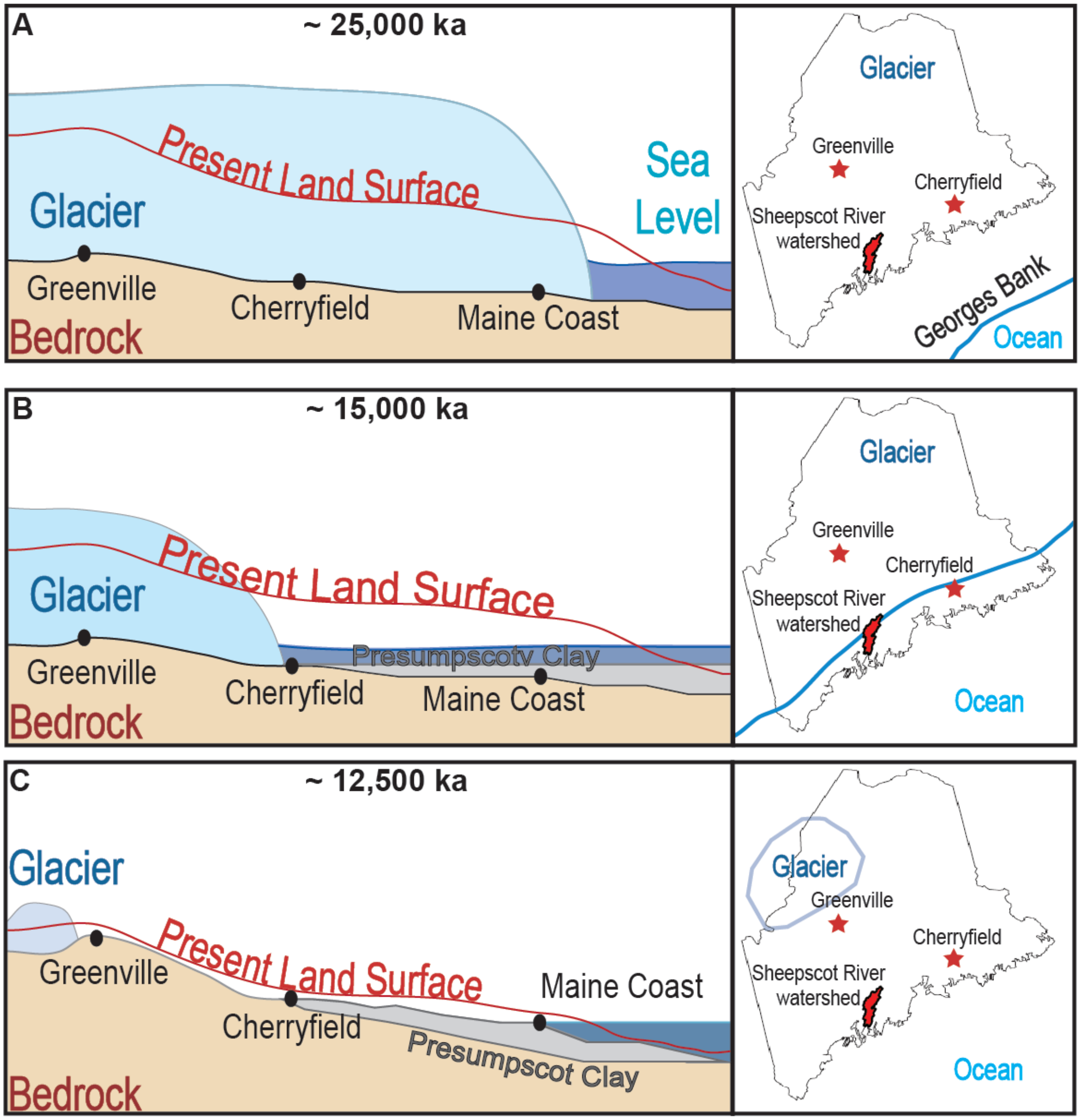

Figure 1.9: Glacial history of Maine showing (A) the state completely covered by the Laurentide Ice Sheet ~25,000 ka. During deglaciation around ~15,000 ka (B), coastal Maine remained depressed and was inundated with seawater. Around ~12,500 ka (C), only remnants of the ice sheet remained throughout the landscape.

derived from glacial sediments, as the river has locally incised up to tens of meters into these deposits. Bedrock exposures within the channel are observable in a few steep reaches (Snyder et al., 2013). Mean annual discharge is 20 m^3/s and is recorded by a USGS gauging station near the town of North Whitefield (figure 1.2). Just north of the gauging station is the confluence joining the West Branch of the Sheepscot River with the main stem (figure 1.2). River kilometers for the Sheepscot River increase upstream, and originate at the bridge crossing the estuary in the town of Wiscasset, ME. Tidal processes play a role over almost a quarter of the river's length but do not extend upstream of Head Tide Dam (figure 1.2).

1.5.2 Historic and Current Land-Use

Landscape alteration initiated by changing land-use practices over the past few centuries is superimposed on the post-glacial response within the Sheepscot River watershed. Extensive alteration of the land began in the late 1600s with the onset of European settlement, where clear-cutting of virgin forests took place to provide land for port towns and agriculture (Laser et al., 2009; Sheepscot Valley Conservation Association, SVCA, 2009). A combination of long winters and thin, rocky soils meant large crop yields were difficult to obtain, leading to a decline in farming throughout the 19th century and the reclamation of the land by dense, second growth forests (SVCA, 2009). Today, forests account for the majority of land in the watershed (89%). Remaining land consists predominantly of agriculture (2.5%) and low density residential (1.5%; Brady, 2007).

Logging activity within the watershed is less prevalent today, but the timber industry left a lasting impression on the landscape in the form of numerous dams along waterways. The river was an effective means to transport large volumes of wood to saw mills built adjacent to run-of-the-river dams (Halstead, 2002). Dams were not limited to the timber industry, and also supported mining, textile, and grain production purposes. In total 44 dams were built throughout the watershed, 19 of which located on either the main stem of West Branch of the Sheepscot River (Halstead, 2002; figure 1.2; table 1.1). Historically, 17 of the dams blocked upstream passage for anadromous fish species; of the ten remaining dams within the river basin, five are believed to still obstruct fish passage (Halstead, 2002; SVCA. 2009; figure 1.2; table 1.1).

The damming of the river was not limited to anthropogenic activity, as beaver dams influenced the fluvial morphology as well. Beavers were inhabitants of this region since pre-Colonial times, and built structures capable of persisting for decades (Halstead, 2002). After being hunted to near extinction, beavers were re-introduced into this region in the 20th century, and they continue to influence fluvial morphology on the reach scale (Rosell et al., 2005).

1.5.3 Selected Study Sites

Four river segments, each 2 km in length, containing Head Tide Dam (HTD), Pinhook Dam (PHK), Kings Mills Dam (KM), and Maxcy Mills Dam (MM) were selected as the study sites used to implement the mapping method comparison (Chapter 2; figure 1.10). The HTD and PHK locations were also used to ground truth DEM-based sediment thickness calculations (Chapter 3; figure 1.10). The terraces at HTD and MM are Anthropocene deposits that formed due to the presence of the dam and associated millpond (Strouse, 2013). It is unknown if the terraces present at PHK and KM formed as a consequence damming, but they are easily identifiable within the lidar DEMs and can provide further assessment on the effectiveness of DEM-based mapping methods. For DEM-based thickness and volume estimates, the inclusion of the PHK will test the accuracy of calculations on a smaller scale site compared to HTD.

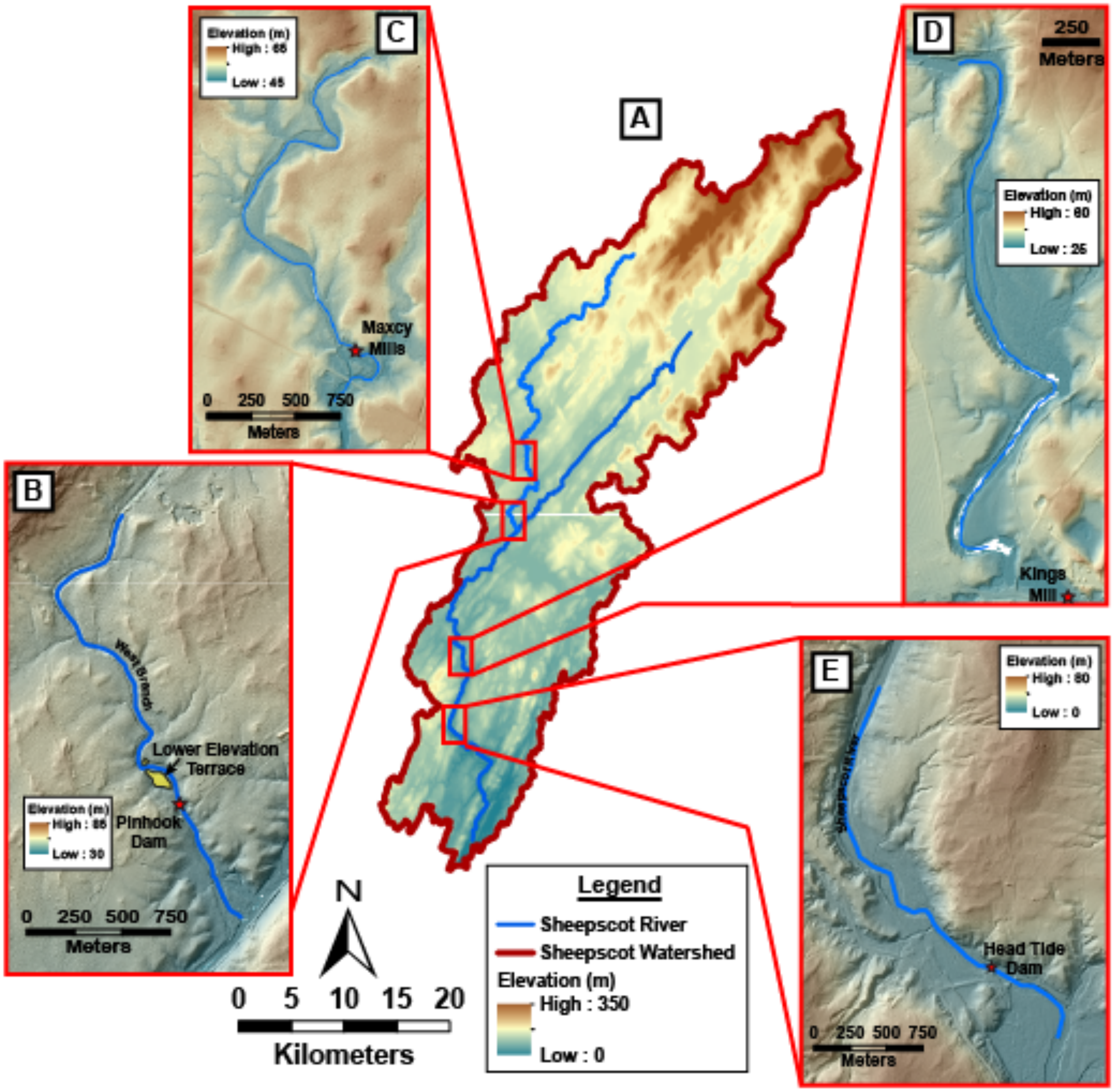

Figure 1.10: DEM of the Sheepscot River watershed (A) with locations of the four selected study regions indicated by the red rectangles. Study sites include the Pinhook Dam (B) and Maxcy's Mills Dam (C) on the West Branch and the Kings Mills Dam (C) and Head Tide Dam (D) on the main stem of the Sheepscot River. Study sites are shown here as DEMs overlain by hillshade rasters.

1.5.3.1 Head Tide Dam

Head Tide Dam (HTD) is the farthest downstream dam present on the Sheepscot River, located just upstream of tidal influences at river kilometer 10.5 near the town of Alna (figure

1.2). It was originally built in the 1760s as a run-of-the-river dam to power sawmills, a gristmill, and a fulling (textile) mill (Halstead, 2002; figure 1.11 A). Upstream of the dam the river is confined on both sides by bedrock. Here the channel is steep (mean gradient ~5%), narrow (< 7 m), and relatively deep (1.5-2 m at flows below bankfull; Strouse, 2013). The surrounding landscape has ~75 m of relief with a mean elevation of 38.36 m (standard deviation 20.68 m)

The dam was rebuilt in 1916, and presently exists as a 4 m high and 40 m wide concrete structure (figure 1.11 B). To promote the passage of Atlantic salmon traveling upstream to spawn, two 1.5 m holes were bored at mid-height in 1952 and 1956 (Halstead, 2002; figure 1.11 B); however, the presence of the dam still contributes to some flow impoundment (but not regulation). Channel narrowing and incision into dam-impounded sediment has occurred as a result of the breaching of the dam, which has formed elevated (~2 m) narrow (10 m) fill terraces vegetated with grass and shrubs (Hazlinsky and Snyder, 2007; Strouse, 2013). Strouse (2013) showed the mill pond associated with HTD extended 1 km upstream and is responsible for trapping the sediment comprising the fill terraces present. The inclusion of anthropogenic artifacts such as tools within terrace deposits provides further indication of dam influenced sedimentation (Strouse, 2013).

1.5.3.2 Kings Mills Dam

Kings Mills was located near the town of Whitefield, ME, on the main stem of the Sheepscot River (figure 1.2). Built sometime around 1774, the dam functioned as a sawmill, gristmill, shingle mill, and power generator throughout its lifetime until Hurricane Edna destroyed it in 1954 (Halstead, 2002; Sacks, 2004). An approximately 6 m concrete wall along the western bank of the Sheepscot River is all that remains of this former dam (figure 1.11).

Upstream of the former dam site, the river channel has a shallow gradient (mean slope of 0.4%) and reaches up to 30 m wide. The surrounding topography has ~35 m of relief and a mean elevation of 35.99 m (standard deviation 6.58 m).

The exact height of the dam remains unknown, but upstream of its historic location exists wide (ranging from 20 to > 100 m) terraces elevated ~ 2 m above the river channel that are clearly visible in bare-earth DEMs (figure 1.10). These terraces have been previously mapped as stream alluvium (Maine Geological Survey, MGS, 1999), and are currently inhabited by forest vegetation or used for agricultural purposes. Land-use within this vicinity is a mix of low-density residential, agriculture, gravel mining, and recreational purposes (there is a golf course within 200 m of the river channel). Surficial geologic mapping of the KM region has classified low-lying regions surrounding the river as Presumpscot Formation with till deposits capping local peaks (MGS, 1999).

1.5.3.3 Maxcy's Mills Dam

Maxcy's Mills dam was an approximately 2 m high dam built in 1809 to power a sawmill along the West Branch of the Sheepscot River (Halstead, 2002; Strouse, 2013; figure 1.2). The dam was in use as a gristmill until 1940, when the mill was torn and the dam was abandoned (Halstead, 2002). Although the dam no longer resides in the channel or causes any impedance to flow, stones used for the structure of the dam are still visible adjacent to the channel and in mid-channel islands (figure 1.11). Part of the original dam's raceway is also still fairly intact and diverts water away from the main channel.

The dam was abandoned in 1940, and Strouse (2013) concluded that the dam breached naturally in the late 1950s. Subsequent channel-narrowing has occurred and is evident through historical air photograph analysis (Hazlinsky and Snyder, 2007; Strouse, 2013). The modern channel is narrow (< 5 m), deep (> 4 m) and has a mean longitudinal gradient of 0.1% (Strouse, 2013). Surrounding the channel is a low-relief landscape (~15 m of relief) with a mean elevation of 53.95 m (standard deviation of 2.73 m). Upstream of the former dam site are wide (> 50 m) floodplains with shrub growth and grasses that transition to a 0.8 m terrace with dense forest (Strouse, 2013). Strouse (2013) classified these terraces as reservoir sediment based on findings of wood and leather artifacts in conjunction with radiocarbon dating that yielded 200 CE (common era) ages.

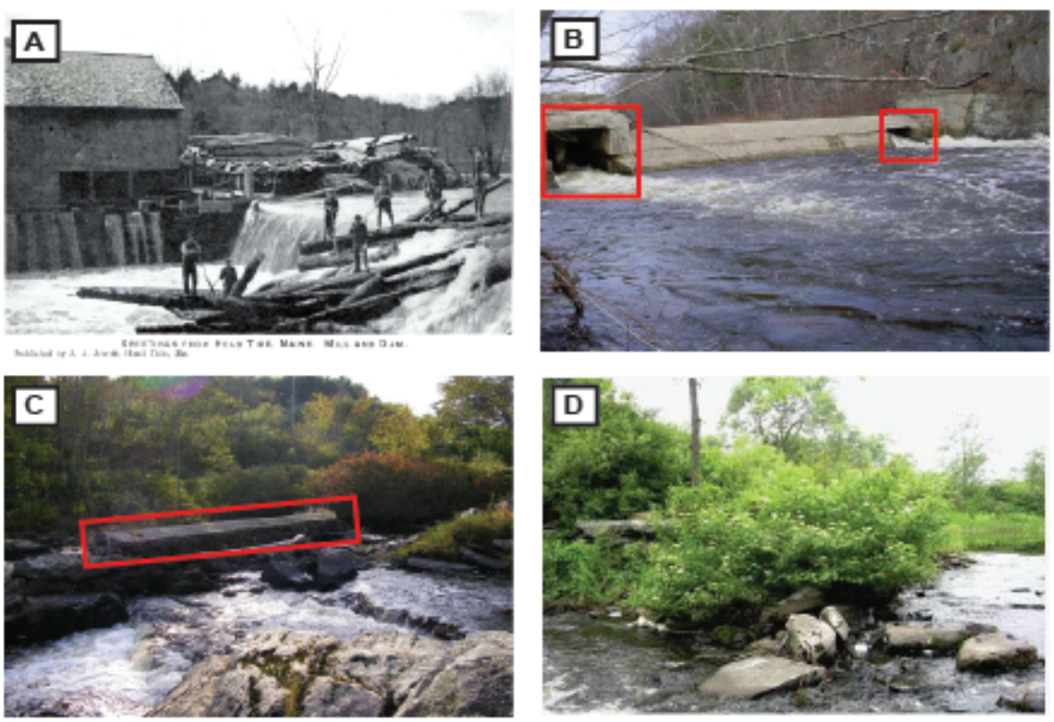

Figure 1.11: Historic and modern images of the dams used as study sites for this research. Images of Head Tide Dam include a postcard circa 1907 (A) and a photograph from 2004 (B) illustrating the two holes bored through the dam to promote fish passage (red rectangles). Photographs (C) and (D) show the remnant structures still visible at the historic Kings Mills and Maxcy's Mills sites, respectively.

Maine Geological Survey (1999) mapped these surfaces as wetland deposits and the surrounding landscape as Presumpscot Formation. Surrounding land use includes agricultural and low-density residential.

1.5.3.4 Pinhook Dam

Pinhook dam was located near the town of Whitefield and was the farthest downstream dam on the West Branch of the Sheepscot River (figure 1.2). Originally built to produce power for a sawmill in 1804, no trace of the dam exists today (Halstead, 2002). Little information is available on the history of the dam, such as the timing of abandonment or the height of the structure, therefore analysis of historic topographic maps must suffice. The dam or any associated millpond is absent from topographic maps dating back to 1893 (U.S. Geological Survey, 1893; figure 1.12), so the dam likely was removed by this time. The current river channel is ~7 m wide with a mean slope of 0.6%, although these values increase as they approach the confluence with the main stem, located ~500 m downstream. Within the channel are numerous bedrock outcrops (figure 1.13). The surrounding landscape has ~40 m of relief and a mean elevation of 51.38 m (standard deviation of 7.16 m).

Even though the dam appears to have been in place for only a short time, terraces are still apparent upstream of the historic location (figure 1.10). Additionally, ~100 m upstream of the former dam site is a small (~600 m^2) terrace tread at a lower elevation relative to the majority of terraces in this region. Although small, this feature tested the capability of each method to distinguish subtle elevation differences between adjacent terrace treads, a situation analogous to studies seeking to map multiple flights of terraces.

The location of terraces immediately upstream of PHK is suggestive of formation due to dam induced base-level change. However, Maine Geological Survey (1999) mapped these units as Presumpscot Formation rather than stream alluvium, indicating that these terraces might be natural "strath" terraces that formed due to the lateral erosion into underlying cohesive glacial clay. The composition of these terraces and the magnitude of anthropogenic control on their development will be addressed further in Chapter 3.

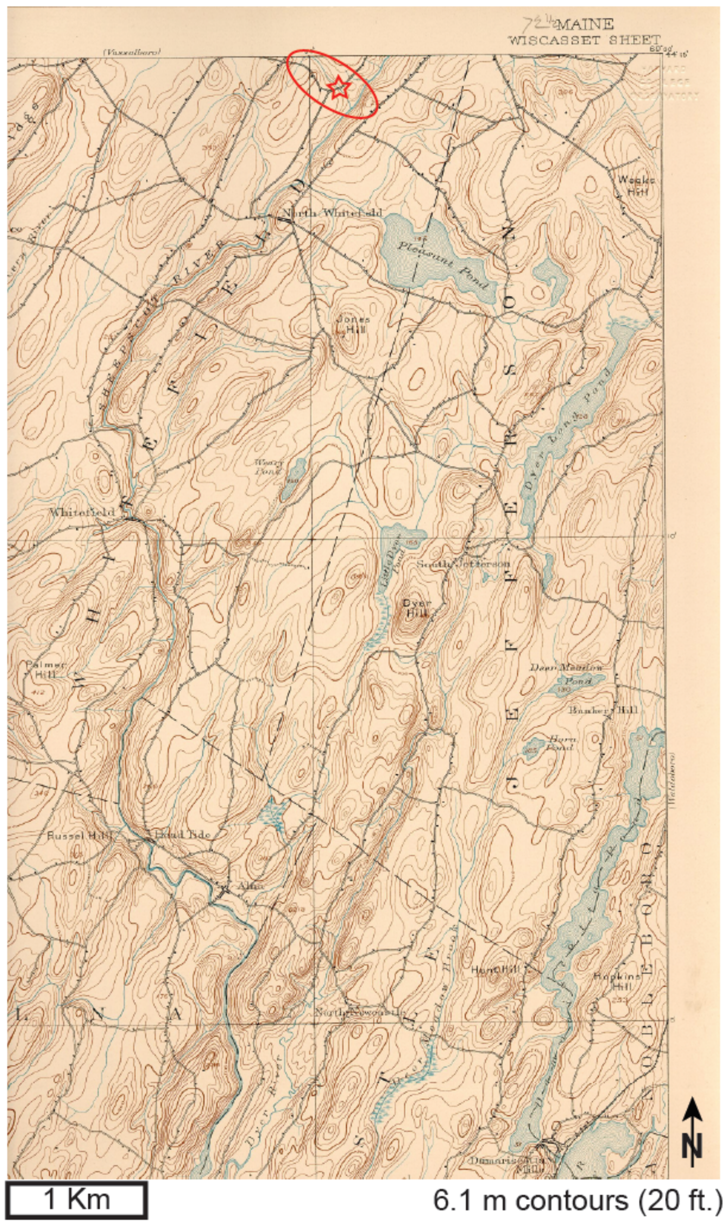

Figure 1.12: Portion of a 1893 topographic map for Wiscasset, ME showing no evidence of Pinhook Dam (red star) or any associated upstream reservoir (red ellipse).

Figure 1.13: Photograph taken looking upstream along the West Branch and showcasing the bedrock outcrops present in the channel near the historic Pinhook Dam location.

2 COMPARISON OF DEM-BASED TERRACE MAPPING METHODS

Numerous studies have developed fully- and semi-automated processes to extract terraces from DEMs, creating a need for a comparison of methodologies. This work compares results among methods and provides information on geomorphic scenarios in which certain methods may perform well or alternatively be unsuccessful at mapping terraces. The goal of this work is to provide insight for future terrace-mapping studies on which method is best suited for their respective study areas.

2.1 Comparison Framework

Terrace mapping was carried out using a bare-earth DEM with 1-m pixel resolution derived from an airborne lidar survey of the Sheepscot River watershed by the National Center for Airborne Laser Mapping (NCALM) in October 2007. Analyses used the computer programs ArcGIS 10.1, MATLAB 10.1, and Landserf 2.3 (Wood, 2009). All mapping methods were implemented at the four selected study sites (figure 1.10). All areas contain terraces that are easily identifiable in a shaded relief raster derived from the lidar DEM (figure 2.1). Each site was arbitrarily divided into five zones: west bank, east bank, incoming river valley, tributaries, and mid-channel islands. These zones were designated to more specifically assess the accuracy of each method across varying geomorphic regimes (figure 2.1). The performance of each DEM-based mapping method was evaluated based on its similarity to manually delineated terrace areas. Terraces at each study site were outlined through visual interpretation of a hillshade raster by tracing the perimeter of the tread, interpreted using the scarp adjacent to the river channel and the change in slope between the flat terrace tread and confining hillslope. The surface area of all

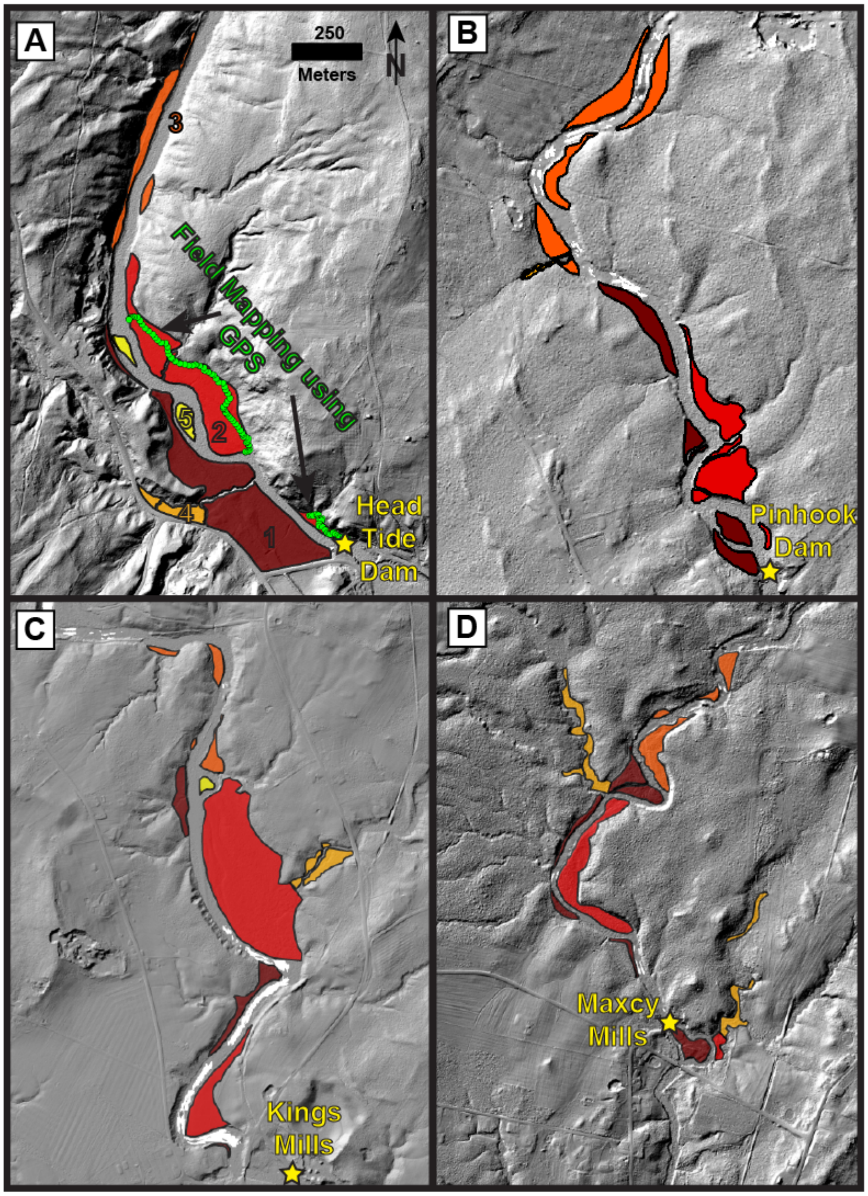

Figure 2.1: Manually delineated terrace extents at Head Tide Dam (A), Pinhook Dam (B), Kings Mills (C) and Maxcy's Mills (D). Manually delineated terrace polygons are divided and colored based upon the zones used for comparison with DEM-based mapping results. Zones include: (1) river right, (2) river left, (3) incoming river channel, (4) tributaries, and (5) mid-channel islands. At Head Tide Dam, GPS field mapping data (green circles) was also collected using a Trimble Juno handheld GPS unit. Base image is a hillshade raster.

mapped terraces was then summed within each designated zone and used as the measured terrace area for comparison with DEM-based results. Within the designated zones at each study site, mapping results obtained from DEM-based methods were first subtracted from corresponding measured areas then divided by the manually defined area to calculate deviation values. Comparison results are discussed in terms of percentages in order to normalize to the varying surface areas across all zones (i.e. 0% is perfect, with negative values corresponding to underestimates and positive values corresponding to overestimates).

The comparison involved two automated and two semi-automated mapping methods, including edge detection using MATLAB, the Rahnis Method documented in Walter et al. (2007), feature classification developed by Wood (1996), and the TerEx terrace mapping toolbox (Stout and Belmont, 2014). The distinction between fully- and semi-automated techniques was that semi-automated procedures required a component of user editing either before or after mapping is completed. Following the practice of Stout and Belmont (2013), a simple rubric was also constructed to assess the performance of each method and their varying degrees of inputs (table 2.1). Scoring criteria included time requirement, degree of landscape interpretation necessary prior to analysis, number of inputs, the amount of manual editing involved, spatial coverage of mapping results, and the overall accuracy compared to manually delineated extents (table 2.1). I defined the range in criterion values (e.g., time requirement, accuracy, etc.) used to assign a score (e.g., 0, 1, 2) based on values encountered while working with all methods, with higher values corresponding to better performance.

2.2 Mapping Methods

2.2.1 Edge Detection in MATLAB

Alongside the three pre-existing methods, I developed a new method of terrace mapping

Time	**1**	**2**	
	> 30 minutes required	< 30 minutes required	
Prior Interpretation of Landscape	**0**	**1**	**2**
	Terraces must be interpreted for successful results	Characteristics of Valley must be determined	No interpretation of landscape required
Number of Input Parameters	**1**	**2**	
	> 5	< 5	
Manual Editing	**0**	**1**	
	Editing required to complete mapping	No editing required	
Spatial Coverage	**0**	**1**	
	Mapped output consists of multiple discrete parcels	Mapped output is continous across tread surface and fully encompasses terrace perimeter	
Accuracy	**0**	**1**	**2**
	Average predicted areas deviate by >±150%	Average predicted areas deviate by >±100%	Average predicted areas deviate by <±100%

Table 2.1: Performance rubric used to assess results of mapping methods and the varying degrees of input requirements necessary to achieve successful delineations.

using edge detection algorithms. This method delineated prominent contrasts within an elevation raster, specifically the border between river terraces and confining valley hillslopes (figure 1.1). Required inputs included an array of elevation data and defined gradient threshold value, which must be exceeded in order to classify a cell as an edge. The MATLAB Image Processing toolbox contains a number of edge detection algorithms that objectively identify cells in a matrix where sharp contrasts exist. To increase the likelihood of these algorithms detecting the border of a terrace, the apparent edge formed by the intersection of the flat terrace surface with the steep valley wall was emphasized. This was achieved by creating a new array that calculated the inverse of the elevation over a region, thus highlighting the low elevation values of terrace surfaces adjacent to the river and deemphasizing the higher elevations of nearby topography (figure 2.2). Next, the Sobel operator (Parker, 1997) edge detection function was used as a 3×3 filter that passed over the inverse elevation raster (figure 2.3). For each cell within a dataset, this filter computed the vertical and horizontal gradient and summed their values together. If the total value exceeded the specified edge threshold, the corresponding cell was deemed an "edge" within the array. Compiling all defined edge cells produced an outline of the terrace landform.

2.2.2 Rahnis Method

Walter et al. (2007) introduced an image-based terrace-mapping method developed by collaborator Michael Rahnis, which has been used in subsequent studies (e.g. Walter and Merritts, 2008; Merritts et al., 2011) to map fill terraces and quantify fill sediment volume throughout the mid-Atlantic Piedmont region of the United States. The Rahnis method is based on the spatial relationship between surrounding topography and the elevation of terrace treads. Initiation of this method required only a DEM as an input; however the presence of terraces within a region must be visually recognized prior to implementation. The user must place points atop interpreted treads and interpolate a surface characterizing its topography (figure 2.4 A-B). A dense array of points was placed atop the terraces at HTD and PHK, and a three-dimensional surface was interpolated using the inverse distance weighting (IDW) interpolation method (figure 2.4 A-B). This surface characterizes the terrace surface elevations over the same extent as the original DEM (figure 2.4 B). An elevation buffer was added to this surface to account for slight variations in topography atop the terrace surface and to avoid producing holes in the mapped terrace extent, with a buffer of 1 m used for both regions.

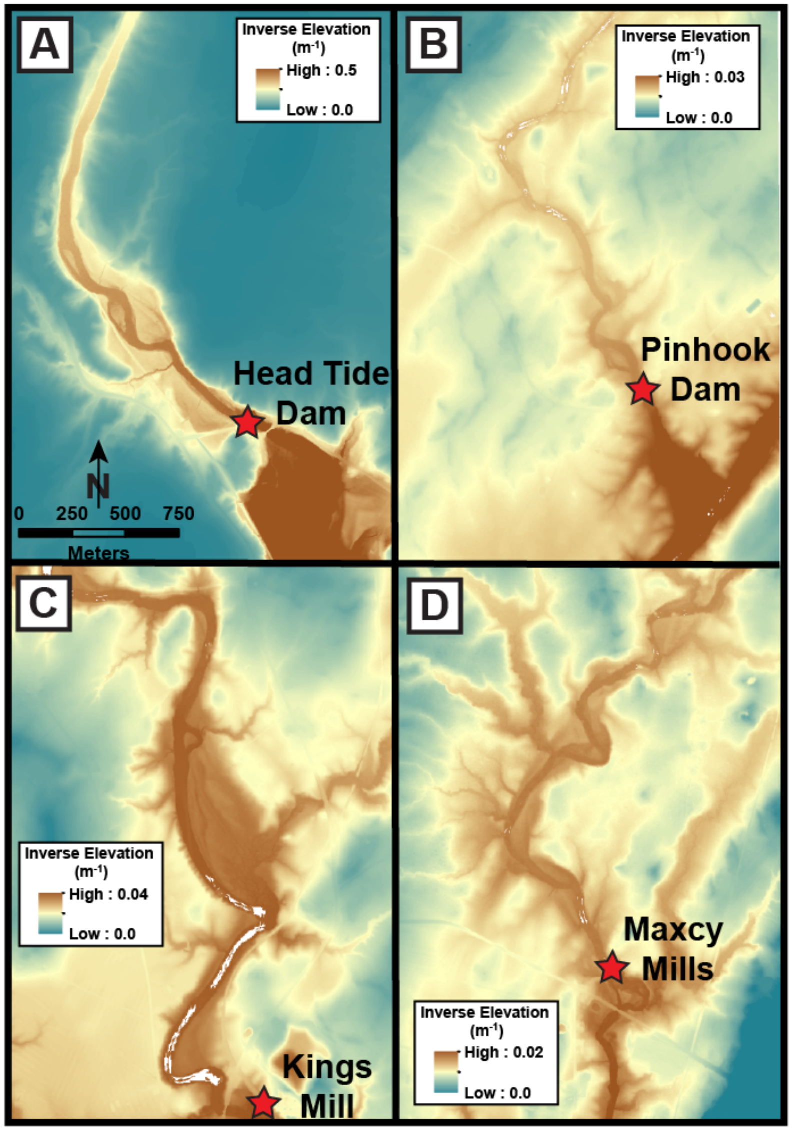

Figure 2.2: Inverse elevation rasters calculated for regions containing (A) Head Tide Dam, (B) Pinhook Dam, (C) Kings Mills, and (D) Maxcy's Mills. These rasters serve as the input to the MATLAB edge detection terrace mapping method.

Elevation values of the original DEM greater than this interpolated surface plus the specified buffer height were then deleted, and the remaining discrete remnants of the original DEM thereby define the terrace extent (figure 2.4 C).

Vertical Filter

-1	0	1
-2	0	2
-1	0	1

Horizontal Filter

1	2	1
0	0	0
-1	-2	-1

Figure 2.3: Vertical and horizontal filters used to identify sharp gradients in the Sobel edge detection method.

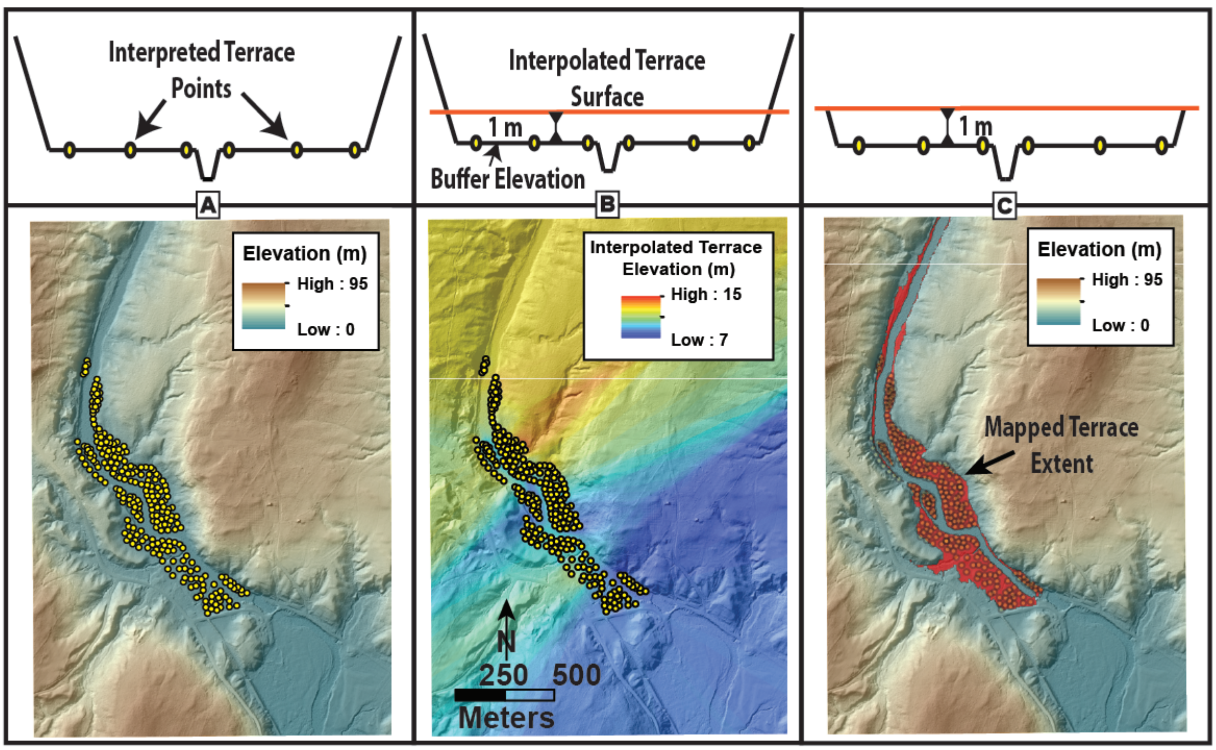

Figure 2.4: Process for implementing the Rahnis Method (Walter et al., 2007) of terrace mapping illustrated in cross-section (top row) and plan form (bottom row). Points are initially placed atop interpreted terrace surfaces (A), and an interpolated surface is constructed based on the elevation of points plus an additional elevation buffer (B). Lastly, original elevation values greater than the interpolated surface are deleted, outlining the extent of terrace landforms (C). All planform images have a DEM base image overlain by a transparent hillshade raster.

2.2.3 Feature Classification

Geomorphometry, or the science of quantitative land-surface analysis, is an offshoot of geomorphology that works with DEMs and seeks to define landscapes using mathematical, statistical, and image-processing techniques. Wood (1996) developed algorithms that classify individual cells of DEM rasters into one of six categories: peaks, troughs, channels, ridges, passes, and planar surfaces (figure 2.5). Classifications are based on elevation, slope, and aspect. These parameters can all be represented by the plan and profile curvature of a landscape, which is calculated as the second derivative of elevation in two orthogonal directions (i.e. x and y; table 2.2). This algorithm is available as the feature classification tool within the open-source GIS software LandSerf (Wood, 2009) or can be coded into any GIS platform. I chose to use the built-in toolbox in LandSerf for classification in this study.

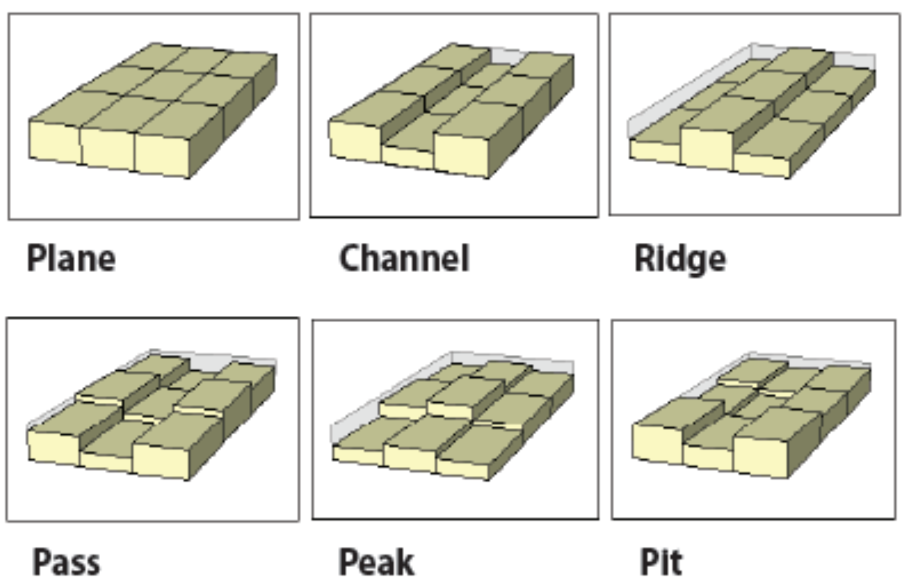

Figure 2.5: Possible surface classifications with corresponding shape developed by Wood (1996).

Although not explicitly designed for mapping terraces, inherent in the feature classification method is the ability to map flat regions that could potentially correspond to terrace landforms. This method requires a DEM as input and user-defined limits of slope tolerance (degrees) and curvature tolerance (dimensionless) for the planar classifications, that were set to 1.0° and 0.1 respectively and are used to account for planar regions that deviate slightly from horizontal. Obtaining terrace extent maps using the feature classification algorithm began by classifying all surfaces in a raster and then extracting all "planar" regions (figure 2.6 A-B).

Feature Name	Derivative Expression	Description
Peak	$\frac{\partial^2 z}{\partial x^2} > 0, \frac{\partial^2 z}{\partial y^2} > 0$	Point that lies on a local convexity in all directions (all neighbors lower).
Ridge	$\frac{\partial^2 z}{\partial x^2} > 0, \frac{\partial^2 z}{\partial y^2} = 0$	Point that lies on a local convexity that is orthogonal to a line with no convexity/concavity.
Pass	$\frac{\partial^2 z}{\partial x^2} > 0, \frac{\partial^2 z}{\partial y^2} < 0$	Point that lies on a local convexity that is orthogonal to a local concavity.
Plane	$\frac{\partial^2 z}{\partial x^2} = 0, \frac{\partial^2 z}{\partial y^2} = 0$	Points that do not lie on any surface concavity or convexity.
Channel	$\frac{\partial^2 z}{\partial x^2} < 0, \frac{\partial^2 z}{\partial y^2} = 0$	Point that lies in a local concavity that is orthogonal to a line with no concavity/convexity.
Pit	$\frac{\partial^2 z}{\partial x^2} < 0, \frac{\partial^2 z}{\partial y^2} < 0$	Point that lies in a local concavity in all directions (all neighbors higher).

Table 2.2: Surface classification criteria based on spatial data developed by Wood, (1996). The values X, Y, and Z are three orthogonal components corresponding to direction of maximum curvature, minimum curvature, and elevation, respectively.

Only surfaces that fell within a specified range were extracted from classified rasters (figure 2.6 B). A small buffer (1 m) was added to the upper elevation bound to account for natural topographic variation within the defined extent, similar to the buffer used in the Rahnis Method (figure 2.6 B). The lower elevation bound was defined as 0.25 m above the water surface elevation, which was necessary to remove all planar classifications that correspond to the water surface in the channel (figure 2.6 B). The remaining remnants of the planar classifications corresponded to fluvial terraces, thereby mapping out their spatial extent (figure 2.6 C).

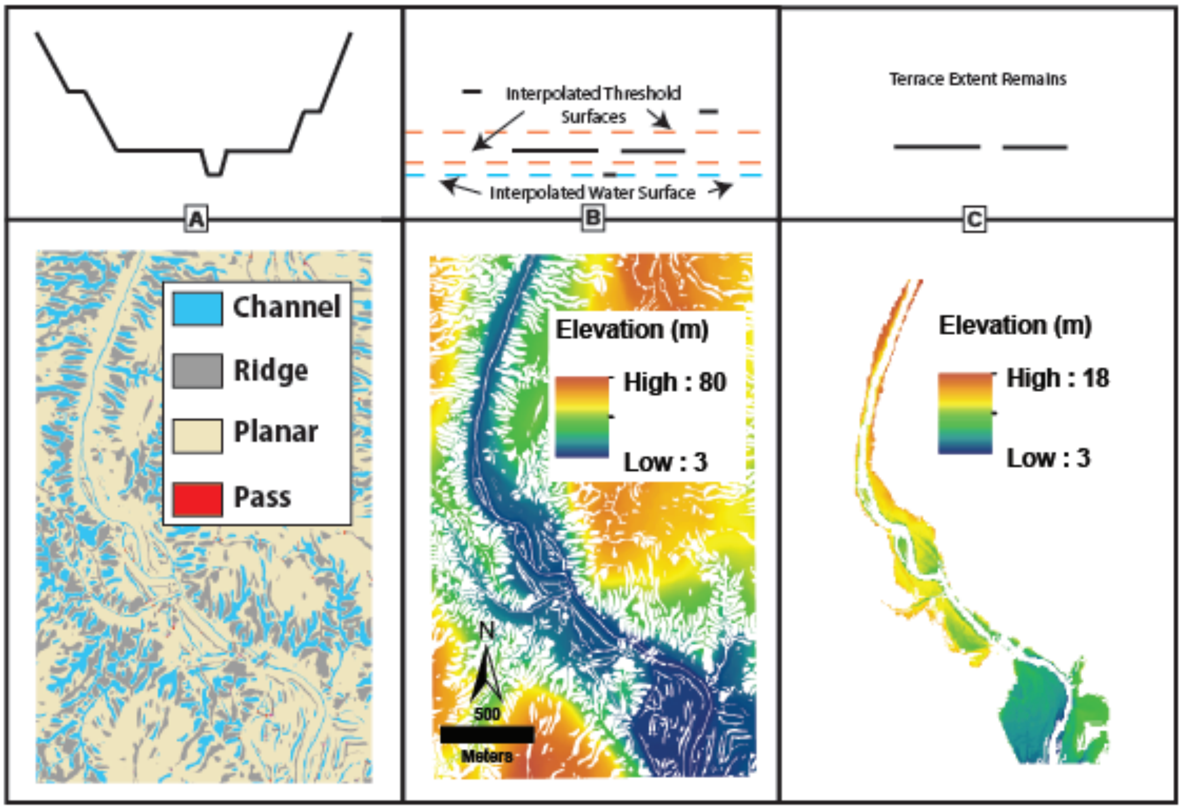

Figure 2.6: The feature classification method for mapping terraces illustrated in cross-section (top row) and plan form (bottom row). Beginning with a classified raster (A), all planar cells are extracted (B). Using an interpolated water surface, threshold elevations are defined, and outlying surfaces are removed from the analysis (C).

2.2.4 TerEx Toolbox

The TerEx Toolbox of Stout and Belmont (2013) was designed specifically as a semi-automated technique for mapping terraces and floodplains on lidar DEMs by identifying areas with small changes in local relief (i.e. flat surfaces adjacent to river channels). Input datasets for the toolbox include a DEM and digitized river channel, along with a number of adjustable parameters including focal window size, change in elevation threshold, maximum valley width, and minimum area threshold. The TerEx toolbox uses an iterative approach to delineate features that incorporates user edits mid-way through the process to increase accuracy of the final product. Flat surfaces were initially found by passing a user-defined focal window (e.g., a 50 m^2 moving window) over the DEM and locating areas with local relief that is less than the user-defined threshold (e.g., 0.5 m). To be considered a terrace or floodplain, identified flat surfaces must exceed the minimum area threshold and partially lie within the designated valley width. At this point, the user is able to employ any prior or intuitive knowledge and edit the polygons generated to remove unwanted features such as roads and bridges or perhaps separate multiple discrete terraces that were mapped as a single unit. Once all edits are complete, terrace areas are re-calculated along with the average elevation of each terrace landform.

For each study area, over 20 trials were run to determine the optimum parameters for best mapping results with final configurations summarized in Table 2.3. For each site, mapping results will be presented in two ways. The first, which will be referred to as the TerEx Raw Output, relied solely on the adjustment of initial parameters to map terraces.

Study Site	Δ Elevation (m)	Focal Window (m^2)	Min. Area (m^2)	Max. Valley Width (m)
HTD	0.5	5	1	300
KM	0.5	7	0.1	150
PHK	0.2	3	0.01	100
MM	0.5	3	1	100

Table 2.3: Final configurations used for terrace mapping with the TerEx toolbox (Stout and Belmont, 2014) for each selected study site.

The second, referred to as TerEx Edited, incorporated user edits into the final mapped extent as the original developers intended. I limited the amount of time allotted for editing at each study site to 30 minutes to insure fairness when comparing results.

2.2.5 Field Mapping of Terraces

Detailed field mapping of river terraces at the Head Tide Dam location was conducted to provide ground truthing for DEM based mapping comparisons at this study site (figure 2.1). The outside perimeter of the terrace surfaces was surveyed using a Trimble Juno handheld GPS unit (horizontal accuracy of ±3 m) to log the location and elevation of the tread extent. While walking the terrace border, progress was recorded by automatically placing waypoints at regularly spaced time intervals of 10 seconds. Field mapping was limited to the perimeter along the east bank of the river due to the presence of a historic railroad bed to the west of the river channel that makes the terrace perimeter less distinct (figure 2.1).

2.3 Mapping Results

2.3.1 Edge Detection in MATLAB

Results obtained from edge detection algorithms are fast and objective; however, the final output is a series of disconnected lines that highlight the strongest contrast in the image rather than a continuous border that encompasses the terrace landform (figure 2.7). This method highlighted the terminal extent of terraces but failed to consistently delineate the banks of the incising river channel at all study sites (figure 2.7). An additional issue was a number of false-positive returns where the method mapped features outside the river valley. False returns are visible at all study sites, but are especially evident within the lower-gradient landscapes of the

Pinhook Dam (PHK) and Maxcy Mills (MM) study sites. This method lacks any control enforced by proximity to the active channel, and is thus more susceptible to identifying non-terrace landforms outside of a river valley.

The edge-detection method is computationally efficient, but the absence of a continuous border becomes problematic when attempting to calculate information about the terrace such as area or thickness. Due to the excessive time required, I refrained from manually connecting all lines to construct a continuous border and excluded the edge-detection results from the quantitative comparison between all methods.

2.3.2 Rahnis Method

The Rahnis Method (Walter et al., 2007) maps terraces based on their elevation above a channel, so elevation exerts the strongest control on results derived using this method (figures 2.8A - 2.11A). The terraces at HTD and KM formed in relatively confined valleys > 5 m below the surrounding terrain. The topographic contrast along terrace perimeters at these sites provides an elevation barrier that can be exploited to delineate a well-defined border (figures 2.8A and 2.9A). Deviations at HTD between manual and computational derived areas using this method ranged from -72% to 9%, with an average deviation of -15% (figure 2.12A). The largest deviation (-72%) occurred within the tributary on the west bank of the river. Deviations were greater at the KM site, ranging from -25% to 240% with an average of 78%. The larger deviation values result from localized low-lying areas in the surrounding landscape that have been modified for agricultural and residential purposes. Deviation values could be potentially improved by increasing the elevation buffer (1 m used for this analysis), but this could cause detrimental effects within other areas.

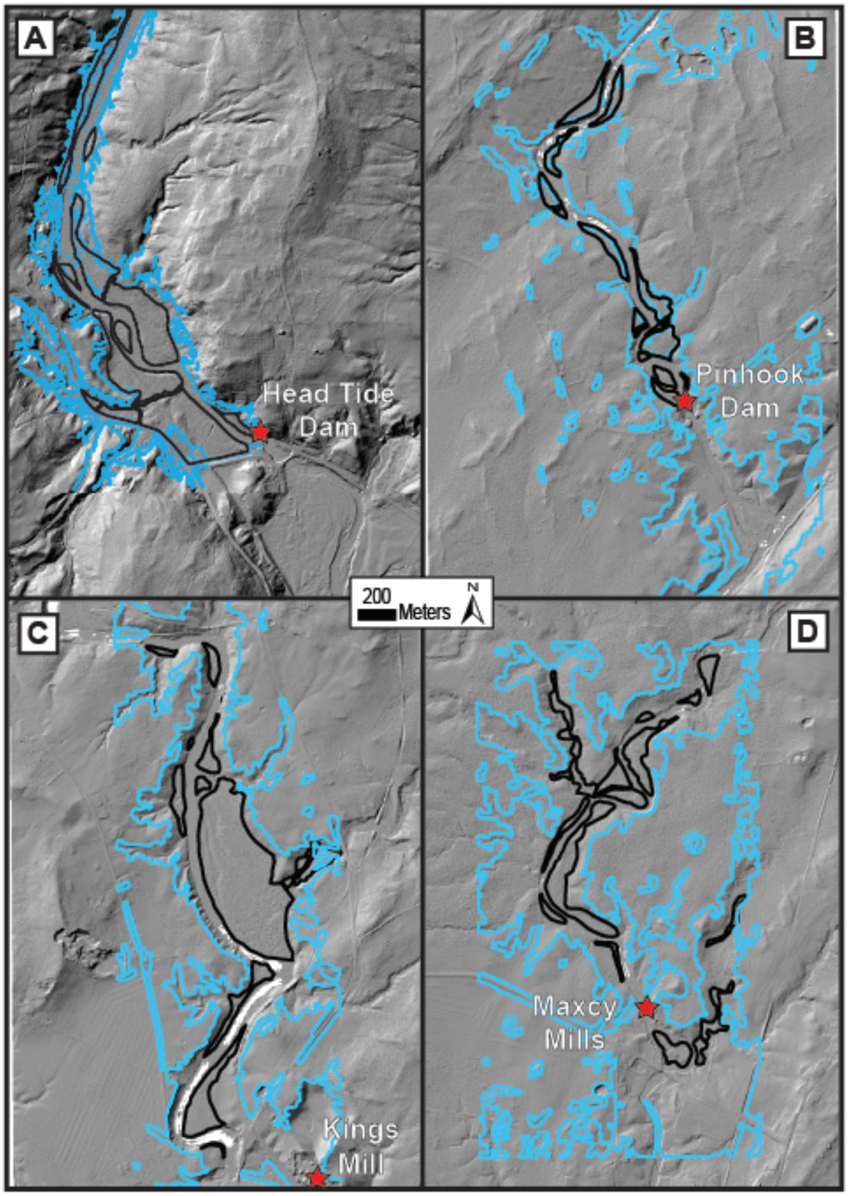

Figure 2.7: Terrace mapping results obtained using edge detection in MATLAB for (A) Head Tide Dam, (B) Pinhook Dam, (C) Kings Mills, and (D) Maxcy's Mills. Results produced discrete lines highlighting the sharpest gradients in the landscape rather than a fully enclosed polygon encompassing terraces, making it difficult to extract further information about terraces. Calculated extents are overlain by the manual delineation of terraces (black lines), each separated based on comparison zones in figure 2.1. Base image is a hillshade raster.

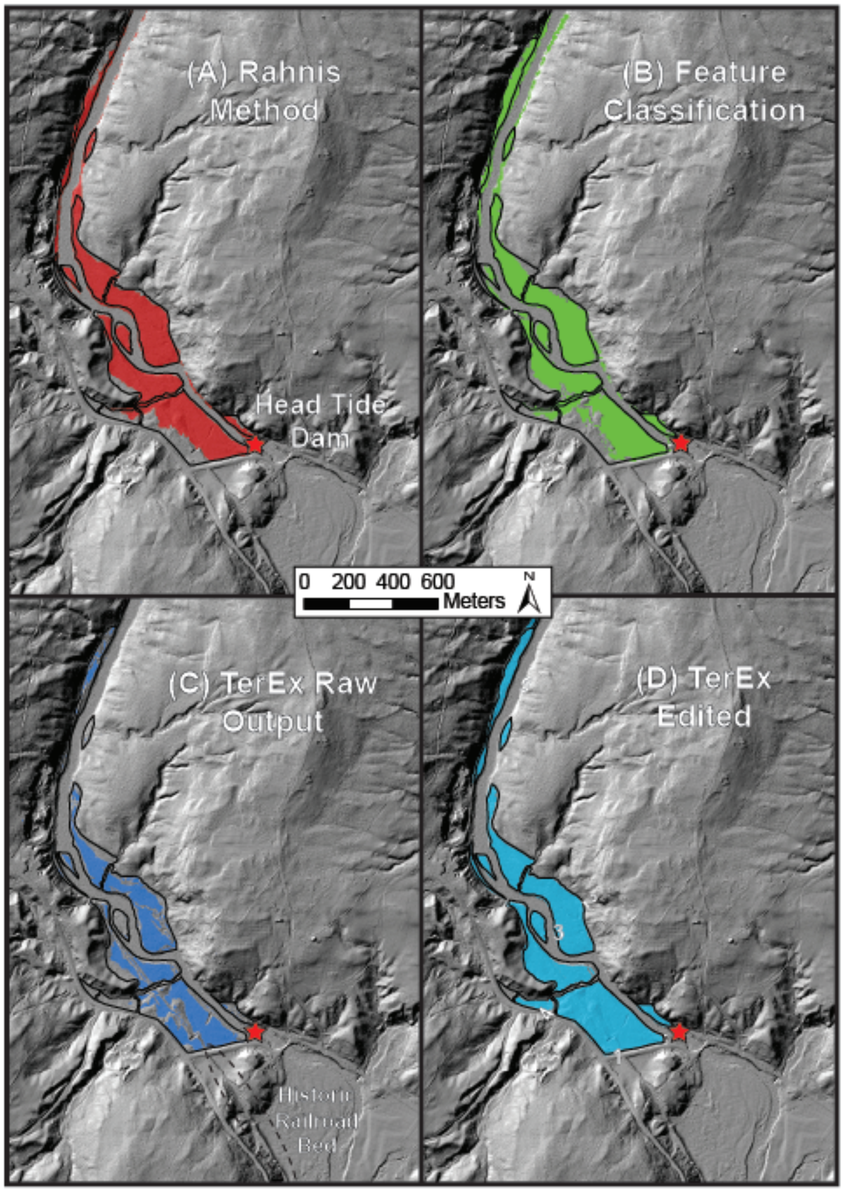

Figure 2.8: Terrace mapping results over the Head Tide Dam study site obtained from: (A) the Rahnis Method (Walter et al., 2007), (B) the Feature Classification Method (Wood, 1996), (C) the raw output from the TerEx terrace mapping toolbox (Stout and Belmont, 2013), and (D) the edited TerEx output. Calculated extents are overlain by the manual delineation of terraces (black lines), each corresponding to an individual comparison zone in figure 2.1 (zones numbered in panel D). Base image is a hillshade raster.

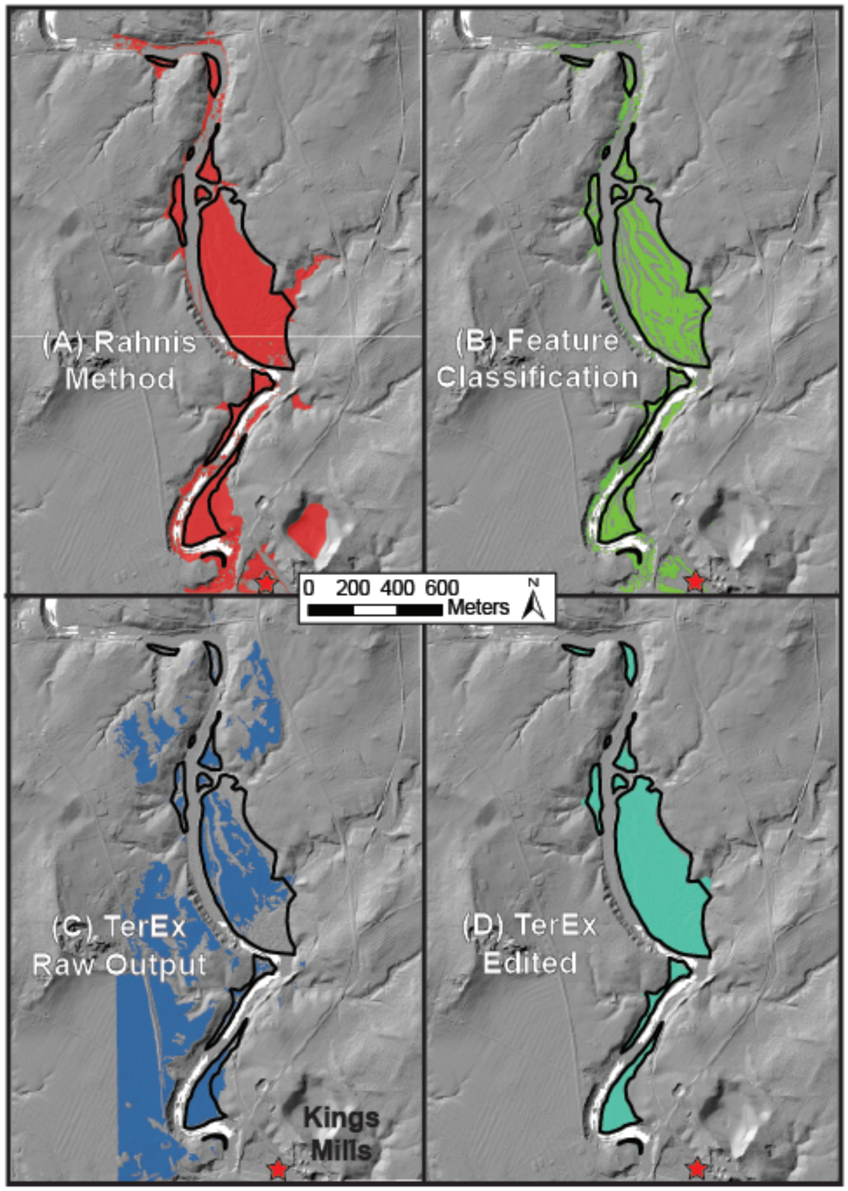

Figure 2.9: Terrace mapping results over the Kings Mills study site obtained from: (A) the Rahnis Method (Walter et al., 2007), (B) the Feature Classification Method (Wood, 1996), (C) the raw output from the TerEx terrace mapping toolbox (Stout and Belmont, 2013), and (D) the edited TerEx output. Calculated extents are overlain by the manual delineation of terraces (black lines), each corresponding to an individual comparison zone in figure 2.1. Base image is a hillshade raster.

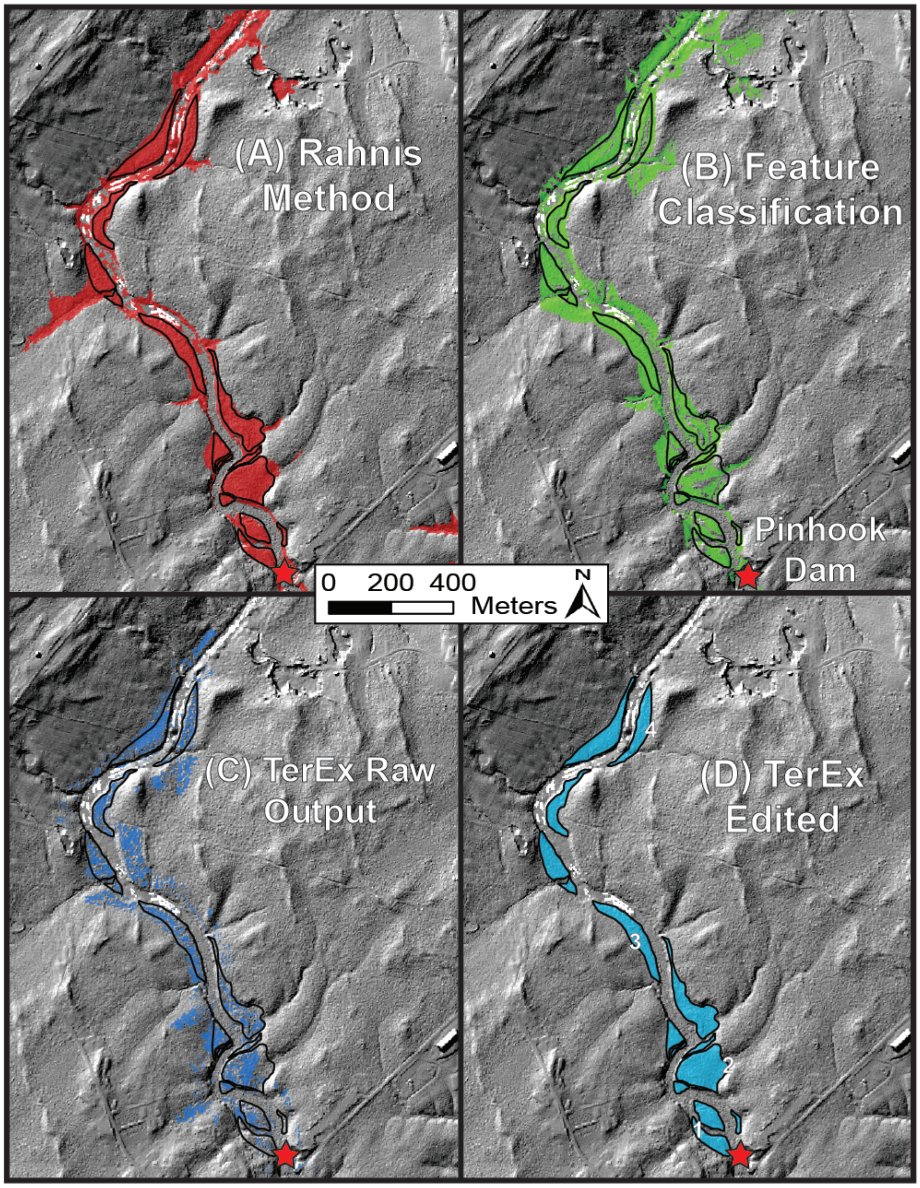

Figure 2.10: Terrace mapping results over the Pinhook Dam study site obtained from: (A) the Rahnis Method (Walter et al., 2007), (B) the Feature Classification Method (Wood, 1996), (C) the raw output from the TerEx terrace mapping toolbox (Stout and Belmont, 2013), and (D) the edited TerEx output. Calculated extents are overlain by the manual delineation of terraces (black lines), each corresponding to an individual comparison zone in figure 2.1 (zones numbered in panel D). Base image is a hillshade raster.

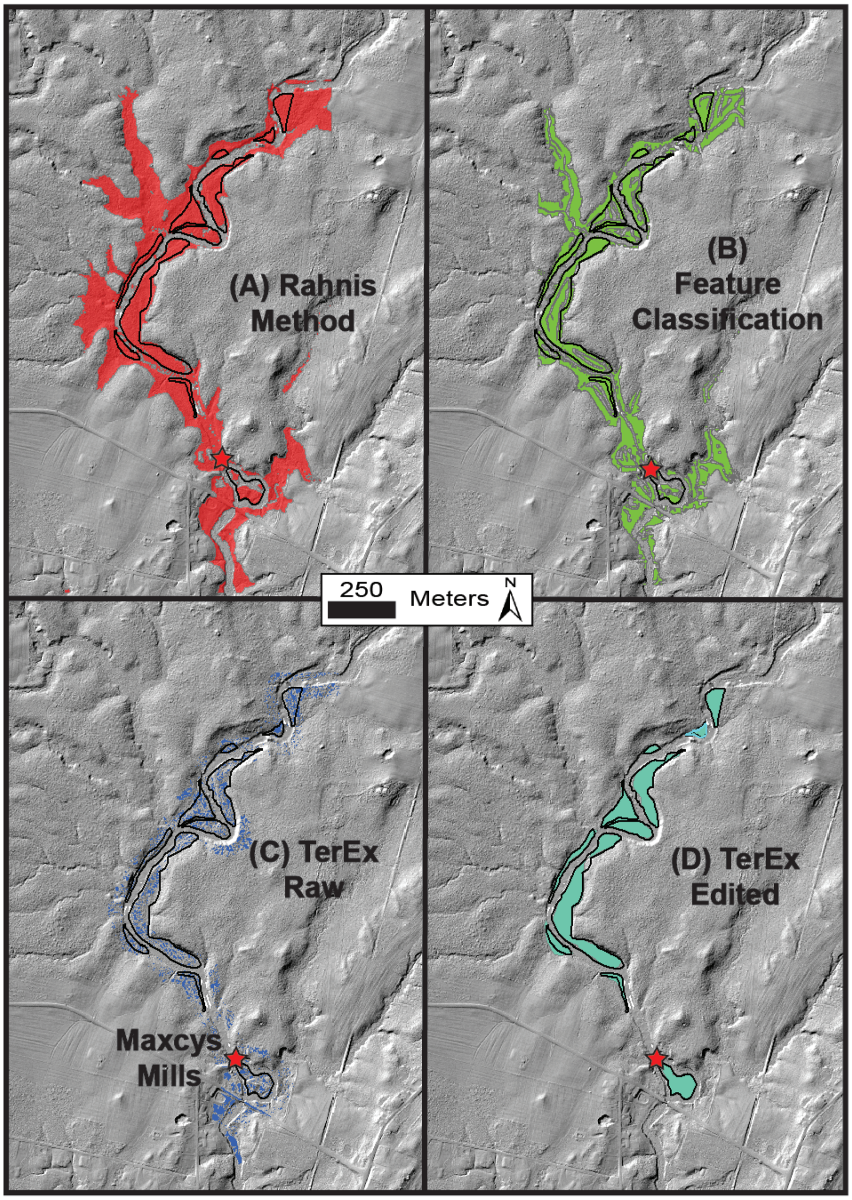

Figure 2.11: Terrace mapping results over the Maxcy's Mills study site obtained from: (A) the Rahnis Method (Walter et al., 2007), (B) the Feature Classification Method (Wood, 1996), (C) the raw output from the TerEx terrace mapping toolbox (Stout and Belmont, 2013), and (D) the edited TerEx output. Calculated extents are overlain by the manual delineation of terraces (black lines), each corresponding to an individual comparison zone in figure 2.1. Base image is a hillshade raster.

The PHK and MM study sites along the West Branch are located in a subtler river valley (local relief across study areas of 43.4 m and 15.9 m, respectively) relative to the surrounding landscape, resulting in a less clear border between terrace and valley hillslope (figure 2.10A and 2.11A). This method overestimated areas across all zones at both study sites, with deviations spanning from 130% to 330% at MM (figure 2.12) and 57% to 850% at PHK. The anomalously high deviation of 850% at PHK occurred within the tributary along the west bank of the river (figure 2.10A). On average, this method overestimated terrace area across all zones by 257% at PHK and 229% at MM. The small lower elevation terraces present at PHK (figure 1.10) were successfully mapped using this method (figure 2.10A), but were incorporated into the adjacent higher elevation terraces rather than mapped as discrete landforms. The interpolated terrace surface with additional buffer value defines an elevation ceiling, below which all identified terraces are mapped as one cohesive unit. If two separate terrace surfaces adhere to this criteria than both will be mapped as a singular terrace using this method. User-edits would be required to identify the break between terraces and manually split these surfaces.

The majority of mapping error at all study sites resulted from the presence of tributaries or a gradual transition from terrace treads to the surrounding terrain. In these situations, the selected elevation buffer and associated contour defining the terrace perimeter extended above terraces and encompassed excess surrounding area. Increasing the value of the elevation buffer can reduce this error, but doing so may adversely affect other zones.

2.3.3 Feature Classification

Feature classification (Wood, 1996) was the only fully automated mapping procedure to adequately map the perimeter of terraces in DEMs (figures 2.8B - 2.11B, 2.12). Calculated areas from this method generally fell between areas derived using semi-automated methods except for at the KM study site, where this method was second only to the manually edited TerEx toolbox (Stout and Belmont, 2014) results (figures 2.9 and 2.12). Total predicted areas were overestimated at all study sites except for HTD (80% of terraces mapped; figures 2.8B and 2.12), with the largest overestimate of 123% occurring at PHK (figure 2.10B and 2.12).

This method performed exceptionally well at the HTD and KM study sites along the main stem of the Sheepscot River, with total predicted areas falling within ±21% of manual delineated areas. Results for individual zones at HTD were on average 18% less than manually defined areas, with minimum and maximum deviations of -1% and -68%. The minimum deviation corresponded to the terraces along the east bank of the river (zone 2: figure 2.8B) while the maximum deviation occurred within the tributary on the west bank of the river (zone 4; figure 2.8B). Average predicted areas at KM were 46% greater relative to manually defined areas, with deviations ranging from -5% to 152%. The maximum deviation occurred along the west bank of the river (zone 1; figure 2.9B) where this method falsely identified slump deposits along the base of the cut bank scarp in the southern region of this study site.

Results at the two West Branch study sites overestimated terrace areas across all zones, with deviation values ranging from 36% to 235% at PHK and 70% to 120% at MM. Average deviations from manual defined extents were 106% at PHK and 94% at MM (figure 2.12). Maximum deviations at MM occurred west of the river, where the subtle transition into a flat adjacent landscape resulted in an excessive amount of flat area being mapped as a terrace. The largest deviations at PHK were recorded in the incoming river channel (zone 3; figure 2.10B), where this method erroneously mapped all land parcels adjacent to the river channel as terraces due to the lack of an apparent perimeter distinguishing terraces from the adjacent flat landscape.

2.3.4 TerEx Toolbox

The multiple trials conducted using the TerEx toolbox (Stout and Belmont, 2014) illustrate the improvements achievable by incorporating user edits into mapping endeavors. Initial outputs from the TerEx method (Stout and Belmont, 2014) showed average deviations at individual sites of 15-200% (figure 2.12). At all study sites, deviation values were reduced to < 20% by editing initial results in a time span of no more than 30 minutes (figures 2.8D-2.11D, 2.12). Unlike previous methods, the raw TerEx toolbox (Stout and Belmont, 2014) output reported similar deviation results for both sites on the main stem and West Branch of the Sheepscot River, and actually produced the best results for the PHK and MM study sites (figures 2.10C and 2.11C). Unedited areas were less than manually defined areas for all zones at MM and all but the incoming river channel (zone 3) at PHK. Raw output maps had average deviations of -28% at PHK and -55% at MM with ranges from -94% to 24% and -96% to -34%, respectively. The largest deviations at PHK and MM occurred within the tributary zones. Underestimates of terrace area within tributaries are a consequence of the channel proximity parameter built into the toolbox and were ubiquitous at all study sites, with deviations ranging from -54% to -96% (figures 2.8C – 2.11C).

Unedited areas at HTD deviated from manual delineations -54% on average, with values ranging from -32% to -84%. The largest deviations at HTD corresponded to the mid-channel islands. Finally, unedited areas at KM ranged from -57% to 1,152% with an average deviation of 193%. The anomalously high deviation recorded at KM occurred west of the river and is a product of the surrounding land use. An approximately 2.5×10^5 m^2 agricultural field is less than 50 m from the river channel and was included in mapping results from the raw output of this tool, resulting in deviations of greater than 1000% for zone 2 at KM. The error was easily remedied, but required user-edits to delete the incorrect mapping results.

2.4 Discussion and Conclusions

This study sought to test prominent DEM-based mapping methods, all of which have been previously validated in their initial applications (Wood, 1996; Walter et al., 2007; Stout and Belmont, 2014). My intention was to more rigorously test these methods by applying them on the post-glacial terrain of the Sheepscot River watershed (figure 1.2) in order to simultaneously assess their performance capabilities in an objective manner and determine which was the most applicable for broad-scale use.

2.4.1 Site-Specific Challenges

Obtaining accurate mapping results requires defining characteristics that are unique to terraces. The uniqueness is vital to ensure that only features corresponding to terraces are extracted. Flat terrace treads generally contrast with adjacent steep valley walls, providing a characteristic that can be exploited by mapping methods. The terraces along the main stem of the Sheepscot River at HTD and KM predominantly display such morphology (figure 2.8 and 2.9). This contributed to the success of all methods at these sites (figure 2.12) because a clear distinction exists between the terraces and the surrounding landscape. Study sites along the West Branch, particularly Maxcy's Mills, have a lower-gradient landscape with less contrast between terrace treads and valley hillslopes (figures 2.10 and 2.11). These characteristics decreased the effectiveness of mapping methods that sought to identify flat regions within an area (feature

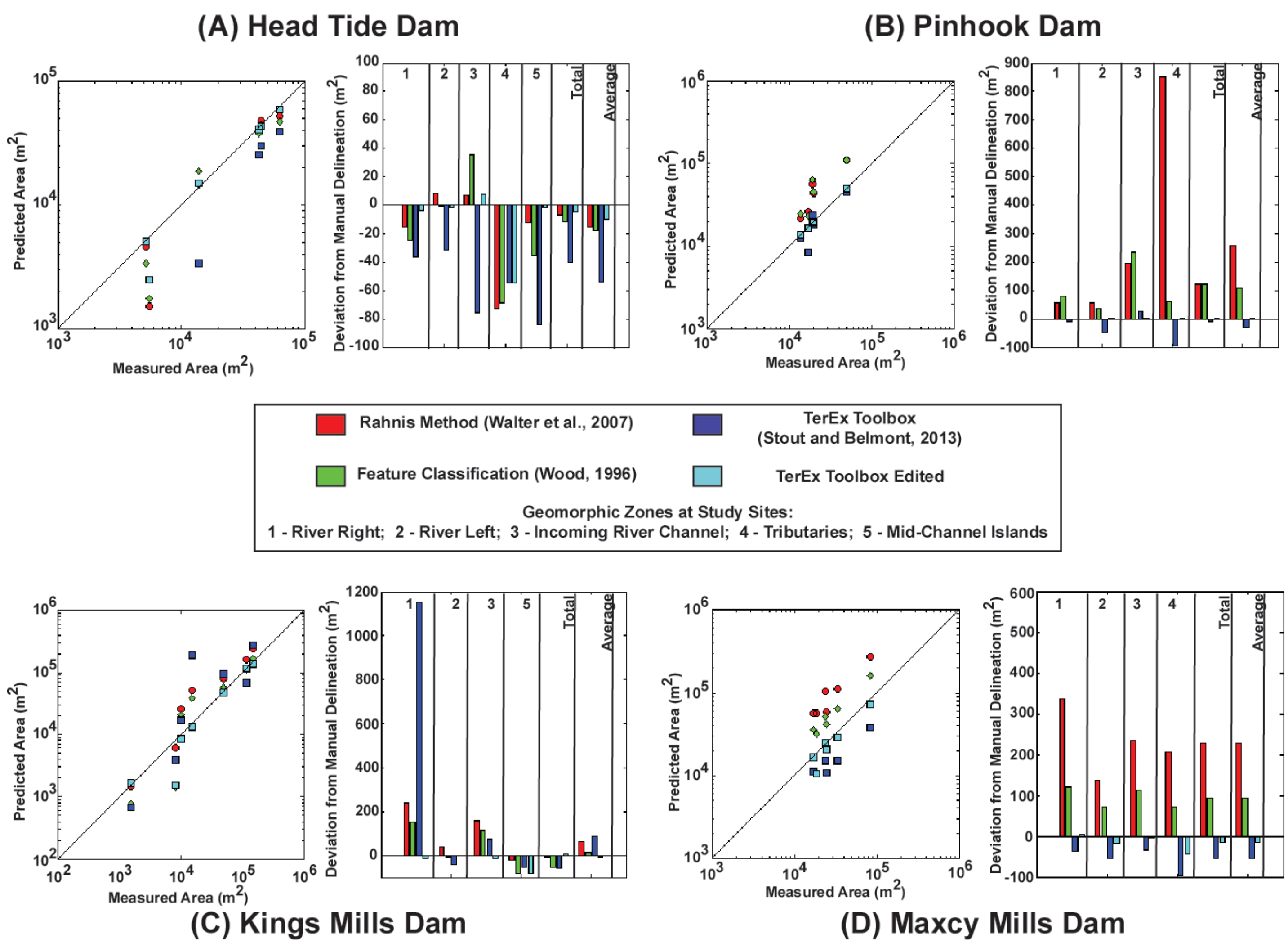

Figure 2.12: Quantitative comparison between terrace mapping methods. Bivariate plots show the predicted areas calculated by each method at all sites versus manual measurement of terrace area in lidar DEMs. Bar plots show deviation values for each method within individual comparison zones delineated in figure 2.1.

classification, Wood, 1996; TerEx Toolbox, Stout and Belmont, 2014) or define an apparent elevation break between terraces and valley hillslopes (edge detection in MATLAB; Rahnis Method, Walter et al. 2007). This more challenging geomorphic setting resulted in less accurate delineations reported by the majority of methods (figure 2.12). The unedited output from the TerEx Toolbox (Stout and Belmont, 2014) was the only method to have equal or better results at the West Branch sites compared to those on the main stem, with total and average deviation values of -7% and -14% at PHK and -55% and -55% at MM, respectively (figure 2.12). The accurate results at study sites on the West Branch achieved by the TerEx Toolbox (Stout and Belmont, 2014) illustrate the importance of methods including parameters accounting for proximity to channel (i.e. maximum valley width). Without this control, methods often return false-positive results for flat regions outside the river valley (figure 2.9).

A distinguishing feature at the PHK study area was the presence of a small (~600 m^2) terrace tread at a lower elevation (~1.5 m) than the surrounding terraces (figure 1.10). This setting is analogous to river valleys containing multiple flights of terraces, and facilitated the testing of each method's ability to map adjacent terraces as discrete features. Both the edge detection and the Rahnis Method (Walter et al., 2007), which map terraces based on their elevations relative to the surrounding landscape, were unsuccessful at appropriately identifying this tread. The Edge Detection method simply failed to detect the perimeter (figure 2.7), while the Rahnis Method (Walter et al., 2007) recognized the smaller tread but incorporated it with the larger, higher elevation terrace tread (figure 2.9B). An iterative approach using the Rahnis Method (Walter et al., 2007) with varying elevation buffers would be required to map the lower elevation tread as a discrete unit. Conversely, the mapping methods that sought to identify flat surfaces (feature classification, Wood, 1996; TerEx Toolbox, Stout and Belmont, 2014) successfully mapped this lower terrace as a single, separate feature (figure 2.9B-C). Therefore, results from PHK suggest that any study working with multiple terraces should utilize a method that extracts terraces based on their defining characteristics, rather than their relation to the surrounding topography.

Lastly, the KM study site contains the greatest variability in land use surrounding the river channel. The majority of methods produced accurate results in this scenario (figure 2.12C), but the initial map outputs from the TerEx toolbox (Stout and Belmont, 2014) erroneously included a large area of agricultural land in its mapped terrace output because it displayed a similar morphology as terraces and was within an acceptable distance to the river channel. The agricultural field sits ~10 m above the river channel, but the TerEx toolbox (Stout and Belmont, 2014) only restricts terrace extents laterally rather than the vertical controls incorporated in the Rahnis Method (Walter et al., 2007) or feature classification method (Wood, 1996). Editing the initial output resolved this issue though, and the edited TerEx (Stout and Belmont, 2014) extents are void of any false inclusions at KM (figure 2.9D).

2.4.2 Comparison of Methods and Recommendations

The edge detection terrace mapping method was developed to compare existing mapping options against a fully automated and objective process. Edge detection algorithms in MATLAB are capable of mapping terrace extents to a first-order approximation (figure 2.7), but it is difficult to extract further information using these defined perimeters. The benefits of this algorithm are that it is rapid and can be completely automated. Studies seeking only to identify the terminal extent of terraces in planform would benefit from this method.

The Rahnis method (Walter et al., 2007) was designed to map single terraces bounded by steep valley walls. This method excelled at mapping the terraces along the main stem (figures 2.8A-2.9A and 2.12), where the landscape displays this scenario. Deviations from this ideal landscape though, such as the overall lower-relief topography along the West Branch or the presence of a small, lower elevation terrace at PHK resulted in larger errors and overestimates of terrace surface area (figures 2.10A-2.11A and 2.12). The primary control exerted by elevation on terrace delineation (figure 2.4) can lead to the erroneous inclusion of land parcels that are not terraces but fall below the elevation threshold designated for mapping.

The performance evaluation (table 2.1) of the Rahnis method (Walter et al., 2007) shows that its major drawback is its reliance on input from the user, specifically the manual placement of points atop interpreted terrace surfaces (Figure 2.4, Table 2.4). The time required to complete this task is negligible for single study sites but would be time consuming and may be undesirable for some studies mapping terraces over entire watersheds. Prior landscape interpretation could also introduce error if points are incorrectly placed upon non-terrace surfaces, which would alter the interpolated terrace surface and possibly misrepresent the spatial relationship between terrace treads and the surrounding landscape. After the placement of points atop terrace surfaces, remaining steps can easily be programmed into an ArcGIS toolbox and greatly reduce the processing time required. The inclusion of the user-placed points with this method requires fewer input datasets and parameters, requiring only the terrace point data and user-defined elevation buffer to complete mapping (Table 2.4). A notable benefit of this method is that it is less susceptible to gaps in defined areal extent caused by deviations from a flat surface, producing outputs that completely cover terrace treads (Table 2.4). I recommend this method for studies seeking to map single terrace treads contained within a steep-sided valley.

Performance Parameters		Rahnis Method					Feature Classification					TerEx Toolbox					TerEx (Edited)				
		HTD	KM	PHK	MM	AVG	HTD	KM	PHK	MM	AVG	HTD	KM	PHK	MM	AVG	HTD	KM	PHK	MM	AVG
Performance Parameters	Time	2	2	2	2	2	1	1	1	1	1	2	2	2	2	2	1	1	1	1	1
	Prior Interpretation of Landscape	0	0	0	0	0	2	2	2	2	2	1	1	1	1	1	1	1	1	1	1
	Number of Input Parameters	2	2	2	2	2	2	2	2	2	2	1	1	1	1	1	1	1	1	1	1
	Manual Editing	1	1	1	1	1	1	1	1	1	1	1	1	1	1	1	0	0	0	0	0
	Spatial Coverage	1	1	1	1	1	0	0	0	0	0	0	0	0	0	0	1	1	1	1	1
	Accuracy	1	1	0	0	0.5	1	2	0	0	0.75	2	0	2	2	1.5	2	2	2	2	2
	Final Score	**7**	**7**	**6**	**6**	**6.5**	**7**	**8**	**6**	**6**	**6.75**	**7**	**5**	**7**	**7**	**6.5**	**6**	**6**	**6**	**6**	**6**

Table 2.4: Final scores for individual methods after mapping terraces at the four study sites. All methods were implemented at Head Tide Dam (HTD), Kings Mills (KM), Pinhook Dam (PHK), and Maxcy Mills (MM). Criteria for point allocation is defined in table 2.1.

The feature classification method (Wood, 1996) also uses elevation as a parameter to extract terraces, but this threshold is only applied to flat areas previously identified by the method (figure 2.6). This decreases the likelihood of including low elevation areas that do not correspond to terraces. Because this method operates by identifying planar regions within a DEM, it struggles when terrace treads deviate from horizontal. Mapping results commonly have a discontinuous texture (e.g., figure 2.9B) that does not fully encompass tread surfaces and underestimates terrace area (Table 2.4). This occurred at all study sites and appears to correspond predominantly to high-flow channels on the terrace surface.

This feature classification method (Wood, 1996) is also objective and automated, requiring only that the user define slope and curvature thresholds and the maximum elevation at which terraces are present. The lack of manual input throughout the mapping process does produce larger errors relative to semi-automated procedures (figure 2.12), but in turn decreases operational time (Table 2.4). Implementing this method requires only a DEM and user-specified maximum terrace elevation, but the need to classify all landforms within the DEM prior to extracting terraces increases the operational time (Table 2.4). The greatest advantage of using the feature classification method (Wood, 1996) is that it does not require any interpretation of a landscape prior to analysis in order to map and construct a continuous border around terrace surfaces (Table 2.4). The efficiency of this method allows results over vast spatial extents (i.e. watershed scale) to be achieved in a relatively short amount of time. I recommend this method to researchers willing to accept slightly less accurate results (figure 2.12) in exchange for a more automated process (Table 2.4)

Overall the raw results from the TerEx toolbox (Stout and Belmont, 2014) perform well relative to the other methods tested (figure 2.12; Table 2.4), and can be easily edited to increase the accuracy of terrace coverage maps (figures 2.8D-2.11D, 2.12). The major drawbacks for this method include the spatial coverage of original outputs and the time required to edit these extents (Table 2.4). Raw terrace delineations are comprised of a number of small polygons atop a single terrace tread rather than one large aggregated unit (figures 2.8-2.11C). This occurred when areas on the terrace tread violated the identification criteria, and appeared to predominantly correspond to high-flow channels on tread surfaces. This toolbox includes the greatest number of adjustable parameters to alter results and correct for incomplete surface coverage (Table 2.4), but I found the effect of changing parameters did not always produce intuitive results. For example, decreasing the minimum area threshold did not always increase the number of returns through the inclusion of smaller parcels of terrace, even with all other variables held constant. Correcting areal coverage and producing highly accurate delineations (<10% deviation) is achievable, but requires nearly the same amount of time as manual delineation (Table 2.4). If edits are necessary, the time required to edit raw outputs is beneficial though because the toolbox automatically derives information about the terrace such as area, height above the channel, and closest river segment.

The TerEx toolbox (Stout and Belmont, 2014) is an excellent introduction to mapping geomorphic features such as terraces in lidar DEMs. The toolbox is readily available, well documented, and the initial implementation is intuitive and familiar to someone with experience using GIS. This method does require a bit of trial-and-error to optimize the input parameters for best results, but this was easily achieved within a time span of 30 minutes at the study sites used in this analysis. Additionally, the edits midway through the mapping process insures that terraces are sufficiently mapped prior to completion. This method can easily be implemented over large channel lengths (10^1-10^3 km), but accurate results may be difficult to obtain in a single trial if the characteristics of the river valley or terraces are variable spatially. This method would also be applicable for studies focusing on a select number of study sites or for those that require terrace areas to reside within a high accuracy threshold.

Performance evaluations for each method tested in this comparison make it difficult to identify a clear best methodology, with average performance scores of: 6.5 for the Rahnis method (Walter et al., 2007), 6.75 for the feature classification method (Wood, 1996), 6.5 for the TerEx toolbox (Stout and Belmont, 2014) raw output, and 6 for the edited TerEx output (Table 2.4). Each method exhibited desirable qualities sought after in DEM-based mapping and should be applied based on requirements of studies and personal preferences. A recurring theme amongst all methods was the optimization of parameters to map all terraces throughout a study area. My efforts focused on mapping terraces within main valley bottoms, and each method was tailored for this task. While my selection of parameter values successfully mapped valley bottom terraces, they often resulted in study sites reporting the highest deviations within tributaries, as the methods were not optimized for these conditions. Before selecting a mapping method, it is important to first define desired expectations and inferences being made based on results. After determining such factors, this research will aid in the selection of an appropriate DEM-based terrace mapping method.

3 Estimating Reservoir Sediment Terrace Extent and Volume in the Sheepscot River Watershed

Along dam-influenced streams within the mid-Atlantic Piedmont region of the U.S., Walter and Merritts (2008) highlighted the lingering effects of dams on stream morphology. Contrary to the classic interpretation that channels are bounded by self-formed floodplains, they instead found that the streams had incised into 1-5 m of slackwater sedimentation behind 17th- to 19th- century milldams, and that channel-adjacent landforms observed were actually fill terraces. Walter and Merritts (2008) refer to these deposits as reservoir-sediment terraces and discussed their potential to negatively affect stream restoration efforts if they fail to be properly identified.

Strouse (2013) extrapolated the work of Walter and Merritts (2008) beyond the unglaciated mid-Atlantic Piedmont region of the U.S. and identified reservoir-sediment terraces upstream of two breached dams within the post-glacial landscape of the Sheepscot River Watershed, Maine. The terraces were classified as milldam-induced Anthropocene deposits based on the analysis of sediment characteristics, observations of historical artifacts within strata units, hydraulic modeling to determine the upstream extent of the millpond, and radiocarbon dating. Results from Strouse (2013) illustrate the pervasiveness of colonial-era damming and its alteration to the natural landscape beyond unglaciated regions in post-glaciated environments. These results also demonstrate the potential existence of reservoir sediment terraces at the remaining dams within the Sheepscot River watershed.

Of the 44 dams that existed throughout the Sheepscot River watershed, 19 were on either the main stem or the West Branch (figure 1.2). At locations where dams have either been removed or breached, fill terraces may store reservoir sediment. This chapter builds upon the results of Strouse (2013) and assesses the magnitude of sediment storage upstream of all of the breached and historic milldams along the Sheepscot River and West Branch using DEM-based methods.

Also discussed are the additional requirements necessary to validate DEM results. The goal of this chapter is to illustrate the potential use of DEM-based procedures to quickly derive first-order estimates on fluvial properties that are important to geomorphologists and stream restoration efforts.

3.1 Methodology

3.1.1 Study Sites used for Ground Truthing

Thickness estimates obtained from three DEM-based models were ground-truthed using terrace stratigraphy measured upstream of the Head Tide Dam (HTD) on the main stem and Pinhook Dam (PHK) on the West Branch of the Sheepscot River (figure 1.2). Elementary statistics were employed to quantitatively compare in situ measurements with values derived using the three models tested. Head Tide Dam is currently still in place within the channel but was breached in the 1950s to allow fish passage, while PHK is completely absent from the landscape. Both locations contain terraces that are easily identifiable within DEMs, but only the terraces at HTD have a confirmed reservoir sediment composition (Strouse, 2013). The origin of terraces visible at PHK will be discussed further in subsequent sections of this chapter.

3.1.2 Field Measurements

3.1.2.1 Stratigraphic Analysis

Fourteen locations at HTD and three locations at PHK were selected from atop terrace treads or along scarps within the river channel to provide point measurements of reservoir-sediment thickness (figure 3.1). Soil pits were manually dug to a depth of 0.4-0.88 m at all locations at PHK and at two locations at HTD, with the remaining locations at HTD consisting of cut bank exposures ranging from 1-2.46 m in height. All soil pit depths were limited by encountering cobbles, which hindered digging to greater depths. Cut bank exposures extended to a depth that was coincident or within 0.5 m of the elevation of the river water surface. When observable within a soil pit or cut bank exposure, the base of reservoir sedimentation was interpreted based on a change in sediment characteristics, described in section 3.2.1.1, and the depth at which the transition occurred was noted. Some subsurface contact relationships were difficult to constrain because the paleo-river valley surface is buried beneath reservoir sediment and the river has not incised deep enough to expose this contact (figure 3.2).

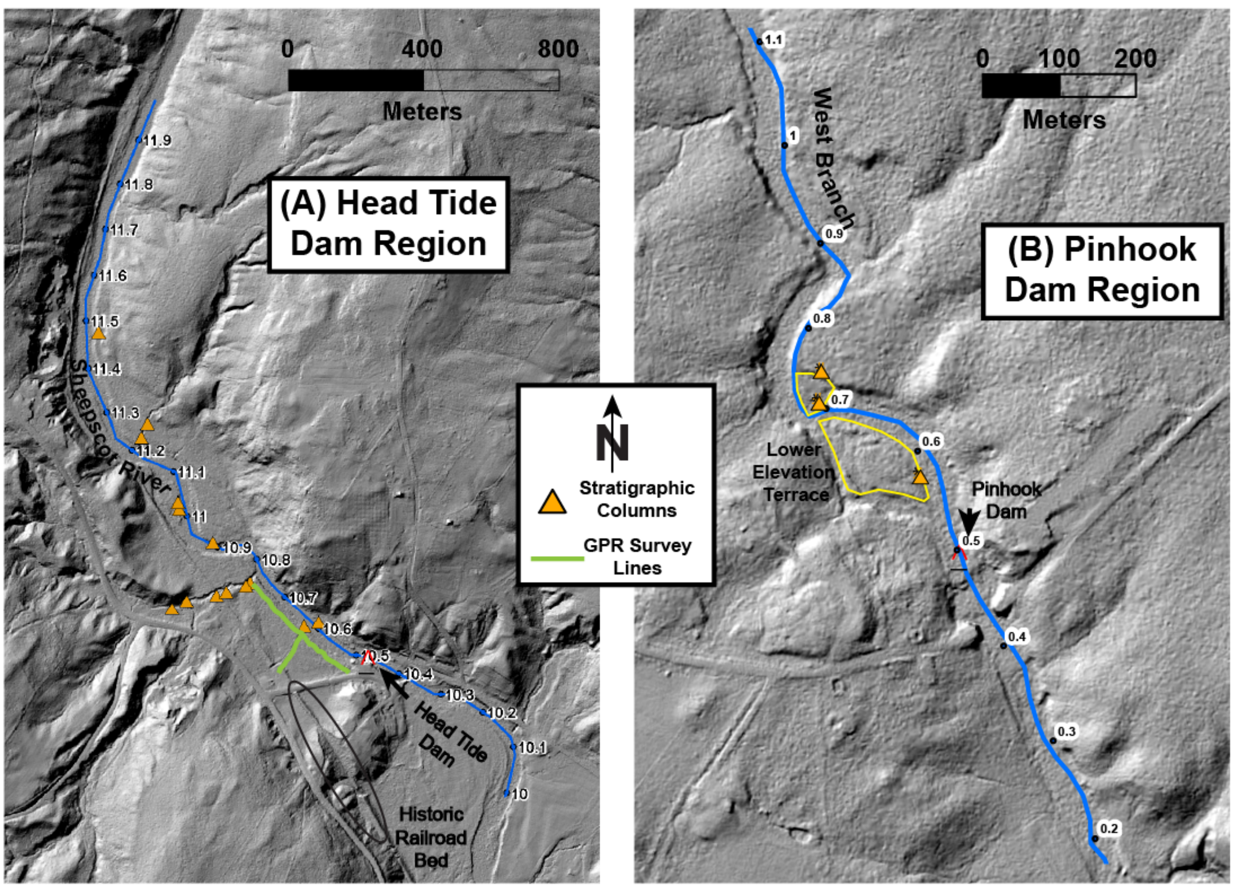

Figure 3.1: Location of field-collected data at (A) Head Tide Dam and (B) Pinhook Dam study areas. Red stars denote the dams, with orange triangles representing measured stratigraphic locations and green lines corresponding to GPR survey lines. Blue line represents centerline of river channel with numbers corresponding to river kilometers. Base images are a hillshade raster constructed from a 1 m pixel size lidar DEM.

Soil pit and cut bank exposure locations were recorded using a Trimble Juno handheld GPS unit (horizontal accuracy of ±3 m and vertical accuracy ±10 m) and uploaded into ArcGIS 10.1 (figure 3.1). Due to the poor vertical resolution, elevations for soil pits were assigned using coincident pixels on a 1-m DEM, while elevations of cut bank exposures were determined by identifying the elevation of the terrace scarp in a DEM within a 3 m radius of the GPS recorded location (figure 3.1). Terrace scarps often slope downwards adjacent to the channel, so cut bank exposure elevations were assigned by analyzing cross-section profiles of terrace treads and identifying the lowest elevation along the tread surface (figure 3.3).

Figure 3.2: Measured soil pit within river right tributary at Head Tide Dam showing contact with the water table and concealment of subsurface contact.

Interpolating between stratigraphic sections and soil pits provided insight on how the basal contact of reservoir sedimentation varies over the study areas. All field-measured thicknesses were compared with coincident terrace thicknesses estimates above DEM datum surfaces (described below) to test which surface is most applicable for use throughout this landscape. Fence diagrams along the main channel at PHK and HTD as well as for the tributary along river right at HTD were constructed to view measured strata in context with the terrace tread and lidar imaged water surface. Fence diagrams also illustrate the reservoir sediment basal contact geometry in channel parallel and perpendicular directions.

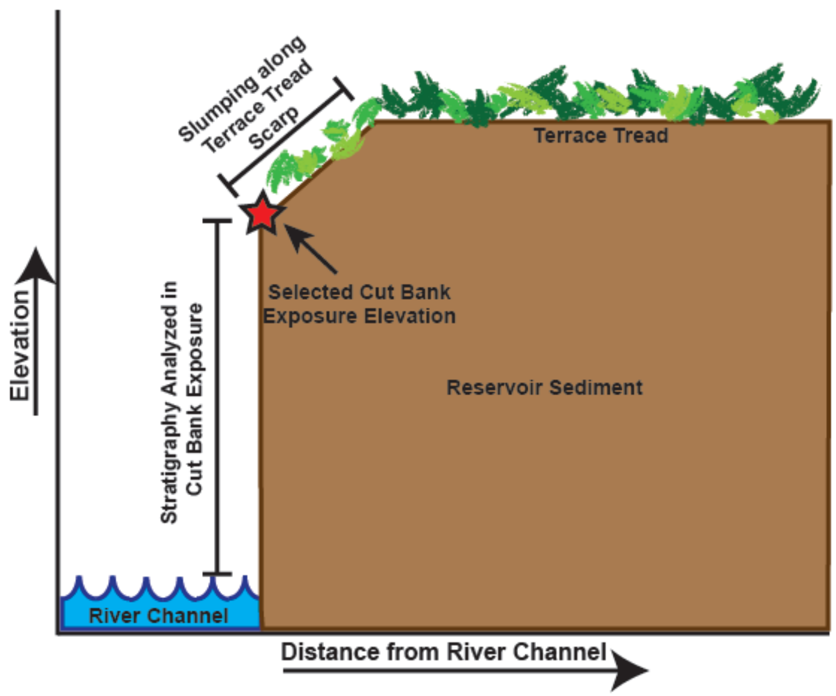

Figure 3.3: Schematic of terrace tread cross-sectional profile illustrating the slumping nature of the tread surface along the incising river channel scarp. Cut bank exposures were measured from the lowest elevation of the terrace tread, and their elevations were manually assigned by identifying this elevation in cross-section profiles (red star) constructed in DEMs.

3.1.2.2 Ground Penetrating Radar

Ground penetrating radar is capable of imaging prominent stratigraphic units in fluvial environments (Clement et al., 2006) and was therefore used to extrapolate beyond the point measurements of soil pits and bank exposures by collecting data along selected survey lines at HTD (figure 3.1). This was done with a Geophysical Survey Systems, Inc. (GSSI) unit with 270 MHz antenna. Highly reflective layers seen in GPR profiles were qualitatively associated with prominent layers observed in stratigraphic columns and soil pits, such as the water table and the contact with the Presumpscot Formation glaciomarine clay. Two GPR survey lines were surveyed along river right (defined in the downstream direction) in between the tributary located at river km 10.8 and HTD (figure 3.1). The first ran parallel to the river, while the second ran perpendicular to the river channel at river km ~ 10.6. The perpendicular profile originated at the river scarp and ran ~ 90 m across the terrace, where it terminated within meters of the transition from the flat terrace tread to the confining valley hillslope (figure 3.1). Two GPR configurations were used for data collection, one with a maximum two-way travel time (twtt) range of 300 ns and the other with a maximum twtt of 200 ns. A total of four GPR profiles were collected for each configuration, two per line in alternating directions. Only the 200 ns range profiles were considered for this analysis because they sufficiently imaged all of the subsurface data of interest.

The GSSI RADAN 7 software was used to vertically adjust collected data along survey lines and remove air space between the antenna and the ground surface. Depth estimates to defined layers were obtained using the cut bank exposure measured on river right at river kilometer 10.62 (figure 3.1; Appendix 1). This column is located at the intersection of the two GPR surveys facilitating the groundtruthing of both GPR scans. Results gave a dielectric constant of 14.96 (unitless), which agrees with expected values for semi-saturated soils and sediments (Keary et al., 2002). This value was applied to the both survey lines in order to estimate depth to reflective layers.

3.1.3 DEM-Based Calculations

3.1.3.1 Terrace Longitudinal Profiles

Terraces were initially mapped along longitudinal profiles to determine where to implement a more complex planform mapping method. Longitudinal terrace maps were constructed using the algorithm developed by Finnegan and Balco (2013), which was designed to automatically identify flat regions adjacent to river channels using DEMs (figure 3.4). Surfaces can correspond to either terraces or floodplains and require user interpretation to distinguish between the two based on surface elevation and stage data for a river during flood events. This method operates under the expectation that the relatively flat surface of terraces will produce peaks in a cross-sectional histogram of elevation, essentially highlighting the location and elevation where terraces are present (figure 3.4). To implement this method, the main stem and the West Branch of the Sheepscot River were divided into 2 km segments, with cross-sectional profiles measured orthogonal to the river every 10 m for a total of 200 cross-sections per segment. Cross-sections were limited to include only elevation values less than 10 m above the channel elevation, although this limit can be changed to optimize results for differing environments. The surface elevation values corresponding to each cross-section were binned into multiple elevation groups spaced every 20 cm (figure 3.4). When terraces were present alongside the river channel, the corresponding elevation bin would show a peak (figure 3.4). The distribution of elevation values for each cross-section is aggregated along the longitudinal profile of the river, and a plot is made in which each cell (x and y values corresponding to horizontal distance and elevation, respectively) is colored according to the number of data points contained within its limits.

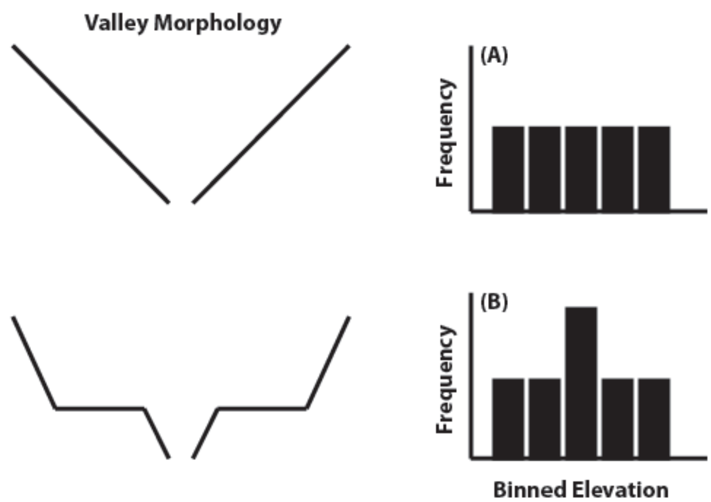

Figure 3.4: Elevation frequency distribution for valley cross-sections with no terraces (A) and with terraces (B). Image taken from Finnegan and Balco (2013).

3.1.3.2 Terrace Delineation

A time-efficient and objective method to extract terraces from DEMs was desired for mapping endeavors throughout the Sheepscot River watershed. The results from the previous chapter (figure 2.12, table 2.3) indicate that the feature classification method (Wood, 1996) would therefore be the most suitable method. The objectiveness and automated procedure of this method make it ideal for mapping terraces spanning watershed scales. The main stem and West Branch were divided into 2 km segments, and each DEM subset was classified into one of six morphologic units (figure 2.5) based on the criteria defined by Wood (1996; table 2.2) using the GIS program LandSerf 2.3 (Wood, 2009). Classified rasters were then imported into ArcGIS 10.1 and all planar regions were extracted (figure 2.6A-B). Planar classifications were further reduced to encompass only terraces by defining minimum and maximum elevation thresholds for each river segment (figure 2.6B). The highest elevation of interpreted terraces within individual elevation frequency plots (Finnegan and Balco (2013) method) was used as a reference to select the maximum elevation thresholds for each 2 km segment, above which all planar surface classifications were deleted (figure 2.6C). This value varied for each segment but never exceeded a value of 4 m above the water surface elevation. All planar surfaces below this threshold except the water surface were included in analysis; therefore floodplains are included in mapping results. The minimum elevation threshold was set to 0.25 m above the river water surface and used to remove planar classifications corresponding to the water surface within the river channel from mapping results. Final results for each 2 km segment were aggregated to produce a single file that contains all mapped terraces along the main stem and West Branch.

At HTD and PHK, terraces were also mapped using the TerEx terrace mapping toolbox (Stout and Belmont, 2013; section 2.2.4). This was done to compare the thickness calculation method used by the TerEx toolbox, which requires the TerEx delineated extent as input in order to calculate thickness and subsequent volume.

3.1.4 Thickness and Volume Calculations

3.1.4.1 Selecting a Base of Reservoir Sedimentation in DEMs

Potential reservoir-sediment terraces were identified within DEMs based on their proximity to a historical dam site; however, once identified it is impossible to constrain subsurface contact information solely using a DEM (i.e., the reservoir sediment basal contact with an underlying paleo-valley deposit in figure 1.3). In order to derive thickness and volume estimates, an appropriate datum for reservoir sedimentation must be defined. After dams have been breached or removed, the incising river will presumably erode back to the original base level prior to the construction of the dam. Therefore, the elevation of the water surface within the river channel imaged by the lidar surveys should be a plausible proxy for the elevation of the base of reservoir sedimentation. This hypothesis was tested using stratigraphic data collected at the HTD and PHK study sites. Stratigraphic data were collected between July 24-29, 2013, over which time the USGS gauging station on the Sheepscot River recorded a mean discharge of 3.75 m^3/sec and mean stage of 0.79 m (figure 3.5) at the North Whitefield gauging station (figure 1.2). The same gauging station recorded an average discharge of 15.83 m^3/sec and stage of 1.17 m during the lidar data collection flights (November 7-8, 2007; figure 3.5). This difference in these values suggests 38 cm as a minimum error bound between the base of reservoir sediment and the lidar-imaged water surface.

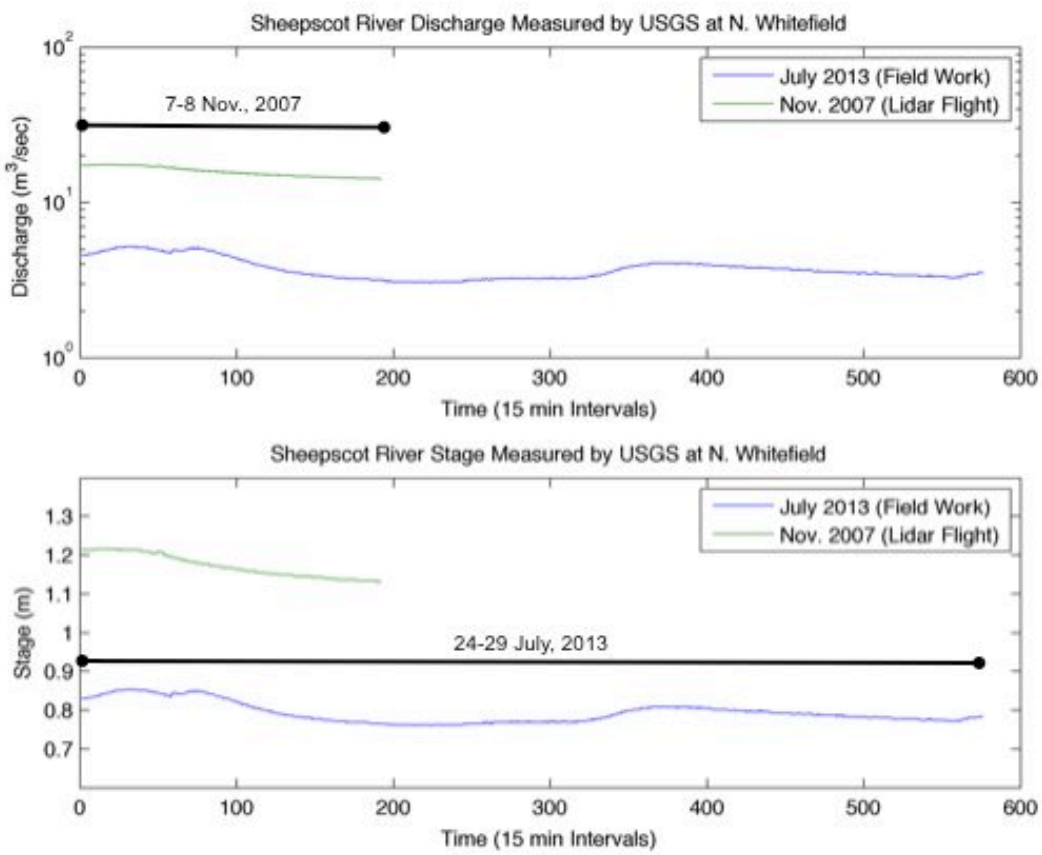

Figure 3.5: Comparison of river discharge and stage data recorded by the U.S. Geologic Survey's gauging station in North Whitefield, ME, during field work carried out in July, 2013, and during the time of the airborne lidar survey (November, 2007).

The river water surface elevation (RWSE) points were the most suitable choice for a datum surface in DEMs because they are continuously imaged along the channel in the dam-influenced region. Interpolating RWSE points using Inverse Distance Weighting (IDW) functions created a projected water surface covering the extent of the original DEM. This projected river water surface (PRWS) is flat orthogonal to the river channel and serves as one of the datum surfaces tested in this analysis (figure 3.6). The second datum surface was constructed by interpolating RWSE points with elevation points along the perimeter of the delineated terrace extents, generating a non-horizontal surface orthogonal to the river channel (figure 3.6). This surface is referred to as the valley-bottom interpolated surface (VBIS).

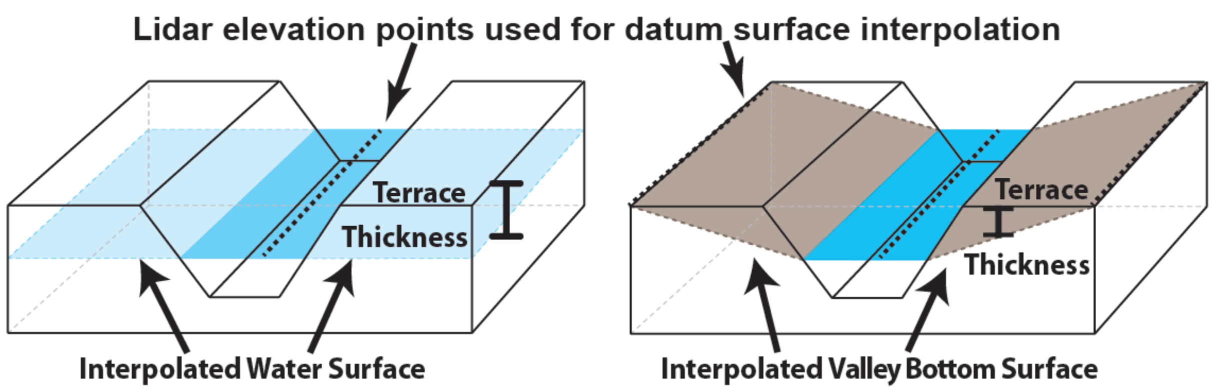

Figure 3.6: Comparison of datum surfaces constructed using (left) only river water surface elevation points (PRWS) and (right) a combination of elevations from the river water surface and outside the defined perimeter of the terrace extent (VBIS).

3.1.4.2 DEM Derived Thickness and Volume

After defining potential bases of fill sediment in the DEM (figure 3.6), thickness and volume estimates were computed for the sediment stored in terraces. Thickness values were calculated above both the PRWS and VBIS within the bounds defined by the feature classification method (Wood, 1996). For both of these surfaces, a simple subtraction of the datum elevation from the coincident terrace surface elevation gives the thickness of the terrace at each pixel. Finally, thickness values above each datum surface were multiplied by their pixel area and summed to provide an estimate of volume.

Although not designed explicitly to calculate the thickness of terrace sediment, the TerEx toolbox can still provide estimates of minimum thickness. This application is only appropriate though under the assumption that the water surface is at an elevation less than or equal to the boundary between fill sediment and underlying lithology, otherwise thickness will be overestimated. To begin, the river channel is segmented into a user specified number of reaches, and all previously mapped terraces and floodplains are associated with the closest segment of river (figure 3.7). Average elevations are calculated for both the river segment and associated terrace landform. Lastly, subtracting the river segment mean elevation from the terrace mean elevation yields the mean thickness of fill sediment applied to the entirety of that particular mapped unit. This method is very similar to the PRWS datum, but relies only on single mean values rather than coincident values on the terrace surface and underlying datum surface.

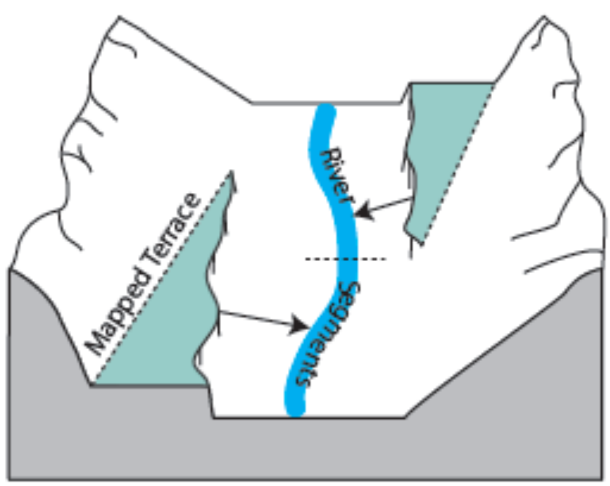

Figure 3.7: Schematic illustrating the TerEx (Stout and Belmont, 2013) thickness calculations. After the river is dissected in equal lengths, all mapped terrace are assigned to the closest river segment, and the average height of the river segment is subtracted from the average height of the mapped terrace.

3.1.5 Statistical Comparisons

The accuracy of sediment thickness calculations above datum surfaces (figures 3.6-3.7) was assessed by comparing results with in situ thickness measurements. Differences (ΔH) between estimated and measured thicknesses of reservoir-sediment at all stratigraphic sections (cut bank exposures and soil pits) were calculated using equation 1:

$$\Delta H = H_{estimate} - H_{stratigraphic} \qquad (1)$$

where $H_{estimate}$ and $H_{stratigraphic}$ correspond to thickness values obtained from DEM analysis and those measured in either soil pits or cut bank exposures, respectively. To compare all values obtained from each method, the standard deviation (σ) for each population was calculated using equation 2:

$$\sigma = \sqrt{\frac{1}{N}\Sigma(H_{estimate} - H_{stratigraphic})^2} \qquad (2)$$

where N is the total number of locations where stratigraphy was measured. Lastly, mean and absolute errors were calculated for each datum surface model.

3.2 Results and Interpretations

3.2.1 Field Derived Results

3.2.1.1 Stratigraphic Section Analysis

Stratigraphic analyses were conducted atop the terraces at Head Tide Dam (HTD) and the two terrace scarps present at Pinhook Dam (PHK), the first ~1 m above the modern channel and the second ~2.5 m above the modern channel (figure 3.8). The terraces at HTD are inundated during high-flow events (Strouse, 2013), and the lower elevation terrace at PHK is likely also inundated during high-flow events, therefore the interpreted terraces would technically be floodplains but are still included in this analysis for completeness. Capping all measured stratigraphy at HTD were massive (0.99 m average thickness) silt-clay deposits with occasional fine-sand lenses (2-5 cm thick) interwoven, a brownish-grayish coloration, and roots present throughout (figure 3.9, table 3.1, Appendix 1). At the PHK site, stratigraphic data were collected from three soil pit locations (figure 3.1, table 3.2, Appendix 1). The soil pits dug atop the lower terrace landform on both sides of the channel displayed a massive (0.89 and 0.68 m thick) silt-clay unit with brownish-grayish coloration and roots present throughout (figure 3.10; Appendix 1). The soil pit dug atop the higher elevation terrace was 0.51 m deep and showed similar stratigraphy (Appendix 1), but contained a number of large (> 5 cm) semi-angular clasts emplaced sporadically throughout the deposit (figure 3.10B).

Figure 3.8: Photograph taken from atop the lower terrace at the Pinhook Dam location looking away from the river channel towards the second, higher elevation terrace.

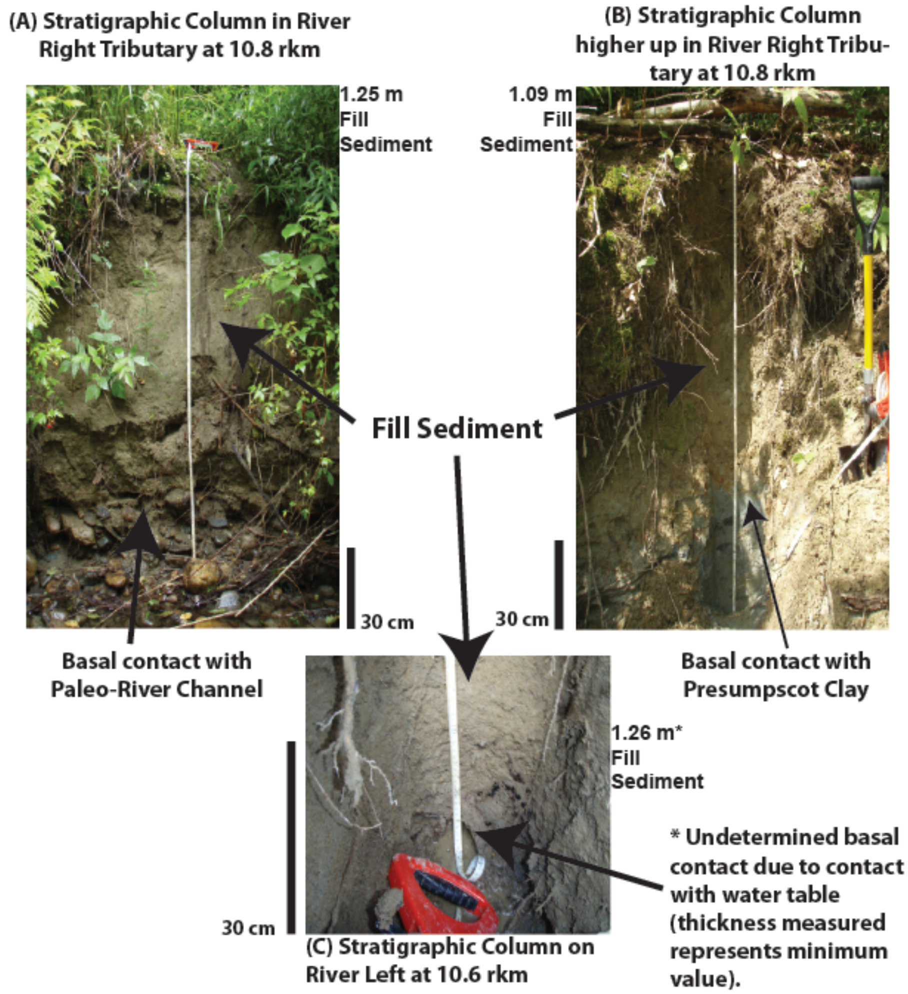

Figure 3.9: Photographs of three stratigraphic columns measured at Head Tide Dam illustrating the typical reservoir sediment profile and the possible lower boundaries used to define the thickness of the deposit. Potential basal contacts include (A) a paleo-river channel, (B) the grey clay Presumpscot Formation, or (C) indistinguishable due to interference with the water table.

The massive, fine-grained deposits observed in cut bank exposures and soil pits were interpreted as reservoir-sediment deposits based on their sediment characteristics. A definitive basal contact for reservoir sedimentation, such as a transition into a paleo-valley deposit (figure 3.8 A-B), was identified at eight locations at the HTD study site. Locations with an identified basal contact included: the two cut bank exposures within river left tributary at river kilometer 11.2, the three cut bank exposures measured at the mid-channel islands located at river kilometer

11-11.2, and at three cut bank exposures within the tributary on river right at river kilometer 10.8 (figure 3.1; Appendix 1). Thickness of reservoir sedimentation ranged from 1 – 1.47 m across the eight locations (table 3.1, Appendix 1). The remaining locations provided minimum estimates of reservoir sedimentation due to interference with the water table (figure 3.8C) or displaying stratigraphy with slight transitions in color or grain-size, which alone is not sufficient to infer a base of valley bottom aggradation. A definitive reservoir-sediment base was interpreted within the two soil pits dug atop the lower elevation terrace at the PHK study site. The maximum depths achieved within these soil pits (0.89 and 0.68 m) were limited due interference with clasts at the bottom of both pits, interpreted as a transition to a paleo-river channel deposit. A basal contact for the higher elevation terrace soil pit was undetermined due to repeated interference with large clasts throughout the soil pit and surrounding region. It is unclear whether the upper terrace formed as a consequence of the dam or is a natural terrace comprised of glacial till. The inclusion of numerous large clasts suggests this is not a millpond deposit. These initial observations of reservoir-sediment deposits are based on sediment characteristics, and require radiocarbon dating to place age constraints on interpreted deposits and confirm their Anthropocene origin.

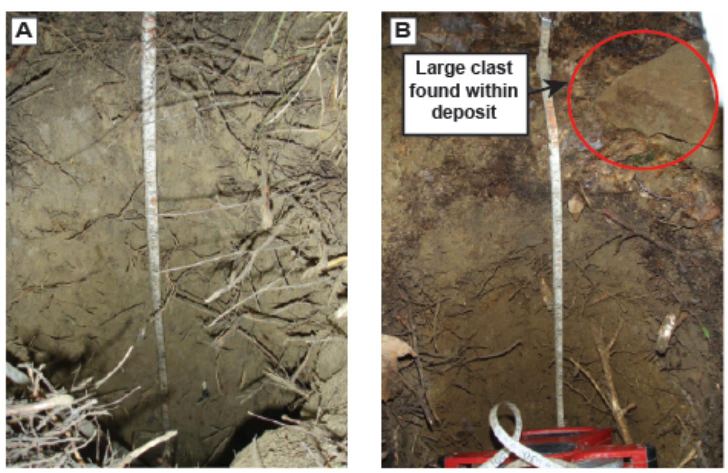

Figure 3.10: Evidence of reservoir sediment apparent in the soil pits analyzed at the Pinhook Dam location. Image (A) is of the soil pit dug on river left on the lower terrace, and (B) is of the soil pit dug atop the upper terrace.

Head Tide Dam Stratigraphic Data	$H_{stratigraphic}$ (m)	$H_{river\ water\ surface}$ (m)	ΔH (m)	Absolute ΔH (m)	$H_{valley\ bottom\ surface}$ (m)	ΔH (m)	Absolute ΔH (m)	H_{TerEx} (m)	ΔH (m)	Absolute ΔH (m)	Notes
Sheepscot_10.61_lbank	1.29	0.83			0.83			1.05			Basal Contact: Undefined
Sheepscot_10.62_rbank	1.26	1.24			1.24			1.42			Basal Contact: Not observed due to contact with water surface, shovel struck clasts ~0.25 m below base
Sheepscot_10.92_lbank	1.47	1.47	0.00	0	1.47	0.00	0	2.28	0.81	0.81	Basal Contact: Clay Layer
Sheepscot_11.02_island1	0.44	0.64	0.2	0.2	0.64	0.2	0.2	0.46	0.02	0.02	Basal Contact: Clay Layer with interbedded sand lenses
Sheepscot_11.02_island2	0.73	0.86	0.13	0.13	0.86	0.13	0.13	1.02	0.29	0.29	Basal Contact: Clay Layer
Sheepscot_11.2_ltrib	1.05	1.86	0.81	0.81	1.86	0.81	0.81	2.28	1.23	1.23	Basal Contact: Clay Layer
Sheepscot_11.2_ltrib2	0.29	1.18	0.89	0.89	1.18	0.89	0.89	2.28	1.99	1.99	Basal Contact: Clay Layer
Sheepscot_11.48_soilpit	0.58	2.11			2.11			3.1			Basal Contact: Undefined. Lots of cobbles present in unit. Potential mass wasting event?
Sheepscot_10.8_rtrib	1.30	1.47	0.17	0.17	1.47	0.17	0.17	2.08	0.78	0.78	Basal Contact: Cobble Layer
Sheepscot_10.8_rtrib2	1.25	2.89	1.64	1.64	2.89	1.64	1.64	2.08	0.83	0.83	Basal Contact: Cobble Layer
Sheepscot_10.8_rtrib3	1.06	3.30			1.10			4.81			Basal Contact: Undefined
Sheepscot_10.8_rtrib4	1.43	3.70			0.17			4.59			Basal Contact: Undefined
Sheepscot_10.8_rtrib5	1.09	3.09	2.00	2	0.10	-0.99	0.99	2.78	1.69	1.69	Basal Contact: Clay Layer
Sheepscot_10.8_rtrib6	0.60	3.62			0.00			4.09			Basal Contact: Undefined due to contact with water surface
Average (m)	0.90	2.10	0.83	0.83	0.99	0.23	0.63	2.09	0.72	0.72	
Standard Deviation (σ)	0.38	1.01	0.62	0.62	0.87	0.62	0.62	1.22	0.63	0.63	

Table 3.1: Stratigraphic data collected throughout the Head Tide Dam study area. Also included are the corresponding DEM thickness estimates from each datum surface method and deviation calculations at each stratigraphic column location.

Pinhook Dam Stratigraphic Data	$H_{stratigraphic}$ (m)	$H_{river\ water\ surface}$ (m)	ΔH (m)	Absolute ΔH (m)	$H_{valley\ bottom\ surface}$ (m)	ΔH (m)	Absolute ΔH (m)	H_{TerEx} (m)	ΔH (m)	Absolute ΔH (m)	Notes
Pinhook_0.71_Lsoilpit	0.885	0.733	-0.152	0.152	0.733	-0.152	0.152	0.49	-0.40	0.40	Basal Contact: Contact with clasts at base of soil pit
Pinhook_0.75_Lsoilpit	0.51	2.09			2.09			2.36			Basal Contact: Undefined
Pinhook_0.58_Rsoilpit	0.68	0.65	-0.03	0.03	0.65	-0.03	0.03	2.09	1.41	1.41	Basal Contact: Contact with clasts at base of soil pit
Average (m)	0.69	0.69	-0.09	0.09	0.69	-0.09	0.09	1.29	0.51	0.90	
Standard Deviation (σ)	0.38	0.06	0.09	0.09	0.06	0.09	0.09	1.13	1.28	0.72	

Table 3.2: Stratigraphic data collected throughout the Pinhook Dam study area. Also included are the corresponding DEM thickness estimates from each datum surface method and deviation calculations at each stratigraphic column location.

Using the DEM-assigned elevations for the stratigraphic sections, fence diagrams illustrate the location of measured stratigraphy along the main channels upstream of HTD and PHK, as well as along the tributary at river kilometer 10.8 within the HTD site (figure 3.11). Figure 3.11 illustrates the position of reservoir sediment deposits relative to the lidar imaged water surface (blue line), terrace treads mapped using the Finnegan and Balco (2013) method (black line), and the river water surface elevation measured during field data collection in July, 2013 (blue circles with dashed line). Included at the HTD site is the cut bank exposure measured by Strouse (2013; Figure 3.11). The base of reservoir sediment was directly measured at nine locations (Appendix 1), with locations where only minimum estimates of reservoir sediment thickness were measured being denoted by a question mark in Figure 3.11. Along the main stem at HTD, minimum elevation estimates for the base of reservoir sedimentation (stratigraphic columns with question marks in Figure 3.11) extend at least to the lidar imaged water surface, with the exception of the soil pit measured atop the terrace tread at river kilometer 11.48 (Figure 3.11). The main channel at PHK displays a similar scenario, with field-measured reservoir-sediment base elevations in the two soil pits atop the lower elevation terrace extending below the lidar imaged water surface (Figure 3.11). The interpreted base of reservoir sedimentation measured within the tributary at HTD was systematically higher than the lidar imaged water surface (up to ~4 m) for all locations, regardless of whether the reservoir sediment basal contact was constrained and unconstrained (Figure 3.11).

3.2.1.2 Ground Penetrating Radar Results

The GPR data collected illustrates the spatial variability of subsurface layers and facilitates depth estimates to layers of interest (Figure 3.12). Along profiles perpendicular to the river channel, a strong reflection layer exists at ~3±1 m depth below the ground surface with diminishing returns deeper (Figure 3.12D). I interpreted this reflective layer as the Presumpscot

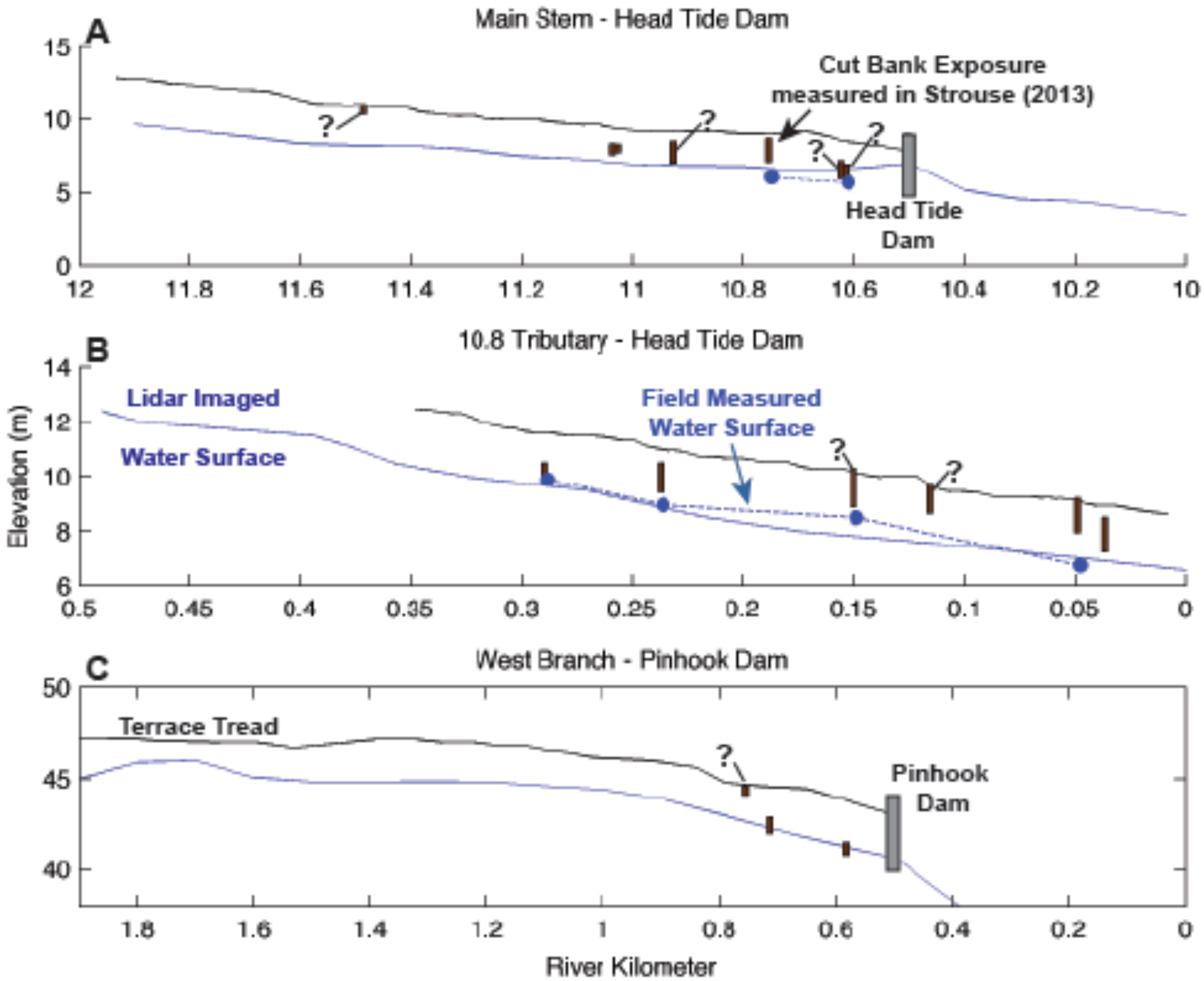

Figure 3.11: Fence diagrams constructed along the main channels of the Pinhook Dam (PHK) and Head Tide Dam (HTD) areas, along with the tributary at river kilometer 10.8 within the HTD site. Stratigraphic columns are simplified to only include reservoir sediment deposits, with question marks denoting locations were the base of millpond sedimentation was not observed. Elevations of the water surface measured in the field (blue dots) are included when the information was recorded in the field.

Formation because clay is known to be a strong reflector in GPR surveys and also highly attenuates electromagnetic waves. Directly above the interpreted Presumpscot Formation is another apparent reflector. Although not as strong, this reflector mimics the topography of the clay and is believed to be the water table surface that is perched above the impermeable Presumpscot Formation (figure 3.12). The terraces at HTD lack any groundwater monitoring equipment, so this interpretation would need to be confirmed by placing piezometers within terraces or through additional near-surface geophysical investigations.

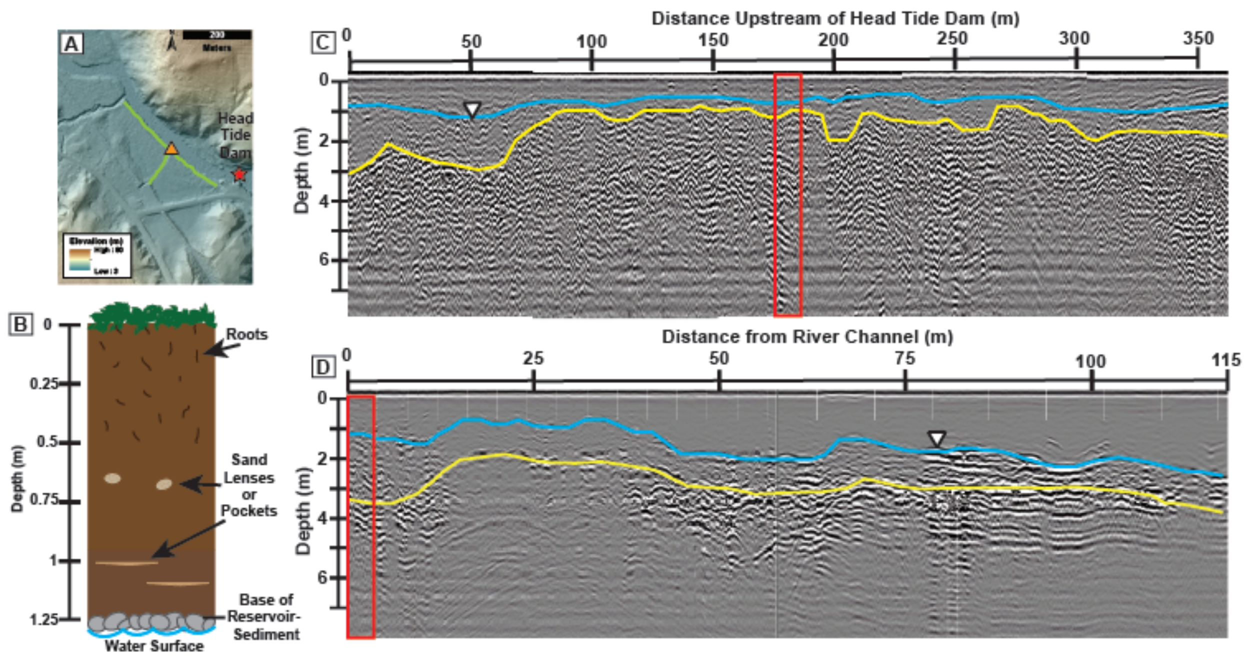

Figure 3.12: Location of ground penetrating radar (GPR) survey lines collected (A) and associated measured stratigraphic column (B) at river kilometer 10.6 used to ground truth GPR data. GPR survey lines illustrate reflective layers parallel to the channel (C) and perpendicular to it (D). Included in both images are the interpreted Presumpscot Formation clay layer (yellow line) and the water table (blue line), as well as the location within the survey at which ground truthing was performed (red rectangle). Depth estimates were achieved using a calculated dielectric constant of 14.96.

Identified layers within GPR scans were used to assess which datum surface model (Figure 3.6) was most representative of the natural system. No paleo-valley deposits (Figure 1.3) were identified in the GPR surveys besides the highly reflective Presumpscot Formation (Figure

3.12), therefore this clay layer was used as a proxy for the ancient valley floor topography and it was assumed that any Holocene deposition and soil development that occurred mimicked this structure. The clay layer extends predominantly horizontal normal to the river channel, and parallels the slope of the terrace tread longitudinally. This geometry is most similar to the PRWS datum model (figure 3.6), which uses only river water surface elevation points to construct a largely horizontal datum surface that follows the slope of the river channel.

3.2.2 DEM Derived Results

3.2.2.1 Terrace Longitudinal Profile

Terrace longitudinal profiles were used to identify prominent terrace landforms upstream of dam sites along the entirety of the main stem and the West Branch of the Sheepscot River (figures 3.13-3.14). Included for identifying reservoir-sediment terraces are the locations and heights of dams, obtained from previous studies and analysis of historical photographs (SVCA, 2002; Strouse, 2013). Tracing the contiguous peaks within and across individual river segments highlights the location and elevation of terraces potentially formed due to the presence of a dam (black ellipses; figures 3.13-3.14).

Terraces upstream of dams identified along longitudinal plots appear to display two idealized gradients (figure 3.15, see figure 3.13-6 for example). The first is predominantly horizontal (i.e. valley flat; Walter and Merritts, 2008) with maximum elevation values that are similar to the dam top, illustrating valley bottom aggradation in the millpond (figure 3.15). These valley flat terraces pinch out in the upstream direction and often coalesce with terraces that are generally parallel to the slope of the modern day channel (figure 3.15). Walter and Merritts (2008) showed that dams ranging in height from 2.5-3.7 m (general milldam heights in mid-

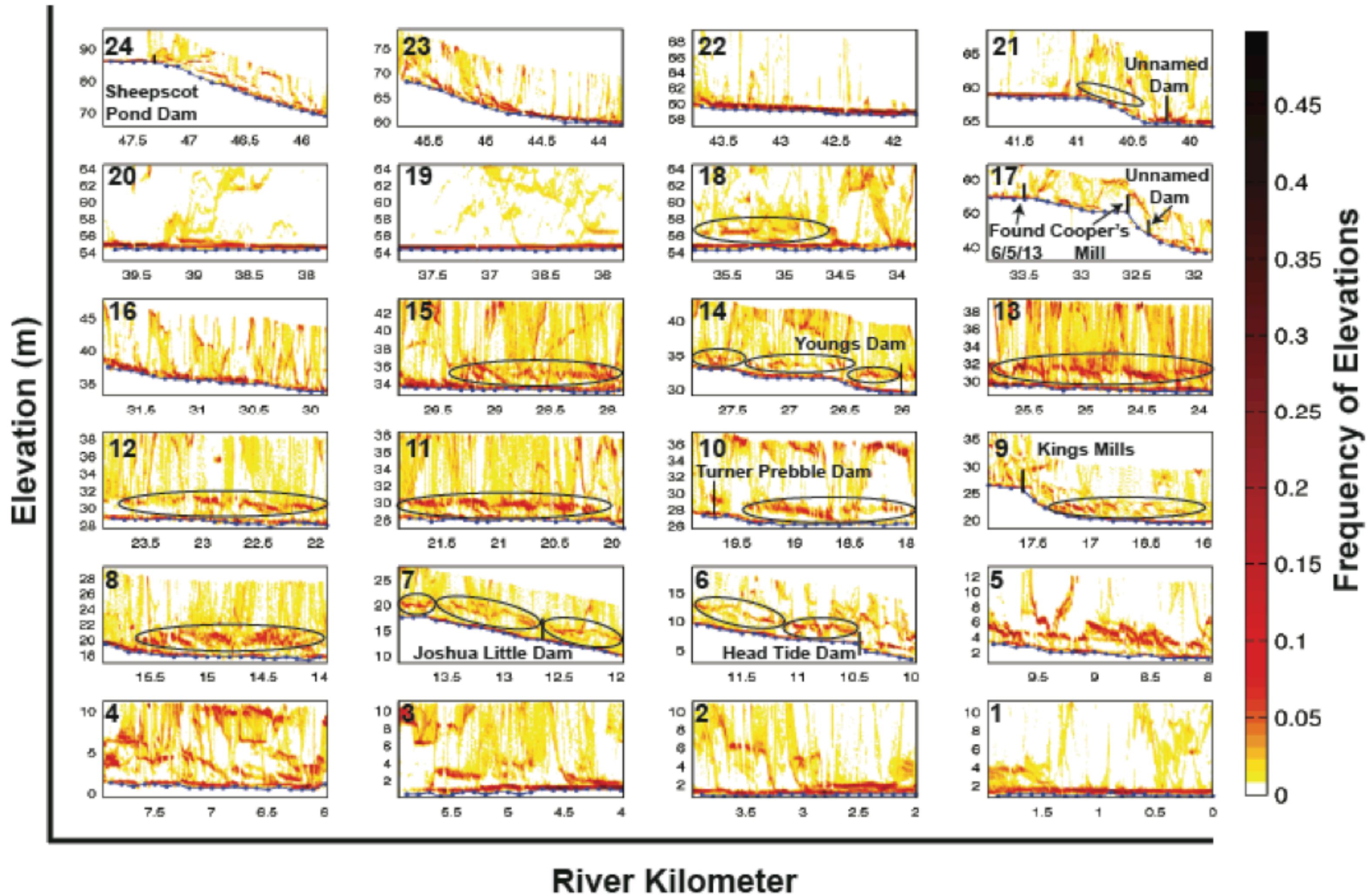

Figure 3.13: Normalized frequency distribution plots along the main stem of the Sheepscot River used to identify terraces along longitudinal profiles. River longitudinal profiles are constructed from lidar imaged elevation points within DEMs (blue circles). Black ovals highlight identified terraces upstream of dam sites. Plots originate in the lower right corner (1) and increase from right to left upwards to the upper left (24).

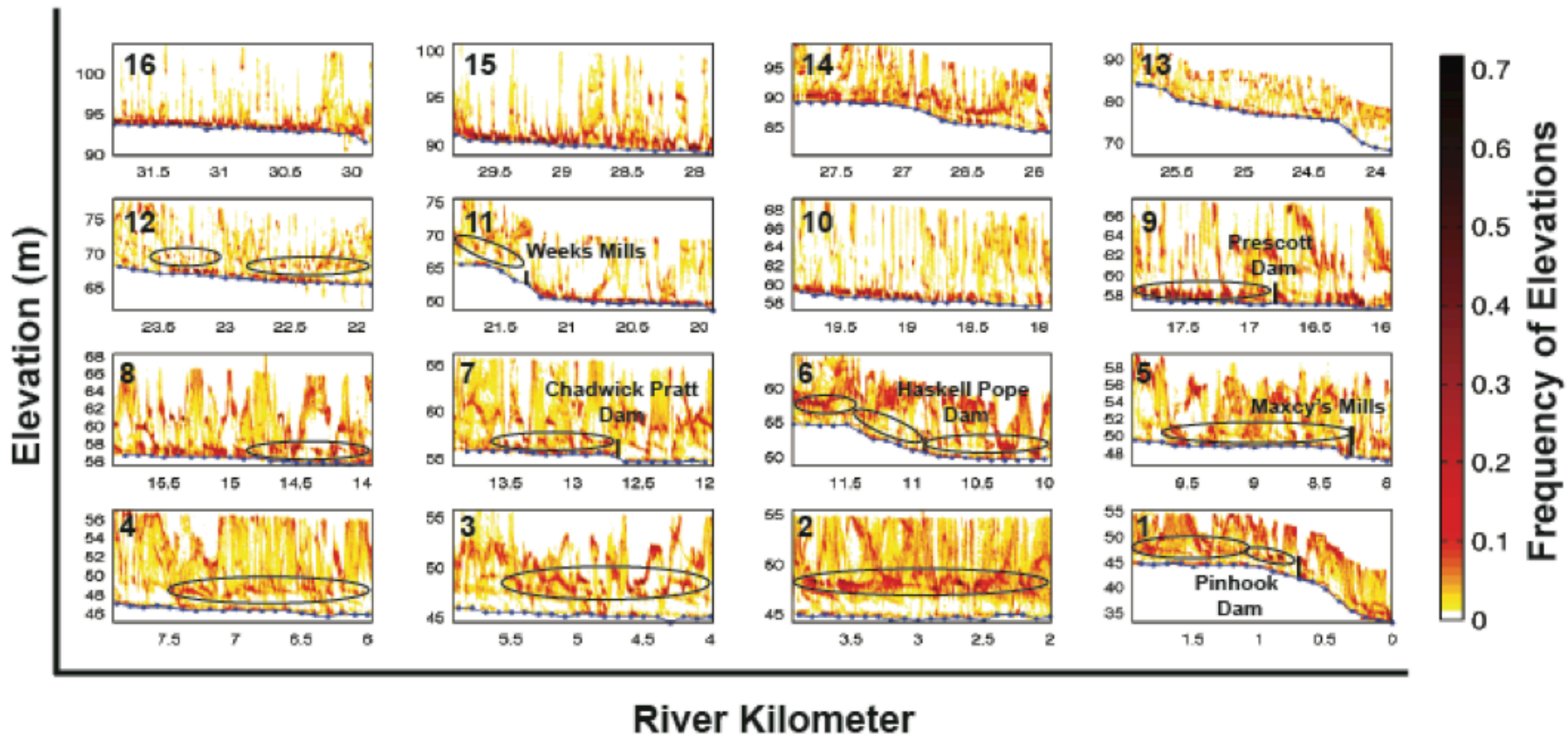

Figure 3.14: Normalized frequency distribution plots along the West Branch of the Sheepscot River used to identify terraces along longitudinal profiles. River longitudinal profiles are constructed from lidar imaged elevation points within DEMs (blue circles). Black ovals highlight identified terraces upstream of dam sites. Plots originate in the lower right corner (1) and increase from right to left upwards to the upper left (16).

Atlantic Piedmont region of U.S.) could impede flow velocity by as much as 60% up to 1-3 km upstream of a dam site. Based on this information, channel parallel terraces were interpreted as a product of millponds and included them in the scope of reservoir-sediment terraces analyzed. This interpretation is supported upstream of Head Tide Dam and Maxcy's Mills Dam by radiocarbon dating or hydraulic modeling conducted by Strouse (2013), but remains unsupported at the remaining dam sites that lack these analyses. If channel parallel terraces are a product of a dam, then the slope of a terrace surface cannot be used as an identifier of reservoir-sediment terraces within DEMs.

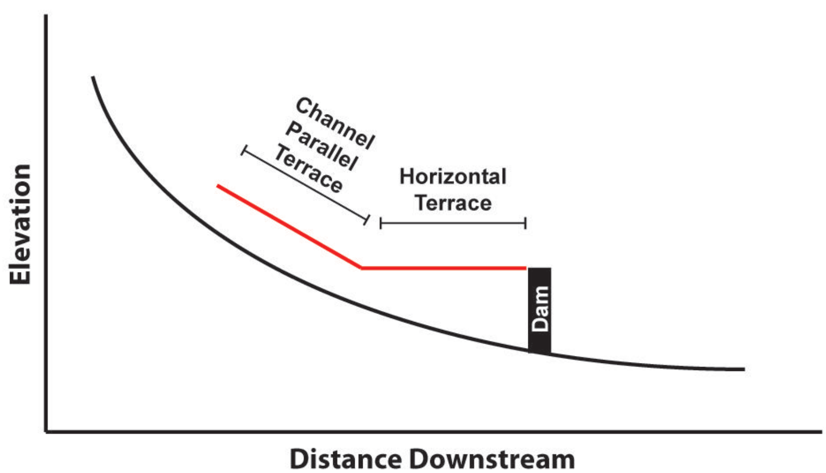

Figure 3.15: Ideal graded river longitudinal profile showing the two prominent gradients of terraces, the first being horizontal and the second parallel to the river channel.

3.2.2.2 Terrace Delineation

Mapping endeavors using the feature classification method (Figure 2.6; Wood, 1996) tested in Chapter 2 were completed in less than 5 hours and successfully delineated tread surfaces within all 2 km segments that contained identified terraces (Figures 3.13-3.14). Certain terrace polygons display holes in their defined coverage, likely due to the presence of high-flow channels atop surfaces that cause a deviation from the planar classification for those particular cells (figure 3.16). These errors can be corrected through manual editing of the map output, but were not carried out in order to illustrate the original output from this method. In total, planform mapping outlined a terrace area of 1.3×10^6 m^2 for the main stem and 1.8×10^6 m^2 for the West Branch. The West Branch watershed has a generally flatter landscape and less bedrock control on valley width, both of which may be contributing to the higher value by increasing the area detected in the feature classification (Wood, 1996) algorithm.

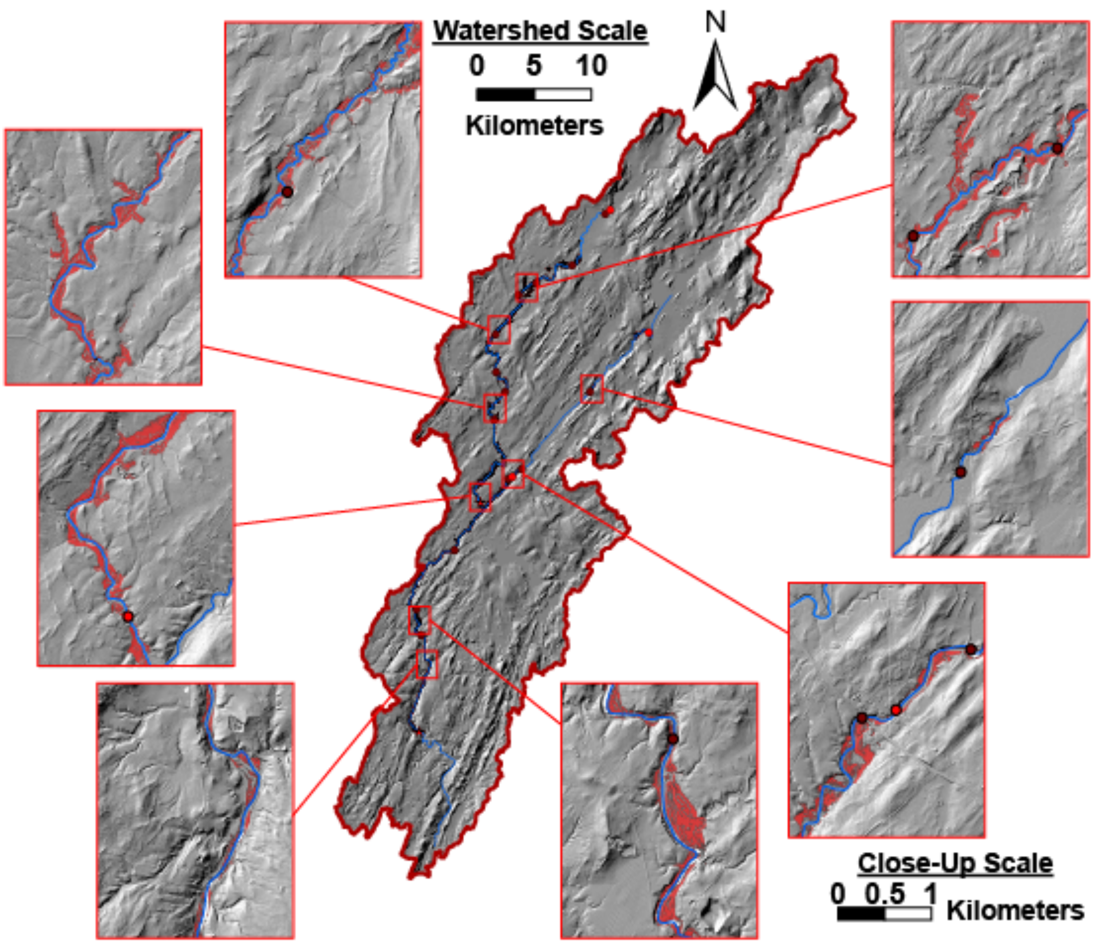

Figure 3.16: Terraces mapped throughout the watershed using the Feature Classification (Wood, 1996) mapping process. Red and maroon circles indicate current and historic dam locations, respectively. Mapping results overlay a hillshade raster of the watershed. Note the separate scales for the watershed and all inset images.

3.2.2.3 Comparison of Potential Datum Surfaces

Obtaining accurate estimates of fill terrace thickness required defining an appropriate datum surface representing the base of reservoir sedimentation. Figure 3.11 demonstrates the potential of using the water surface imaged during the 2007 lidar survey for use in constructing datum surfaces corresponding to the base of reservoir sedimentation. In situ measurements of terrace stratigraphy were collected during a time of lower discharge and stage values (figure 3.5) relative to the timing of the lidar flights. At certain locations, particularly those closest to the dams, the base of reservoir sedimentation remained unexposed during these periods of lower discharge and stage. For these locations, a minimum estimate of reservoir-sediment thickness could be obtained using the water surface elevations as a basal proxy. Within the tributary at HTD, four cut bank exposures contained an observable reservoir-sediment basal contact exposed approximately 0.5-2 m above the current water surface; thus, the use of the main channel water surface for datum surface construction would overestimate the thickness of reservoir sedimentation at these locations. The tributary water surface was not utilized in the construction of datum surfaces, which is likely contributing to this error. These results support the use of the water surface imaged during the 2007 lidar survey as an appropriate proxy for the base of reservoir sedimentation, but illustrate that this proxy will not systematically yield under or over estimates of terrace thickness. To truly evaluate the accuracy of the DEM water surface as a basal proxy, the relationship between millpond sedimentation and the river water surface must be constrained by obtaining survey-grade elevation control for the stratigraphic contacts observed in the field.

Using the DEM-derived datum surfaces (Figures 3.6-3.7) defined for this research, maximum calculated thicknesses were ~8 m at HTD and ~ 4 m at PHK. Variations between the continuous thickness rasters (A-B; D-E) calculated above the projected river water surface (PRWS) and valley bottom interpolated surface (VBIS) are most evident along the perimeters of the terrace extents (figure 3.17), where thicknesses are a maximum above the PRWS (figure 3.5A) and minimum above the VBIS (figure 3.6B). While using the VBIS datum for calculations, some peripheral cells returned negative thickness values and were adjusted to a value of zero. This arises due to the sloping nature of the VBIS surface, which can interpolate over localized low points in topography and produce a negative thickness value when subtracted. Thickness values derived by the TerEx toolbox (Stout and Belmont, 2013; Figure 3.17C & F) are similar to the PRWS results, but are a much lower resolution because entire mapped treads are prescribed a single thickness value. DEM-derived thickness values were compared to coincident stratigraphic columns where reservoir-sediment was identified and measured in situ (tables 3.1-3.2). Using only locations where the base of reservoir sedimentation was observed and measured, the three methods reported average deviations (ΔH) ranges of 0.09 – 1.19 m at HTD and -0.09 – 0.51 m at PHK. The valley bottom interpolated surface (VBIS) results reported the lowest mean error, absolute error, and σ values at both study sites out of all methods tested, suggesting the VBIS is the best suited datum surface for thickness calculations.

At HTD, volumes were calculated using each datum surface and compared to estimates from Strouse (2013), where volume was calculated by multiplying a manually delineated terrace area by one thickness value collected from a measured stratigraphic column (table 3.3). The similarity between the 70% slab volume, which attempts to account for a non-horizontal valley bottom, from Strouse (2013) with the VBIS derived volume lends further support to the use of this datum for thickness and volume calculations.

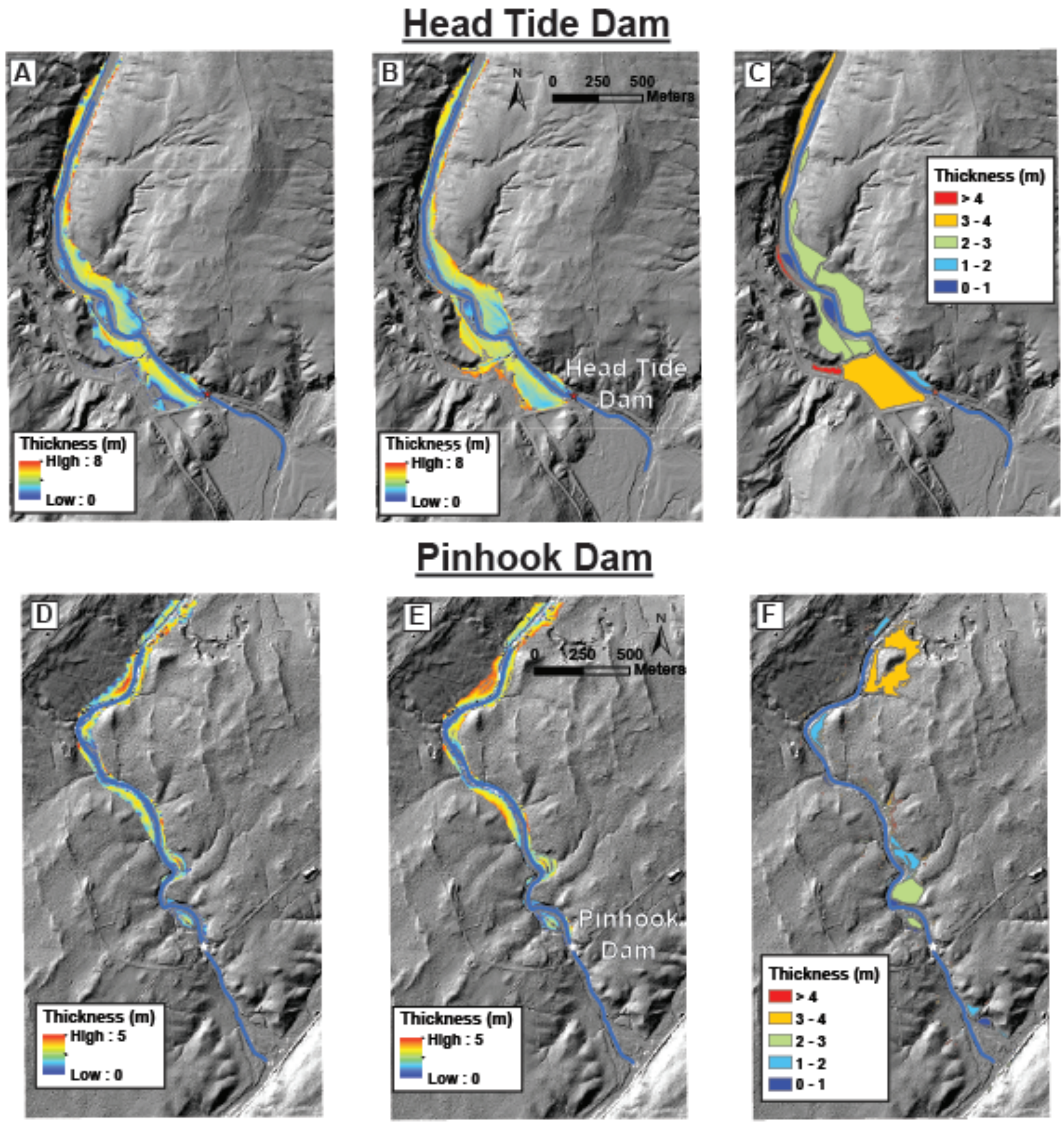

Figure 3.17: Sediment thickness rasters for the Head Tide Dam (A-C) region and Pinhook Dam (D-F) region. Calculations were done using the valley bottom interpolated surface (VBIS) datum surface (A & D), the projected river water surface (PRWS) datum surface (B & E), and by subtracting average terrace elevations from average elevations of river subsections (C & F). Terrace extent is defined using the Feature Classification (Wood, 1996) method for A, B, D, and E, while C and F used the output from the TerEx toolbox (Stout and Belmont, 2013). Base image is a hillshade raster.

Water Table Datum Volume (m^3)	Valley Bottom Datum Volume (m^3)	TerEx Toolbox Volume (m^3)	Strouse (2013) Slab Volume (m^3)	Strouse (2013) 70% of Slab Volume (m^3)
3.4×10^5	1.9×10^5	2.2×10^5	3.0×10^5	2.1×10^5

Table 3.3: Comparison of DEM based volume estimates of legacy sediment storage at Head Tide Dam with previously calculated estimates from Strouse (2013).

3.2.2.4 Volume Estimates of Reservoir Sediment Storage along the Sheepscot River

As discussed previously in section 3.2.2.1, the presence of millponds appears to be forming both valley-flat and channel-parallel terraces upstream of breached and historic dam locations (figure 3.15). Accounting for both of these terrace types, the extent of reservoir-sediment terraces upstream of former dam sites can be on the order of 1-3 kilometers. Results from the Finnegan and Balco (2013) method (figures 3.13-3.14) combined with knowledge of reservoir-sediment terrace profiles were used to discern the maximum upstream extent of a dam's influence. These values served as the terminal distance for the extent of mapped reservoir-sediment terraces upstream of a dam.

Within these bounds along channel profiles, terrace perimeters derived from the feature classification (Wood, 1996) method were used as the extent over which thickness and volume estimates were calculated. Results from GPR surveys and stratigraphic data indicate the use of the VBIS as an appropriate datum surface for thickness and volume calculations (Figure 3.12; tables 3.1-3.2). However, due to minimal time requirements, thickness and volume estimates were calculated above both the PRWS and VBIS datum surfaces (figures 3.18-3.19). Terraces observed at both study sites (HTD and PHK, figure 1.10) were interpreted as impounded sediment deposits, and this observation was extrapolated to the remaining dam locations by assuming that all mapped terraces upstream of dams were comprised of reservoir sediment. If this assumption is valid, reservoir terraces present at individual dam sites on the main stem store an average volume of 2.5×10^5 m^3. Along the West Branch, individual dam sites store and average volume of 2.6×10^5 m^3 of millpond sediment in the form of terraces. Total volume of reservoir sediments stored at five dam sites along the main stem is 9.3×10^5 m^3 using the PRWS and 5.7×10^5 m^3 using the VBIS. Along the West Branch, total volume of reservoir sediments stored at six dam sites are 1.0×10^6 m^3 using PRWS and 6.3×10^5 m^3 using VBIS. In total, the main stem and West Branch of the Sheepscot River store approximately 3.1×10^6 m^3 of reservoir sediment contained within terraces. Because the sediment stored in these terraces is derived from the surrounding landscape, it was assumed that the bulk densities for reservoir and hillslope sediment were equal for the entirety of the 576 km^2 Sheepscot River watershed. Under this assumption the total volume of reservoir sediment stored in terraces was divided by the watershed area, which corresponds to an average thickness of ~5 mm of sediment eroded from the landscape that is still stored in valley bottom deposits.

3.3 Conclusions and Future Work

Overprinting the Pleistocene glacial activity recorded in the Sheepscot River watershed is a landscape heavily influenced by anthropogenic processes that have occurred over the past ~300 years. Detailed field analyses have elucidated the lingering effect of damming at two locations along the river (e.g. Strouse, 2013). This research built upon these results by analyzing the remaining dam locations along the main stem and West Branch using DEM-based procedures. DEM analyses offer an efficient means to gain first-order insight on the magnitude of

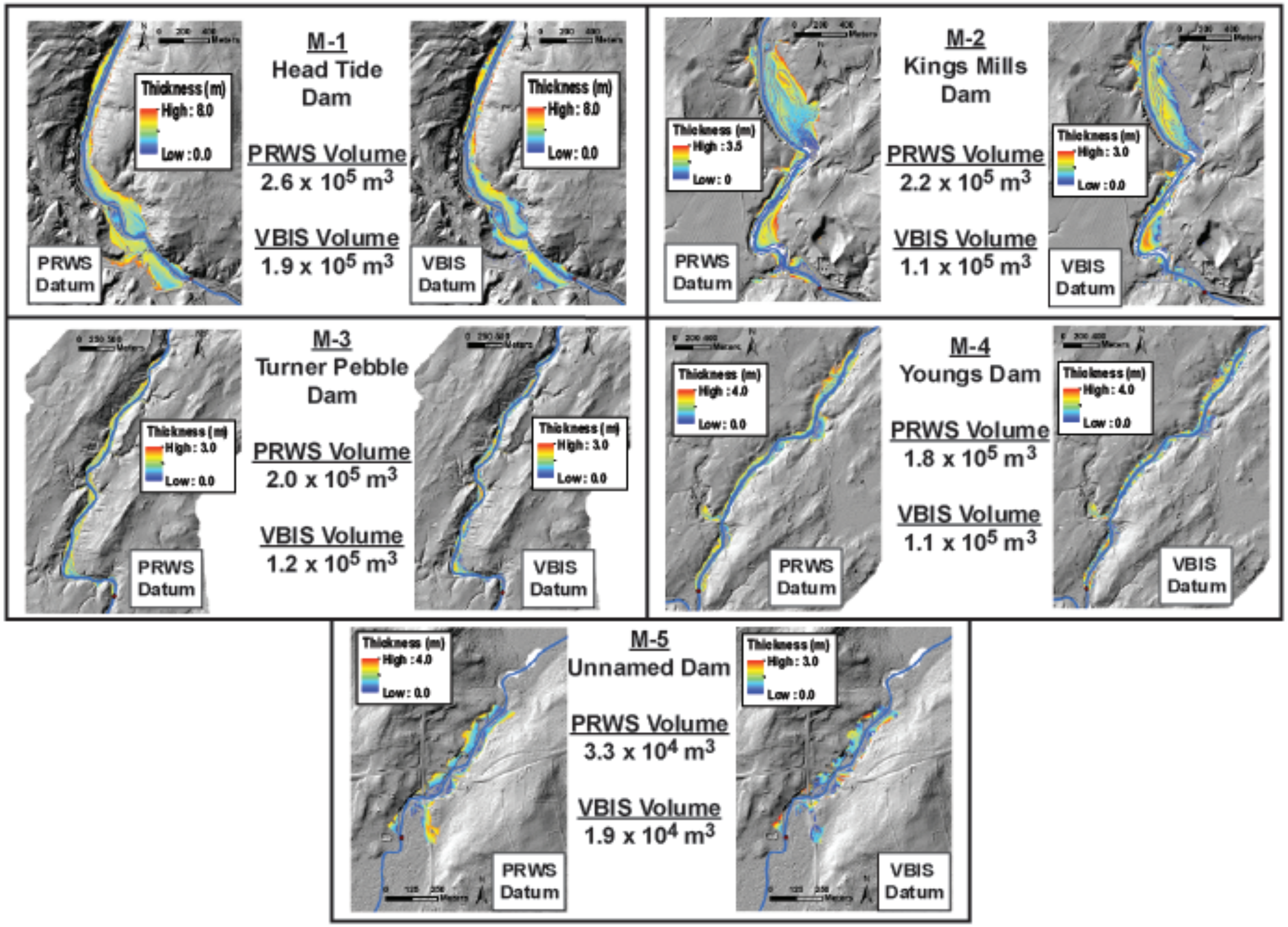

Figure 3.18: Reservoir sediment thickness rasters calculated for historic and breached dam locations along the main stem of the Sheepscot River. Base image is a lidar derived hillshade raster.

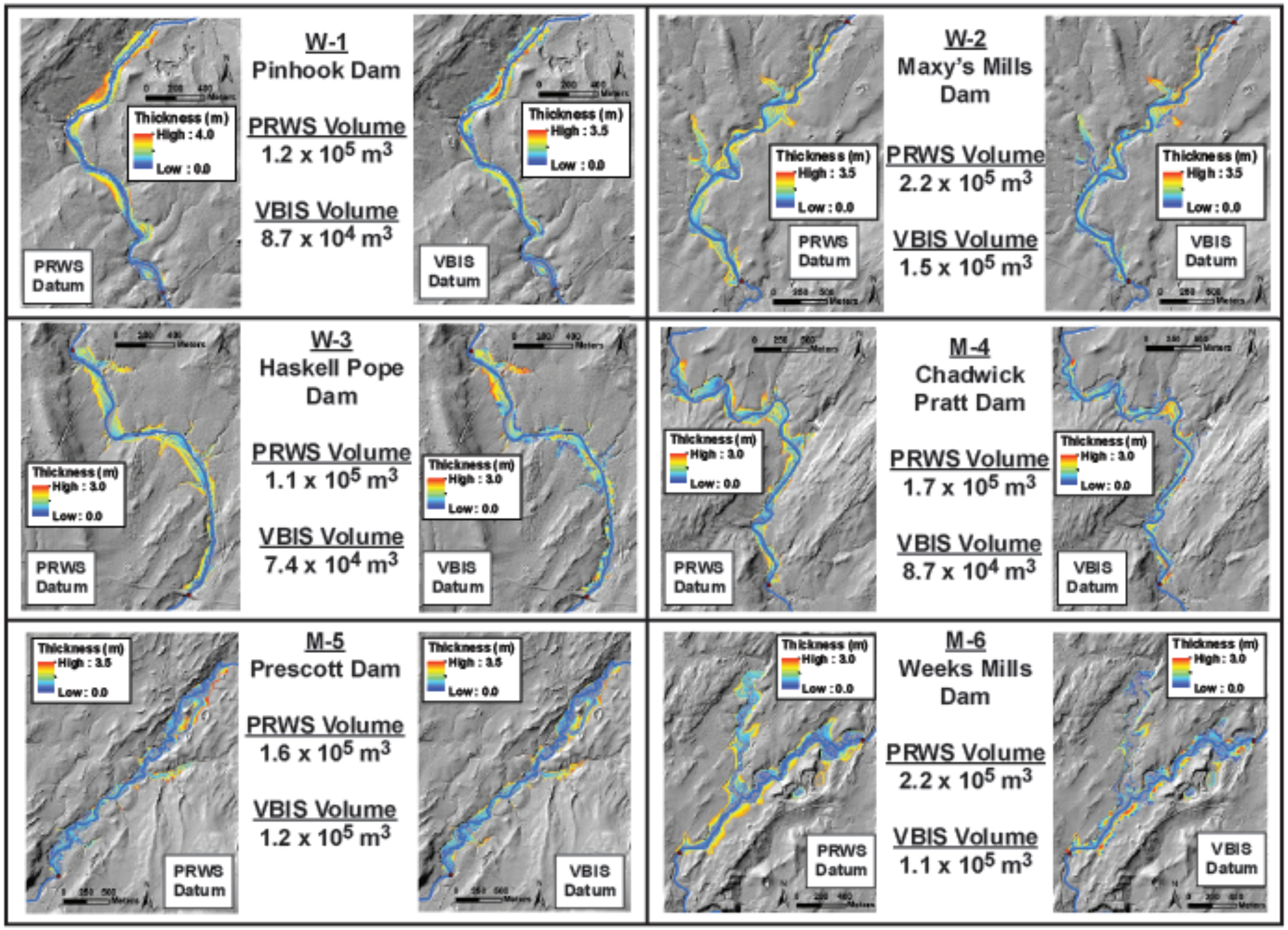

Figure 3.19: Reservoir sediment thickness rasters calculated for historic dam locations along the West Branch of the Sheepscot River. Base image is a lidar derived hillshade raster.

anthropogenic modification that has occurred over watershed scales, but these results are still preliminary and require further field-based analyses such as stratigraphic observations with survey-grade elevation control at multiple dam sites along with radiocarbon dating on all interpreted reservoir sediment deposits for validation. Nonetheless, the methods described herein illustrate the use of DEM-based analyses as a complimentary initial step used to guide future field excursions.

A variety of DEM-based terrace mapping procedures exist (Chapter 2), but the feature classification method (Wood, 1996) was selected for this work based on its fast processing time and inherent objective nature. This method was successful at mapping over 3.0×10^6 m^2 of terrace landforms along the main stem and west branch of the Sheepscot River. All terraces mapped were in accordance with those identified by visual examination along the channels, with no prominent terraces being excluded from final results. Gaps in mapped surface area exist atop certain terraces (figure 3.16) and appear to correspond to high-flow channels that failed to be classified as planar regions.

Reservoir-sediment thicknesses and associated terrace volumes were calculated at the two representative study sites using the projected river water surface (PRWS), valley bottom interpolated surface (VBIS), and the TerEx toolbox (Stout and Belmont, 2013) method as datum surfaces, all of which are derived from lidar DEMs. All datum surfaces generally overestimated thickness relative to field measured cut bank exposures and soil pits, and no datum surface was unquestionably the most favorable. Stratigraphic data favor the VBIS (tables 3.1-3.2), while the GPR results support a more horizontal datum such as the PRWS (figure 3.12). Field-measured stratigraphy left the base of reservoir sediment unconstrained at six locations throughout the HTD study site and one location at the PHK study site (Figure 3.11). At three of the locations at the HTD study site, the minimum estimates of millpond sedimentation measured in cut bank exposures extended to the DEM water surface or below (Figure 3.11), indicating that the use of the DEM water surface as a proxy for the base of reservoir sedimentation should underestimate thickness estimates at these location. The remaining unconstrained locations had observable reservoir-sediment deposits extending to within 2-4 m of the DEM water surface and require further field analysis to determine their relation with the DEM water surface. At locations where the base of reservoir sedimentation was observed and measured, DEM-based thickness calculations across both sites reported average errors (ΔH) ranging from -0.09 – 1.19 m, suggesting that DEM-based thickness calculations utilizing the DEM water surface will not provide systematic over or under estimates of reservoir sediment thickness. Volume calculations differed by over 1.0×10^5 m^3 between the two datum surfaces for some individual sites (figure 3.20). Despite such a large difference reported at certain locations, I suggest both methods should be implemented to define a probable range of potential values. Both datum methods are easily programmable into ArcGIS and essentially involve the same procedure, with the only major difference being the one additional input for the VBIS (i.e. the points along the terrace extent). Volumes calculated in this analysis reflect a maximum estimate in which all terraces identified upstream of dams are comprised of reservoir sediment. While the composition of these terraces remains uncertain after this analysis, if the assumptions made for this work hold true then this sediment could be a potential point-source disrupting downstream channel dynamics if mobilized through stream bank erosion. Further, this sediment could have negative chemical effects if any contaminants are adhered to particles such as is the case along the mid-Atlantic Piedmont region of the U.S. (Walter et al., 2007). Both of these circumstances illustrate the importance or obtaining estimates of sediment volume in order to assess potential impacts of dam removal or stream alteration that might increase the mobilization of reservoir-sediment stored in terraces.

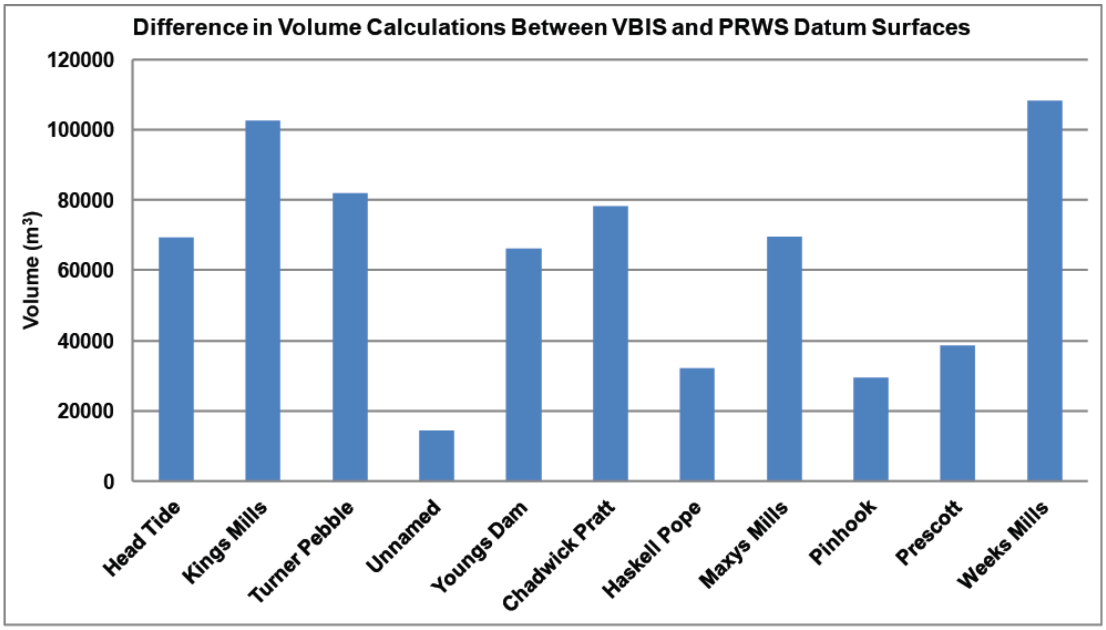

Figure 3.20: Variations in fill sediment volume calculations at current and historic dam sites within the Sheepscot River watershed based on the selection of datum surface. Datum surfaces considered in this plot include the Projected River Water Surface (PRWS, figure 3.5A) and the Valley Bottom Interpolated Surface (VBIS, figure 3.5B)

The results of this study will serve as a guide for future work seeking to confirm the magnitude of millpond sedimentation throughout the Sheepscot River watershed. The extent of reservoir sediment terraces upstream of historic and breached dams was defined through visually examining terrace longitudinal profiles (Figures 3.13-3.14) and lidar-derived hillshade rasters. Testing this interpretation at individual dam sites using hydraulic modeling programs such as the one dimensional Hydrologic Engineering Centers River Analysis System (HEC-RAS) will facilitate estimation of the maximum upstream extent of ponding behind dams (Strouse, 2013). For spatially-delineated terraces (Chapter 2; figure 3.16) that reside within the HEC-RAS-modeled upstream extent of a dam's reservoir, a massive fine-grained composition consistent with the reservoir-sediment characteristics must be observed in soil pits, cut bank exposures, or sediment cores. Analyzed stratigraphy must probe deep enough to identify paleo-valley bottom deposits (figure 1.3) in order to thoroughly compare between the PRWS and VBIS datum and identify a truly appropriate model for use in this environment. At each location were stratigraphy is measured, survey-grade elevation data must be collected as well to facilitate the comparison between in situ and DEM datasets. Lastly, radiocarbon dates must be collected to confirm the Anthropocene origin of all interpreted millpond sediment deposits. Strouse (2013) obtained a minimum of three radiocarbon dates at each analyzed dam site to confirm ages, and it is advisable that this standard should be adhered to at all subsequent study sites.

The primary function of these results was to illustrate the capability of using DEM analysis to rapidly obtain a first-order approximation of reservoir sediment volume stored within a watershed. These results will serve as the foundation for future studies involving reservoir-sediment terraces in the Sheepscot River watershed. Additionally, the DEM-based methods described herein can easily be applied to any watershed where lidar surveys have been flown and assist in the identification and preliminary analysis of reservoir sediment terraces.

References

Belknap, D.F., J.T. Kelley, and A.M. Gontz (2002), Evolution of the glaciated shelf and coastline of the northern Gulf of Maine, USA. *Journal of Coastal Research, Special Issue 36*, 37–55.

Belknap, D.F., C. Shipp, and J.T. Kelley (1986), Depositional Setting and Quaternary Stratigaphy of the Sheepscot Estuary, Maine: A Preliminary Report, *Géographi Physique et Quaternaire*, *40*, 55-69.

Bloom A.L. (1963), Late-Pleistocene fluctuations of sea level and postglacial and crustal rebound in coastal Maine, *American Journal of Science*, *261*, 862-879.

Blum, M.D. (1993) Genesis and architecture of incised valley fill sequences; a late Quaternary example from the Colorado River, Gulf Coastal Plain of Texas. In: Weimer, P., Posamentier, H.W. (Eds.), *Siliciclastic Sequence Stratigraphy,* Recent Developments and Applications, *American Association of Petroleum Geologists*, Memoir, Tulsa, OK, *58*, 259–283

Brady, M. (2007), Major Land Uses, *USDA Economic Research Service*.

Bull, W.B. (1991) Geomorphic Responses to Climate Change. *Oxford University Press*, Oxford, 326.

Campbell, M.R. (1929) The river system, a study in the use of technical geographic terms. *Journal of Geography*, *28*, 123–128.

Collins, S.H. (1973), Terrain parameters directly from a digital terrain model. Publication of American Congress on Surveying and Mapping.

Demoulin, A., B. Bovy, G. Rixhon, and Y. Cornet (2007), An automated method to extract fluvial terraces from digital elevation models: The Vesdre valley, a case study in eastern Belgium, *Geomorphology*, *91*, 51-64.

Finnegan, N.J., and G. Balco (2013). Sediment supply, base level, braiding, and bedrock river terrace formation: Arroyo Seco, California, USA, *GSA Bulletin, 125*, doi: 10.1130/B30727.1.

Finnegan N.J., R. Schumer, and S. Finnegan, (2014), A signature of transience in bedrock river incision rates over timescales of 104-107 years, Nature, 505, 391-394.

Finnegan N.J., and W.E. Dietrich, (2011), Episodic bedrock strath terrace formation due to meander migration and cutoff, *Geology*, *39*(2), 143–146.

Gran K.B., P. Belmont, S.S. Day, C. Jennings, A. Johnson, L. Perg, and P.R. Wilcock (2009), Geomorphic evolution of the Le Sueur River, Minnesota, USA, and implications for current sediment loading. *Geological Society of America Special Papers*, *451*, 119–130.

Halstead, M. (2002), *The Sheepscot River, Atlantic Salmon, and Dams: A Historical Reflection*, SVCA, Alna, ME, 36.

Hancock, G.S., R.S. Anderson, O.A. Chadwick, and R.C. Finkel (1999), Dating fluvial terraces with ^{10}Be and ^{26}Al profiles: application to the Wind River, Wyoming, *Geomorphology*, *27*, 41-60.

Hazlinsky, E.J., and N.P. Snyder (2007), Documenting 20th century changes in river morphology using aerial photographs and field surveys; Narraguagus and Sheepscot rivers, Maine, *Abstracts with Programs-Geological Society of America*, *39*(1), 44.

Keary, P., Brooks, M., and I. Hill (2002), *An Introduction to Geophysical Exploration*, Blackwell Publishing, Malden, MA.

Laser, M. J. Jordan, and K. Nislow (2009), Riparian forest and instream large wood characteristics, West Branch Sheepscot River, Maine, USA, *Forest Ecology and Management*, *257*, 1558-1565.

Lavé, J., Avouac, J.P. (2000), Active folding of fluvial terraces across the Siwaliks Hills, Himalayas of central Nepal, *Journal of Geophysical Research*, 105, 5735-5770

MacMillan R.A., T.C. Martin, T.J. Earle, and D.H. McNabb (2003), Automated analysis and classification of landforms using high-resolution digital elevation data: applications and issues, *Canadian Journal of Remote Sensing* 29(5), 592–606.

Maine Department of Conservation, (1999), Surficial Geology of Maine, Maine Geological Survey, Augusta, ME, July 1, 1999. Accessed June 23, 2014.

Merritts, D.J., K.R. Vincent, and E.E. Wohl (1994), Long river profiles, tectonism, and eustasy: A guide to interpreting fluvial terraces, *Journal of Geophysical Research*, *99*, 14,031-14,050.

Merritts, D.J., R. Walter, M. Rahnis, J. Hartranft, S. Cox, A. Gellis, N. Potter, W. Hilgartner, M. Langland, L. Manion, C. Lippincott, S. Siddiqui, Z. Rehman, C. Scheid, L. Kratz, A. Shilling, M. Jenschke, K. Datin, E. Cranner, A. Reed, D. Matuszewski, M. Voli, E. Ohlson, A. Neugebauer, A. Ahamed, C. Neal, A. Winter, and S. Becker (2011), Anthropocene streams and base-level controls from historic dams in the unglaciated mid-Atlantic region, USA, *Phil. Trans. R. Soc.*, *369*, 976-1009.

Molnar, P., B. Erik Thorson, B.C. Burchfiel, Q. Deng, X. Feng, J. Li, G.M. Raisbeck, J. Shi, W. Zhangming, F. Yiou, and H. You (1994), Quaternary climate change and the formation of river terraces across growing anticlines on the north flank of the Tien Shan, China, *Journal of Geology*, *102*, 583–602, doi: 10.1086/629700.

Osberg PH*, A.M.* Hussey II*, and G.M.* Boone *(1985),* Bedrock Geologic Map of Maine. *Maine Geological Survey*.

Parker, James R. (1997), *Algorithms for Image Processing and Computer Vision,* New York, John Wiley & Sons, Inc., 23-29.

Pazzaglia FJ (2013), 9.22 Fluvial terraces, In *Treatise on Geomorphology*, John FS (ed). Academic Press, San Diego, CA, 379–412.

Pazzaglia, F.J., and M.T. Brandon (2001), A fluvial record of long-term steady-state uplift and erosion across the Cascadia forearc high, western Washington State, *American Journal of Science*, *301*, 385–431.

Pazzaglia F.J., T.W. Gardner, and D.J. Merritts (1998), Rivers over rock: fluvial processes in bedrock channels. In *Geophysics Monograph Series*, Tinkler J, Wohl E (eds). AGU: Washington, DC.

Rahnis, M. (2012). Personal Communication [e-mail].

Riebe C.S., J.W. Kirchner, D.E. Granger, and R.C. Finkel (2001) Strong tectonic and weak climatic control of long-term chemical weathering rates, Geology, 29(6), 511–514.

Ritter, D.F., R.C. Kochel, J.R. Miller (2002), *Process Geomorphology*, Waveland Press, Long Grove, IL.

Rockwell, T. K., E. A. Keller, M. N. Clark, M. N., and D. L. Johnson (1984) Chronology and rates of faulting of Ventura River terraces California, *Geological Society of America Bulletin*, *95*, 1466-1474.

Rosell, F., O. Bozser, P. Collen, and H. Parker (2005), Ecological impacts of beavers *Castor fiber* and *Castor Canadenis* and their ability to modify ecosystems, *Mammal Review*, *35*(4), 248-276, doi: 10.1111/j.1365-2907.2005.00067.x.

Sacks, M.L. (2004), *A Brief History of Whitefield, 1760-2004*, Whitefield Historical Society, Whitefield, ME.

Sheepscot Valley Conservation Association (SVCA) (2005), KRIS Sheepscot, http://www.krisweb.com/krissheepscot/krisdb/html/krisweb/index.htm.

Smith, G.W. (1985). Chronology of Late Wisconsinan deglaciation of coastal Maine, *Geological Society of America*, Boulder, CO, *Special Paper 197*, 29–44.

Snyder, N. P., M. R. Castele, and J. R. Wright (2008). Bedload entrainment in low gradient paraglacial coastal rivers of Maine, U.S.A.; implications for habitat restoration, *Geomorphology, 103*(3), 430-446

Stone, B.D., and H.W. Borns (1986), Pleistocene glacial and interglacial stratigraphy of New-England, Long Island, and adjacent Georges Bank and Gulf of Maine. *Quaternary Science Reviews 5*, 39–52.

Stout, J.C., and P. Belmont (2013), TerEx Toolbox for semi-automated selection of fluvial terrace and floodplain features from lidar, *Earth Surface Processes and Landforms*, doi:10.1002/esp.3464

Strouse, S. (2013). The Effect of Millponds on Sedimentation in a Post-Glacial Mid-Coast Maine River Valley, MS thesis. Boston College. Chestnut Hill, MA. Print.

Thompson, W.B., Borns, H.W. (1985), Surficial Geologic Map of Maine. Maine Geological Survey, Augusta, ME.

U.S. Geological Survey (1893), Wiscasset, ME Quadrangle, University of New Hampshire Library, Accessed 02.02.2014

U.S. Geological Survey Real-Time Water Data for the Nation, http://waterdata.usgs.gov/usa/nwis/uv?01038000, Gauging station located at North Whitefield, ME. [Accessed 04.12.2014]

Walter, R.C., Merritts, D.J., Rahnis, M. (2007), Estimating volume, nutrient content, and rates of stream bank erosion of legacy sediment in the Piedmont and Valley and Ridge physiographic provinces, southeastern and central PA, A report submitted to the PA Department of Environmental Protection.

Walter, R. C., and D.J. Merritts (2008), Natural streams and the legacy of water-powered mills, *Science*, *319*, 229–304, doi:10.1126/science. 1151716.

Wegmann K.W., and F.J. Pazzaglia (2002), Holocene strath terraces, climate change, and active tectonics: the Clearwater River basin, Olympic Peninsula, Washington State. *Geological Society of America Bulletin*, *114*(6), 731–744.

Wegmann K.W., and F.J. Pazzaglia (2009), Late Quaternary fluvial terraces of the Romagna and Marche Apennines, Italy: climatic, lithologic, and tectonic controls on terrace genesis in an active orogen, *Quaternary Science Reviews*, *28*(1-2), 137–165.

Wood, J.D. (1996) The geomorphological characterization of digital elevation models *PhD Thesis, University of Leicester, UK*, http://www.soi.city.ac.uk/~jwo/phd

Wood, J.D. (2009), Geomorphometry in LandSerf. *Geomorphometry – Concepts, Software, Applications*, *33*, 333-349, doi:10.1016/S0166-2481(08)00014-7.

Appendix 1: Stratigraphic Data Collected from Soil Pits and Cut Bank Exposures

Sheepscot_10.8_righttrib		
Depth (m)	Description	Interpretation
0.3	Brown massive silt layer with roots and soil development. Grades into lower unit.	Top of Reservoir-sediment deposit
0.85	Massive fine grained sand/silt layer with bug burrows. Graded upper and lower contact.	Reservoir-sediment
1.1	Massive silty layer with sand lenses present near base.	Reservoir-sediment
1.3	Silt layer with blue and rust colored staining. Buried organic material present. Interbedded sand and silt. Sharp upper and lower contact.	Reservoir-sediment/ Floodplain deposit or Wetland
1.55	Rounded gravel layer. Average clast size ~ 20 cm.	Paleo river channel
1.64	Muddy sand with lots of organics buried, producing black color.	Potential buried Holocene wetland

Sheepscot_11.2_lefttrib		
Depth (m)	Description	Interpretation
0.51	Brown massive silt layer with roots and soil development. Basal contact infered based on change in cohesion.	Top of Reservoir-sediment deposit
0.85	Massive silt layer with some roots present. Brownish coloration, slightly visible basal contact.	Reservoir-sediment
0.98	Massive silt/clay layer. Very cohesive. Sharp upper and lower contacts.	Reservoir-sediment
1.05	Fine-grained sand with lots of organics present. Some interbedded clay/silt layers.	Reservoir-sediment
1.25	Massive light gray clay layer with 1-2 mm clasts present sporadically. Basal contact undetermined.	Presumpcot Clay

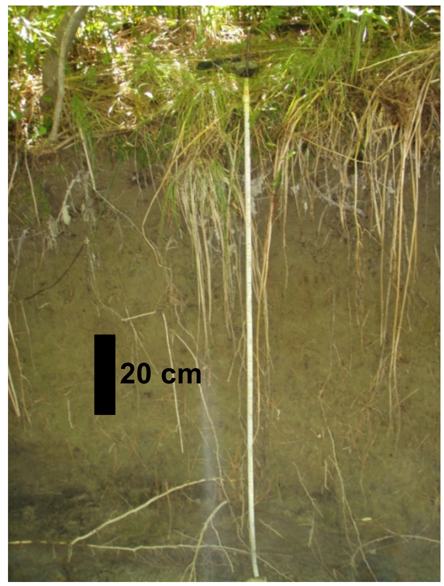

Sheepscot_11.48_soilpit		
Depth (m)	Description	Interpretation
0.58	Massive brown silt with roots and cobbles present sporadically. Piece of brick found within top 10 cm of deposit.	Legacy-sediment

Sheepscot_11.2_lefttrib2		
Depth (m)	Description	Interpretation
0.29	Brown massive silt layer with roots and soil development. Sharp basal contact apparent by color change.	Reservoir-sediment deposit
0.34	Black silty/clay layer with lots of organics present. Sharp upper and lower contacts.	Potential buriend wetland/flood plain
1	Massive grey clay layer. Very cohesive. Basal contact undetermined.	Presumpscot Clay

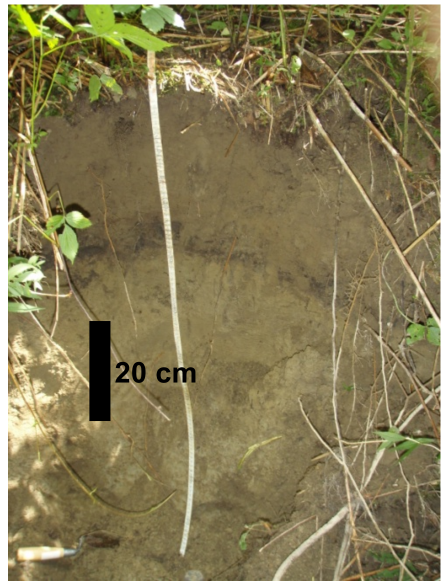

Sheepscot_11.2_island		
Depth (m)	Description	Interpretation
0.4	Massive brown silt layer with small sand lenses. Active flood deposits on surface.	Reservoir-sediment deposit
0.58	Grey silt/clay layer. Subtle upper contact. Some roots present, but less than above unit.	Potential buriend wetland/flood plain
1	Rounded cobbles, average diameter ~5 mm.	Ancient river bed.

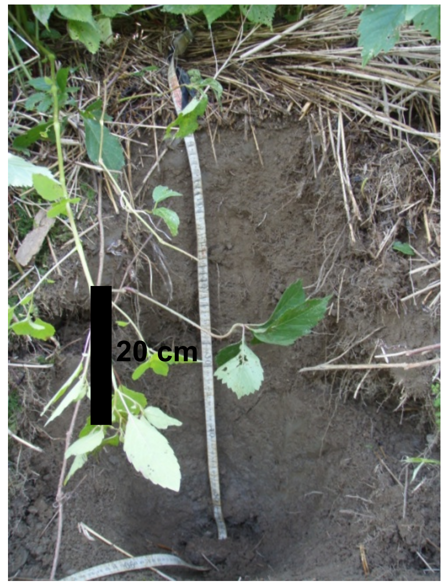

Sheepscot_11_island1		
Depth (m)	Description	Interpretation
0.44	Massive brown silt with some clay. Roots and animal/insect burrows visible. Clear basal contact based on change in grain size.	Reservoir-sediment deposit
0.58	Medium sand unit with cobble bed. Cobbles are ~3-5 mm and well rounded. No structures clearly apparent in unit.	Ancient Floodplain
0.63	Fine grained sand with some wood particles found. No apparent structure in unit.	Ancient Floodplain or Wetland
1.26	Light grey clay layer with interbedded layers of sand. Sand layers range from 5-10 cm apart.	Presumpscot Clay

Sheepscot_11_island2		
Depth (m)	Description	Interpretation
0.32	Massive brown silt with some clay unit. Roots and burrows present throughout.	Reservoir-sediment
0.73	Continuation of upper unit, but slight change to more greyish color.	Reservoir-sediment
0.82	Coarse sand with some intermixed fine sand regions. Clear upper and lower contacts determined by change in grain size.	Floodplain Deposit
1.17	Fine-grained sand with interbedded organic layers. Layers and dark brown in color	Floodplain Deposit
1.46	Grey clay layer with interbedded sand lenses.	Presumpscot Clay

Sheepscot_10.8_righttrib2		
Depth (m)	Description	Interpretation
1.25	Massive brown silt/clay layer. Subtle transition to greyer color at 0.6 m. Many roots present, with large burrow at 0.5 m.	Reservoir-sediment
1.47	Black/dark grey layer. Lots of organics , some interbedding visible.	Potential buried Holocene wetland
2.03	Grey silt/clay layer with interbedded fine-sand layers.	Paleo-floodplain
2.46	Rounded cobbles in fine-sand/mud matrix. Bottom defined by contact with the water surface.	Buried paleo-river bed

Sheepscot_10.8_righttrib3		
Depth (m)	Description	Interpretation
1.02	Massive light brown silt/clay with roots present throughout.	Reservoir-sediment
1.06	Fine-grained sandy silt unit with some organics visible at boundary with upper unit. True depth undetermined.	Reservoir-sediment/ Potentially Floodplain deposit

Sheepscot_10.8_righttrib4		
Depth (m)	Description	Interpretation
1.43	Dark brown silt unit with lots of roots present. Some cobbles found sporadically throughout deposit.	Reservoir-sediment
1.8	Soil pit dug on adjacent lower surface ~1.5 m away from upper unit. Silt/clay unit greyish in color with black staining. Potential transition to clay at depth, but not confirmed	Buried Paleo-Floodplain/ Transition to Presumpscot Formation

Sheepscot_10.9_riverleft		
Depth (m)	Description	Interpretation
1.27	Massive light brown silt/clay with roots present throughout.	Reservoir-sediment
1.39	Buried decaying log.	
1.47	Massive grey silt/clay unit with some fine sands disperesed throughout.	Reservoir Sediment

Sheepscot_10.6_riverleft		
Depth (m)	Description	Interpretation
0.63	Massive silt unit with some clay. Light brown in color. Roots and decaying wood present.	Reservoir-sediment
1.29	Subtle shift to more greyish color with some fine-grained sand lenses and charcoal present. Base determined due to contact with water surface.	Reservoir-sediment. Color shift could be caused by anoxic conditions.

Sheepscot_10.6_riverright		
Depth (m)	Description	Interpretation
0.98	Massive light brown silt/clay unit with roots present. Two sand pocketes visible at ~0.75 m depth.	Reservoir-sediment
1.26	Subtle tranistion to grey fine-sand/silt unit. Rust coloration and has sand lenses present. Cobble layer basal contact determined through contact with shovel.	Reservoir-sediment. Color shift could be caused by anoxic conditions.

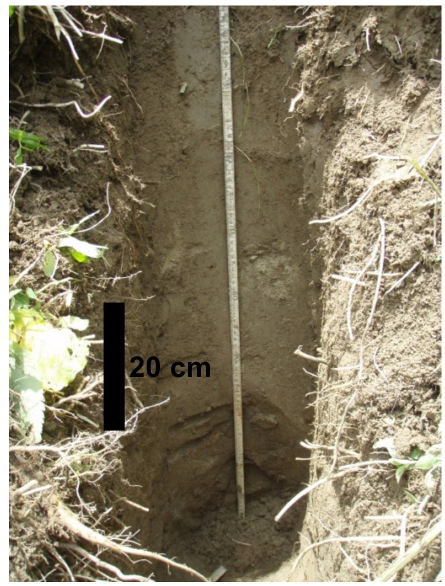

Sheepscot_10.8_righttrib5		
Depth (m)	Description	Interpretation
1.09	Massive light brown silt/clay with lots of roots present throughout. Some tiny potential charcoal pieces at bottom contact. Rust staining at base.	Reservoir-sediment
1.54	Light grey clay layer with fine-grained sand lenst at 1.29 m depth. Some localized build-up of organics above and below sand lens. Unit extends down until it contacts the water surface.	Presumpscot Clay

Pinhook_riverleft_1		
Depth (m)	Description	Interpretation
0.39	Massive light brown silt/clay with roots present throughout.	Reservoir-sediment
0.885	Subtle transition to more grey/clay. Some charcoal seen. Cobble layer basal contact determined through contact with shovel.	Reservoir-sediment

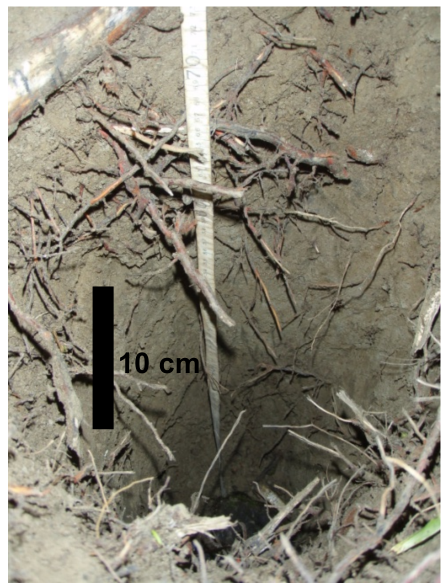

Pinhook_riverleft_upperterrace_2		
Depth (m)	Description	Interpretation
0.29	Dark brown massive silt/clay with lots of roots present. Numerous large clasts (~5 cm) found within unit.	Reservoir-sediment with inclusion of colluvial clasts.
0.51	Reddish/brown silt/clay layer with roots present. Cobble layer basal contact determined through contact with shovel.	Reservoir-sediment

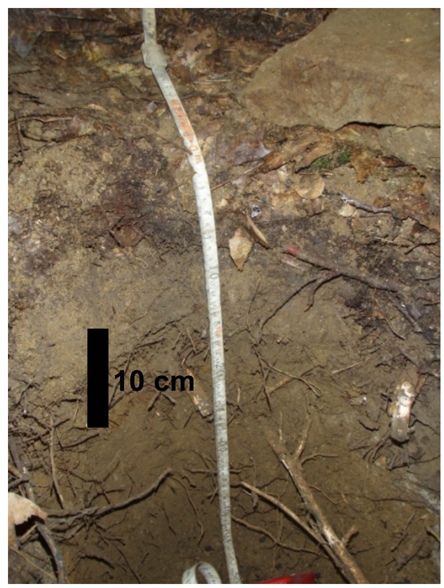

Pinhook_riverright_3		
Depth (m)	Description	Interpretation
0.68	Massive fine-grained silt/clay unit. Light brown in color with lots of roots present. Large cobble (~5 cm) observed at 0.2 m depth. Cobble layer basal contact determined through contact with shovel.	Reservoir-sediment with inclusion of colluvial clasts